

11-2021

## **MATERIAL CHARACTERIZATION FOR MICROWAVE ABSORBING AND SHIELDING APPLICATIONS**

Muhammed Shafeeque Kallumottakkal

Follow this and additional works at: [https://scholarworks.uaeu.ac.ae/all\\_theses](https://scholarworks.uaeu.ac.ae/all_theses)

 Part of the [Engineering Commons](#)

---

United Arab Emirates University

College of Engineering

Department of Electrical and Communication Engineering

**MATERIAL CHARACTERIZATION FOR MICROWAVE  
ABSORBING AND SHIELDING APPLICATIONS**

Muhammed Shafeeque Kallumottakkal

This thesis is submitted in partial fulfilment of the requirements for the degree of  
Master of Science in Electrical Engineering

Under the Supervision of Prof. Mousa Hussein

November 2021

### **Declaration of Original Work**

I, Muhammed Shafeeque Kallumottakkal, the undersigned, a graduate student at the United Arab Emirates University (UAEU), and the author of this Master thesis entitled “*Material Characterization for Microwave Absorbing and Shielding Applications*”, hereby, solemnly declare that this thesis is my own original research work that has been done and prepared by me under the supervision of Prof. Mousa Hussein, in the College of Engineering at the UAEU. This work has not previously formed the basis for the award of any academic degree, diploma or a similar title at this or any other university. Any materials borrowed from other sources (whether published or unpublished) and relied upon or included in my thesis have been properly cited and acknowledged in accordance with appropriate academic conventions. I further declare that there is no potential conflict of interest with respect to the research, data collection, authorship, presentation and/or publication of this thesis.

Student’s Signature:



Date: 18 November 2021

Copyright © 2021 Muhammed Shafeeque Kallumottakkal  
All Rights Reserved

## Approval of the Master Thesis

This Master Thesis is approved by the following Examining Committee Members:

- 1) Advisor (Committee Chair): Prof. Mousa Hussein

Title: Professor

Department of Electrical and Communication Engineering

College of Engineering

Signature: 


Date: 9/12/2021

- 2) Member: Dr. Mahmoud Al Ahmad

Title: Associate Professor

Department of Electrical and Communication Engineering

College of Engineering

Signature: 


Date: 17/12/2021

- 3) Member: Dr. Hamad Alkhoori

Title: Assistant Professor

Department of Electrical and Communication Engineering

College of Engineering

Signature: 

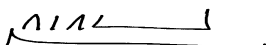
Date: 17/12/2021

- 4) Member (External Examiner): Prof. Mohammad S. Sharawi

Title: Professor

Department of Electrical Engineering

Institution: Ecole Polytechnique de Montréal: Montreal, QC, Canada

Signature: 

Date: 09/12/2021

This Master Thesis is accepted by:

Acting Dean of the College of Engineering: Professor Mohamed Al-Marzouqi

Signature Mohamed AlMarzouqi Date 02/02/2022

Dean of the College of Graduate Studies: Professor Ali Al-Marzouqi

Signature Ali Hassan Date 02/02/2022

Copy \_\_\_\_ of \_\_\_\_

## Abstract

The rapid advancement and widespread of microwave and RF-communication systems have contributed to an abundant rise in electromagnetic energy radiation in our living environment. Such an increase in microwave sources is due to the development and advancement in communication techniques (mobile phones, laptops, and antennas for aeronautics or automobile) and electronic warfare in the military field (radar and satellite). To address these concerns, EM absorbing materials are used to ensure public safety and the safety of military operations. Various types of EM absorbing materials made up of composite materials have been produced and studied. This thesis, discusses the microwave properties of different sets of composite materials. Firstly, the samples of polymer with varying concentrations of weight (wt. %) (1%, 5%, 8%, and 10%) of Multi-Wall Carbon Nanotube (MWCNT) are studied. Secondly, the CNT sample is functionalized with metal alloy oxides, such as Cobalt oxide, Cobalt Iron oxide, and Iron oxide in three different concentrations (5%, 10%, and 20%) are embedded in a polyurethane matrix are investigated. The dielectric properties of the samples are studied using an open-ended coaxial probe technique in the wide frequency range (5 - 50 GHz). The reflection loss at normal incidence is then used to calculate the composites' absorption efficiency, a minimum reflection of -43dB was obtained at 8 GHz frequency with a small thickness of 3.5mm. The results reveal that by varying the CNT content and material thickness, the spectrum range of absorption can be modified. The absorption efficiency of polyurethane/CNT composites was improved by functionalized CNT with various alloyed metal. Thus, functionalized composites can be used as a lightweight material for microwave absorption and shielding.

**Keywords:** Functionalized CNT, Microwave Absorption, Dielectric.

## Title and Abstract (in Arabic)

### توصيف المواد لتطبيقات امتصاص الميكروويف والتدريع

#### الملخص

ساهم التقدم السريع والواسع النطاق لأنظمة اتصالات الميكروويف والترددات اللاسلكية في ارتفاع كبير في إشعاع الطاقة الكهرومغناطيسية في بيئتنا المعيشية. ترجع هذه الزيادة في مصادر الميكروويف إلى التطور والتقدم في تقنيات الاتصال (الهواتف المحمولة وأجهزة الكمبيوتر المحمولة وهوائيات الطيران أو السيارات) والحرب الإلكترونية في المجال العسكري (الرادار والأقمار الصناعية). لمعالجة هذه المخاوف، يتم استخدام مواد امتصاص EM لضمان السلامة العامة وسلامة العمليات العسكرية. تم إنتاج ودراسة أنواع مختلفة من المواد الممتصة EM المكونة من مواد مركبة. تناقش هذه الأطروحة خصائص الميكروويف لمجموعات مختلفة من المواد المركبة. أولاً، تمت دراسة عينات البوليمر بتركيزات مختلفة من الوزن (بالوزن%) (1%، 5%، 8%، 10%) من الأنابيب النانوية الكربونية متعددة الجدران (MWCNT). ثانياً، يتم توظيف عينة CNT بأكاسيد سبيكة معدنية، مثل أكسيد الكوبالت، وأكسيد الحديد الكوبالت، وأكسيد الحديد في ثلاثة تركيزات مختلفة (5%، 10%، 20%) مدمجة في مصفوفة البولي يوريثين. تمت دراسة الخصائص العازلة للعينات باستخدام تقنية مسبار متحد المحور مفتوح النهاية في نطاق تردد واسع (5 - 50 جيجاهرتز)، ثم يتم استخدام فقدان الانعكاس عند الوقوع الطبيعي لحساب كفاءة امتصاص المركبات، بعد أدنى تم الحصول على انعكاس -43 ديسيبل بتردد 8 جيجاهرتز وبسمك صغير يبلغ 3.5 مم. تكشف النتائج أنه من خلال تغيير محتوى CNT وسمك المادة، يمكن تعديل نطاق الامتصاص الطيفي. تم تحسين كفاءة امتصاص مركبات البولي يوريثين/الأنابيب النانوية الكربونية بواسطة الأنابيب النانوية الكربونية الوظيفية مع العديد من المعادن المخلوطة. وبالتالي، يمكن استخدام المركبات الوظيفية كمادة خفيفة الوزن لامتصاص الميكروويف والحماية.

**مفاهيم البحث:** CNT وظيف، امتصاص الميكروويف، عازل.



## **Acknowledgements**

It is my proud privilege to express my deepest gratitude to my thesis supervisor Prof. Mousa Hussein, Electrical and Communication Engineering department of UAE University. His inspiration, enthusiasm, deep knowledge, guidance, and support helped at all times to complete my thesis.

I would like to thank Dr. Mahmoud Al Ahmad, and all faculty members of Department of Electrical & Communication Engineering for their support and assistance throughout my study and research. And also, thanks to all my friends who are more or less contributed to the preparation of this thesis.

Special thanks to my parents, my wife, brothers, and sisters who helped me along the way.

## **Dedication**

*To my beloved parents and family*

## Table of Contents

|   |      |
|---|------|
| Title .....   | i    |
| Declaration of Original Work .....                            | ii   |
| Copyright .....   | iii  |
| Approval of the Master Thesis .....                           | iv   |
| Abstract .....  | vi   |
| Title and Abstract (in Arabic) .....                          | vii  |
| Acknowledgements .....  | viii |
| Dedication .....  | ix   |
| Table of Contents .....                                       | x    |
| List of Tables .....  | xii  |
| List of Figures .....   | xiii |
| List of Abbreviations .....                                   | xv   |
| Chapter 1: Introduction .....                                 | 1    |
| 1.1 Overview .....  | 1    |
| 1.2 Classification of Materials .....                         | 2    |
| 1.2.1 Dielectric Materials .....                              | 3    |
| 1.2.2 Magnetic Materials .....                                | 4    |
| 1.2.3 Composite Materials .....                               | 5    |
| 1.2.4 Nano-composite Materials .....                          | 6    |
| 1.3 Types of Absorbers .....                                  | 6    |
| 1.3.1 Impedance Matching Absorber .....                       | 6    |
| 1.3.2 Resonant Materials Absorber .....                       | 7    |
| 1.4 Statement of the Problem .....                            | 8    |
| 1.5 Relevant Literature .....                                 | 8    |
| Chapter 2: Theory of Microwave Absorption .....               | 12   |
| 2.1 Multiple Reflection Method .....                          | 19   |
| Chapter 3: Materials and Morphological Study .....            | 23   |
| 3.1 Functionalized CNT .....                                  | 25   |
| Chapter 4: Measurement Techniques .....                       | 31   |
| 4.1 Vector Network Analyzer and Scattering Parameters .....   | 32   |
| 4.2 Calibration .....   | 35   |
| Chapter 5: Measurements and Characterization of Samples ..... | 40   |
| 5.1 Permittivity Measurements .....                           | 40   |
| 5.2 Attenuation Calculation .....                             | 44   |

|   |    |
|---|----|
| 5.3 Impedance Calculation.....                        | 45 |
| Chapter 6: Reflection Loss Study of the Samples ..... | 47 |
| 6.1 Reflection Loss for One-layer composite .....     | 47 |
| 6.2 Reflection Loss for Two-layer composite.....      | 54 |
| Chapter 7: Conclusion.....                            | 60 |
| References .....                                      | 61 |
| List of Publications .....                            | 65 |
| Appendices.....                                       | 66 |
| Appendix 1 .....                                      | 66 |
| Appendix 2.....                                       | 72 |
| Appendix 3.....                                       | 73 |

## List of Tables

|   |    |
|---|----|
| Table 1: Microwave frequency bands .....                                  | 1  |
| Table 2: CNT based composites for microwave absorption .....              | 10 |
| Table 3: Elements present in the sample at different areas .....          | 27 |
| Table 4: Performance of composite with Co functionalization .....         | 48 |
| Table 5: Performance of composite with CoFe Oxide functionalization ..... | 50 |
| Table 6: Performance of composite with Fe Oxide functionalization .....   | 53 |
| Table 7: Performance of double layered composite.....                     | 58 |

## List of Figures

|  |    |
|--|----|
| Figure 1: Polarization due to electric field.....  | 3  |
| Figure 2: Impeding absorbing charges.....  | 5  |
| Figure 3: Set up for matched layer absorber.....   | 7  |
| Figure 4: Wave propagation through absorbing material.....                               | 12 |
| Figure 5: Dielectric salisbury screen.....   | 15 |
| Figure 6: Dielectric salisbury screen transmission line model.....                       | 17 |
| Figure 7: Transmission matrix representation.....  | 17 |
| Figure 8: Equivalent circuit.....  | 17 |
| Figure 9: Multiple reflection in one layer.....  | 20 |
| Figure 10: Multiple reflection in two layers.....  | 22 |
| Figure 11: SEM image of CNT.....   | 23 |
| Figure 12: Samples with PU and different Wt.% of CNT.....                                | 24 |
| Figure 13: SEM of MWCNT in PU matrix.....  | 24 |
| Figure 14: SEM images of CNT with cobalt-iron oxide nanoparticles.....                   | 26 |
| Figure 15: TEM images of CNT with cobalt-iron oxide nanoparticles.....                   | 28 |
| Figure 16: Elemental mapping of cobalt-iron oxide nanoparticle.....                      | 29 |
| Figure 17: Functionalized CNT samples.....   | 30 |
| Figure 18: Schematic diagram of the measurement setup.....                               | 32 |
| Figure 19: Measurement setup used in our lab.....  | 32 |
| Figure 20: Instruments used.....   | 33 |
| Figure 21: Schematic of a two-port network.....  | 34 |
| Figure 22: Calibration setup.....  | 36 |
| Figure 23: Measurement of teflon using O-L <sub>1</sub> -L <sub>2</sub> calibration..... | 37 |
| Figure 24: Measurement of teflon using OSL calibration.....                              | 38 |
| Figure 25: PU with different concentration of CNT.....                                   | 41 |
| Figure 26: Functionalized with different concentration of Co.....                        | 42 |
| Figure 27: Functionalized with different concentration of CoFe.....                      | 43 |
| Figure 28: Functionalized with different concentration of Fe.....                        | 43 |
| Figure 29: Attenuation factor.....   | 45 |
| Figure 30: Comparison of impedance.....  | 46 |
| Figure 31: Reflection loss without functionalization.....                                | 48 |
| Figure 32: Reflection loss of Co functionalized composite.....                           | 49 |
| Figure 33: Comparison of reflection losses for different wt.% of Co.....                 | 49 |
| Figure 34: Reflection loss for CoFe functionalized composite.....                        | 51 |
| Figure 35: Comparison of reflection losses for different wt.% CoFe.....                  | 51 |
| Figure 36: Reflection loss of Fe functionalized composite.....                           | 52 |
| Figure 37: Comparison of reflection losses for different wt.% of Fe.....                 | 53 |
| Figure 38: Reflection loss for PU 5% CNT 10% Co & PU composite.....                      | 55 |
| Figure 39: Reflection loss for PU 5% CNT 10% Co & PU with no metal.....                  | 55 |
| Figure 40: Reflection loss for PU 5% CNT 20% Co & PU composite.....                      | 56 |
| Figure 41: Reflection loss for PU 5% CNT 20% CoFe & PU composite.....                    | 56 |

Figure 42: Reflection loss for PU 5% CNT 10% Fe & PU composite ..... 57

## List of Abbreviations

|                                  |                                  |
|----------------------------------|----------------------------------|
| CNTs                             | Carbon Nanotubes                 |
| CoFe                             | Cobalt Iron                      |
| CVD                              | Chemical Vapour Deposition       |
| DAK                              | Dielectric Assessment Kit        |
| EM                               | Electromagnetic                  |
| EMI                              | Electromagnetic Interference     |
| Fe                               | Iron                             |
| MAMs                             | Microwave Absorbing Materials    |
| MWCNT                            | Multi Wall Carbon Nanotube       |
| O-L <sub>1</sub> -L <sub>2</sub> | Open-Load1-Load 2                |
| OSL                              | Open-Short-Load                  |
| PEC                              | Perfect Electric Conductor       |
| PU                               | Polyurethane                     |
| RCS                              | Radar Cross Section              |
| SEM                              | Scanning Electron Microscopy     |
| SNA                              | Scalar Network Analyzers         |
| SWCNT                            | Single Wall Carbon Nanotube      |
| TEM                              | Transmission Electron Microscopy |
| VNA                              | Vector Network Analyzer          |
| Wt. %                            | Weight Percentage                |



## Chapter 1: Introduction

### 1.1 Overview

Microwave is a set of frequency bands in the Electromagnetic (EM) spectrum with a frequency range of  $10^9$ – $10^{12}$  Hz [1], and having a wavelength ranges from 1 mm to 30 cm. Microwave frequency lies in between infrared radiation and radio waves in the EM spectrum. Microwave is further divided into sub-bands such as L, S, C, X, Ku, K, Ka, and mm wave. Table 1 depicts the different microwave bands with frequency ranges and their corresponding wavelengths.

Table 1: Microwave frequency bands

| Bands   | Frequency Range (GHz) | Wavelength (cm) |
|---------|-----------------------|-----------------|
| L       | 1-2                   | 30-15           |
| S       | 2-4                   | 15-7.5          |
| C       | 4-8                   | 7.5-3.8         |
| X       | 8-12                  | 3.8-2.5         |
| Ku      | 12-18                 | 2.5-1.7         |
| K       | 18-27                 | 1.7-1.1         |
| Ka      | 27-40                 | 1.1-0.75        |
| mm Wave | 40-300                | 0.75-0.1        |

The availability of these various bands made microwaves useful for a wide range of applications in society and industry, such as television broadcast, satellite

communication, mobile phones, medical treatments, navigation, food preparation and radar technology. These are sources of microwave radiation. Thus, to reduce the radiation, efficient microwave absorbers are essential. The microwave absorber is a specially engineered material that dissipates the electric/magnetic fields of the waves into heat to remove the reflected EM energy incident on its surface.

With the advancement of stealth technology, Microwave Absorbing Materials (MAM) research has accelerated, and substantial progress has been made [2]. In aerospace engineering, light weight absorbing material covering a wide range of frequencies is considered an essential factor in such industry. MAMs investigation has started before World War II; the Germans developed a ferrite-based paint that was considered the first MAM in reaction to the Allies' success with radar sets. During this time, the United States and Germany began working on projects to put the EM wave absorber ideas that had emerged from research into practice, including production, design tests, and field evaluation for use in a limited number of defense applications. The focus of the USA was on designing absorbers that would improve radar efficiency by reducing interfering reflection from nearby objects [3]. It has now transitioned from conventional MAMs to advanced MAMs, which is depicted by Nano-MAMs [4]. Materials science, solid-state physics, and electrical and electronic engineering are developing MAMs and studying their properties at microwave frequencies [2].

## **1.2 Classification of Materials**

EM waves have electric and magnetic components; thus, an absorbing material must be capable of canceling out microwave radiation's electric and magnetic components. MAM's, also known as radar absorbing materials (RAMs), can be divided into dielectric, magnetic, and composite absorbing materials.

### 1.2.1 Dielectric Materials

An insulator that can be polarized by an applied electric field is known as a dielectric material. When a dielectric material is exposed to an external electric field, the electric charges do not move through the material at the atomic level; however, specific changes in charge configuration may occur and form a dipole, as shown in Figure 1. The degree to which the dipoles align themselves to the electric field is called the material's polarizability[5].

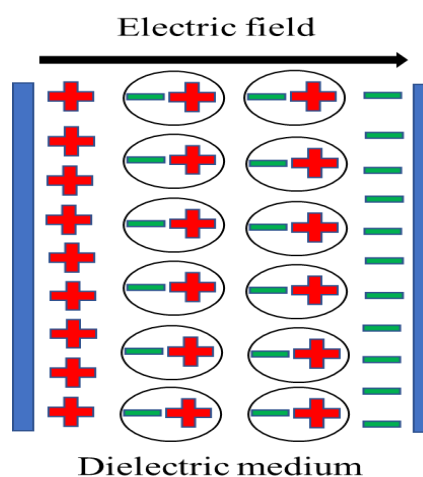


Figure 1: Polarization due to electric field

When an EM wave strikes a dielectric material, it dissipates electric energy, which is then converted into heat energy, and this energy is referred to as dielectric loss. A material's overall permittivity may be influenced by a several dielectric loss mechanisms or polarization effects such as electronic and atomic polarization, orientation polarization, ionic conductivity, and space charge polarization. In the presence of an electric field, free charge carriers cannot completely migrate into an absorber made of more than one material. The carriers may become trapped inside the absorber's interfaces, causing charges to accumulate and leading to an increase in

permittivity. This happens due to the space charge polarization. If there are only electronic and atomic polarizations, then the material is almost lossless in the microwave region. Frequency dependence of space charge and orientation polarization explains the dielectric relaxation. Its effects associated with permanent and induced molecular dipoles cause the loss in the microwave region.

To evaluate microwave absorption, dielectric absorbers use electronic polarization, ion polarization, and intrinsic electrical dipolar polarization in their materials [6]. Considering the dielectric absorber has light-weight but has a low absorptivity compared to magnetic absorbers [1]. To control the complex permittivity, dielectric absorbers use conductive fillers like nano-composites. These nano-composites have a low density, and their mixing ratios are quite low as compared to magnetic fillers.

### **1.2.2 Magnetic Materials**

Magnetic materials are categorized as diamagnetic, paramagnetic, or ordered magnetic based on the responses of their atoms' magnetic moments to an external magnetic field. Diamagnetic materials have a balanced magnetic movement. The materials having unpaired electrons that leads to unbalanced magnetic movements are paramagnetic material. While the ferromagnetic material has unpaired electrons but their magnetic movements are parallel to the applied magnetic field. Like in the dielectric material, the magnetic material also has some loss mechanism when interacting with EM waves such as eddy current loss, hysteresis loss, and residual loss. Magnetic losses are more significant at lower frequencies, and at higher frequencies, electromagnetic absorption is accounted by the material's electric properties [7].

Magnetic absorbers have good absorption properties, but their densities are typically too high.

### 1.2.3 Composite Materials

This thesis focused on composite materials to study its microwave properties for having a highly efficient microwave absorber. In general, the composite material constitutes two or more components having a different property. When the components of composites come together, they form a new substance with properties that are distinct from the individual components. A host matrix and fillers are commonly used in composite materials. This kind of material is developed by impeding absorbing charges (magnetic or dielectric) into a host matrix material, as shown in Figure 2.

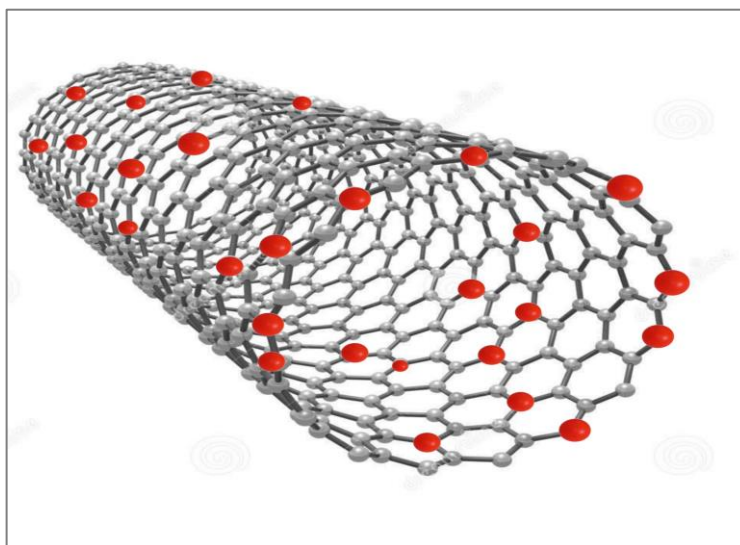


Figure 2: Impeding absorbing charges

The constituent properties depend on different parameters. Thus, tuning the microwave properties can be possible by changing the properties or the amount of the constituents. So, the composite materials are very efficient for microwave absorption applications.

### **1.2.4 Nano-composite Materials**

Nano-composites are a diverse class of materials of one or more dimensions in the nanometer (nm) scale that exhibit unusual material properties. These multiphase materials have at least one constituent with a dimension of less than 100 nm. Nano-composites are made by combining nanoparticles with a base material to strengthen the properties of the base material, such as optical, mechanical, thermal, dielectric, and electrical properties. According to conventional composite principles, a composite's permittivity should be somewhere between the filler and content. Nano-composites, on the other hand, never follow this pattern [8]. Three significant variables, particle size, shape, and surface characteristics, determine the filler material's reinforcing ability. Nano-scale fillers are just a few hundred nanometers in size, but they have a very high aspect ratio and surface area, offering excellent reinforcement with the base material [9]. Nano MAM is a potential absorber for industrial applications because of its light-weight, excellent compatibility, and wide bandwidth.

### **1.3 Types of Absorbers**

To prevent the reflection of electromagnetic waves incident on the absorber surface, microwave absorbers are usually made of blocks of wave-absorptive material and comes in various designs [10]. Graded interfaces or Impedance matching and resonant absorbers are two types of microwave absorbers.

#### **1.3.1 Impedance Matching Absorber**

Impedance matching absorber portrays a graded interface to match impedance or a progressive change in material properties for impedance matching, which involves pyramidal, tapered loading, and matched layer absorbers. Figure 3 shows the set-up for the matched layer absorber. The thickness and impedance values of the

matching layer are set between the two impedances to be matched, that is, the absorber and incident media. This matching occurs when the thickness of the matching layer is quarter of a wavelength of the radiation in the layer. The impedance matching occurs only at the frequency that equals the optical thickness. The magnitude of the impedance step between the incident and transmitting media would be proportional to the magnitude of the reflection experienced by a propagating wave working on an interface. One or more wavelengths of material are needed for complete attenuation of the incident wave, which makes them bulky [11].

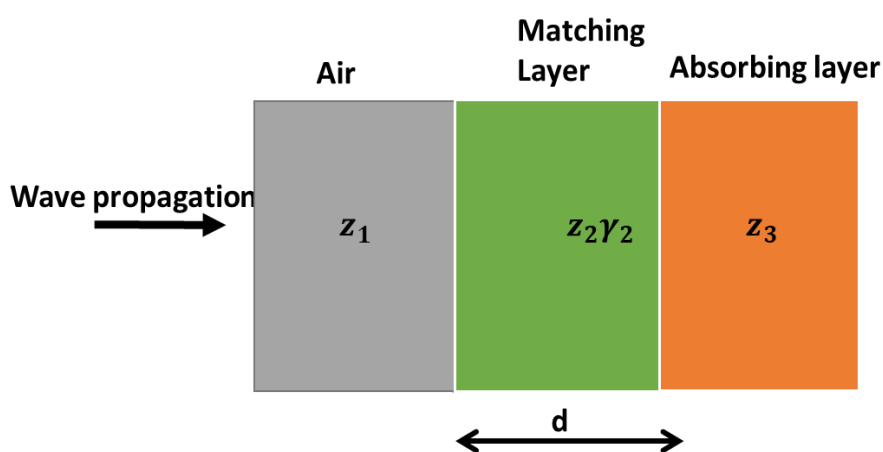


Figure 3: Set up for matched layer absorber

### 1.3.2 Resonant Materials Absorber

Dallenbach layers, Salisbury Screen, and Jaumann layers are examples of resonant materials, also known as tuned or quarter wavelength absorbers. The impedance of the incident and absorbing media is not balanced in this class of materials, and the material is thin, and not all of the power is absorbed. The phase of the reflected wave is reversed by  $\pi$ , and the transmitted wave is reflected from a metal

backing after passing through the absorbing medium. Before the wave propagates back to the incident medium, this second reflection causes a phase reversal of  $\pi$ .

#### **1.4 Statement of the Problem**

This study, focused to find solutions to ensure a sound EM radiation absorbing material. Studies are centered on EM absorbing materials with light-weight and broad absorption capability to ensure public safety and the safety of military operations. Especially in military operations to reduce the magnitude of the radar cross-section. Various types of materials are researched to find the efficient microwave absorber, especially the composite materials. The composite materials can combine both the magnetic and dielectric materials and have a better absorption performance than the magnetic and dielectric materials using alone [6]. Thus, used a polymer-based metal functionalized CNT to have a light-weight and wide band microwave absorber.

#### **1.5 Relevant Literature**

Advances in material science and engineering have led to the development of composite materials with excellent microwave absorption properties. Impeding absorbing magnetic or dielectric charges into a host matrix material produces this type of material [12]. Because of the potential changes in the physical properties of nano-composites, the use of nanoparticles in matrix systems has become a subject of interest in engineering applications. Extensive research has been done to combine the dielectric loss of Carbon Nano Tubes (CNTs) with the magnetic loss of ferromagnetic or compound materials. Some composites of this kind have been investigated, including CNTs/CoFe<sub>2</sub>O<sub>4</sub>, raw MWCNTs/Fe catalyst, Co/CNT, and iron nano-granule/MWCNT [13]. Polymer Nano-composites are high-performance composites made by adding nanoparticles to a polymer matrix, also known as nano-filled polymer composites.



These are made up of nano-fillers that are uniformly distributed across the polymer matrix. Only about 10% of nano-fillers are needed to alter the intrinsic polymer properties [14]. Significant differences in composite properties can be achieved depending on the nature of the filler, the weight percentage used, and the method of preparation. Recently, nano-carbon-based reinforced composites have been proposed to improve traditional materials' performance while reducing the overall multilayer thickness [1]. Cylindrical-shaped Carbon Nano Tubes (CNT) consisting of either Single-Wall CNT (SWCNT) or Multi-Wall CNT (MWCNT) are well-known as wideband absorbing materials among different allotropic types of carbon atoms. These materials have strong mechanical and thermal properties and are lightweight [15].

CNT-based polymer composites are being considered as an alternative to conventional smart materials [16]. By utilizing the light-weight of CNT and high absorption efficiency of magnetic material lead to the development of functionalized composites, and functionalization can do in either by filling or coating on the CNT will allow tuning the absorption properties [17]. In a functionalized polymer nano-composite absorption is determined by the lossy filler concentration and the thickness of the lossy sheet [1]. Because of their excellent mechanical properties, good biocompatibility, designable flexibility, light-weight, and low cost, Polyurethanes (PUs) are commonly used as matrices in coatings, composites, and other applications [5]. But the CNT/PU composite used for microwave absorption application is less. Liu et al, studied the EM wave absorption properties of SWNT/PU nano-composites prepared by solution filming using SWNTs dispersed in PU solutions for the first time. They discovered that the EM wave absorption improved from 18.3 to 45.9 dB [18]. Chemical vapor deposition was used to synthesize CNT/CoFe<sub>2</sub>O<sub>4</sub> spinel nano-

composite, high complex permittivity of  $\text{CoFe}_2\text{O}_4$  helped to attain strong absorption of microwaves in the high-frequency range [19]. CNT filled with Fe nanoparticles is investigated and obtained 90% absorption at 11.8-14.7 GHz and minimum reflection loss value of -37.71 dB [20]. The electrical properties of the material have a strong influence on how electromagnetic energy interacts with it. Material composition and content can interact with the electric and magnetic forces produced by the electromagnetic fields, resulting in this type of interaction [21]. Table 2 describes some composites with their performances.

Table 2: CNT based composites for microwave absorption

| Nanomaterial  | Thickness (mm) | Minimum Reflection loss (dB) | Freq (GHz) | Bandwidth (GHz)              | Reference  |
|---|----------------|------------------------------|------------|------------------------------|------------|
| CNTs/ $\text{CoFe}_2\text{O}_4$                               | 1.4            | -18.00                       | 9          | 7                            | [19]       |
| Fe filled CNT /epoxy  | 1              | -31.71                       | 13.2       | 2.9                          | [20]       |
| MWCNTs)/Fe  | 3.36-5.57      | -39                          | 2.68       | 2.04-3.47<br>(-20)<br>(1.43) | [21]       |
| MWCNT / $\text{Fe}_3\text{O}_4$ hybrid                        | 2.0–5.0        | -41.61                       | 5.5        | 3.0 - 11.4<br>(8.4)          | [6]        |
| $\text{Ni}_{0.5}\text{Zn}_{0.5}\text{Fe}_2\text{O}_4$ / MWCNT | 3              | -19.34                       | 8.46       | 1.24                         | [22]       |
| MWCNT/ $\text{Fe}_3\text{O}_4$ /epoxy                         | 4              | -27                          | 10.3       | 1.2                          | [23, p. 4] |

Most of the composite in the above table uses the epoxy resin as the host matrix, Similarly, in majority of the research works in the literature studies the

composite Where the CNT is dispersed in the epoxy resin matrix and it is lesser in polyurethane host matrix, in context of aerospace applications, polyurethane is usually preferred and it has been certified due to its excellent mechanical properties such as flexibility, resistance to bending, ease of production in large quantities, However, few studies have been conducted polyurethane/CNT composite as microwave absorbers. Similarly, the major studies are carried out in a small bandwidth of (2-18 GHz) but in this study uses a wide bandwidth of (5-50 GHz).

## Chapter 2: Theory of Microwave Absorption

EM wave absorption is a mechanism in which the energy of an electromagnetic wave is absorbed and then converted into another source of energy, such as thermal energy, based on the conservation of energy principle and preventing the wave from being reflected or transmitted through the materials [5]. By adjusting the electrical and magnetic properties of the respective medium and material for the desired frequency range, the absorber characteristics can be attained. Three processes occur as an electromagnetic wave passes through a material: reflection, absorption, and transmission. There is also evidence of retransmission and secondary reflections [24], as shown in Figure 4.

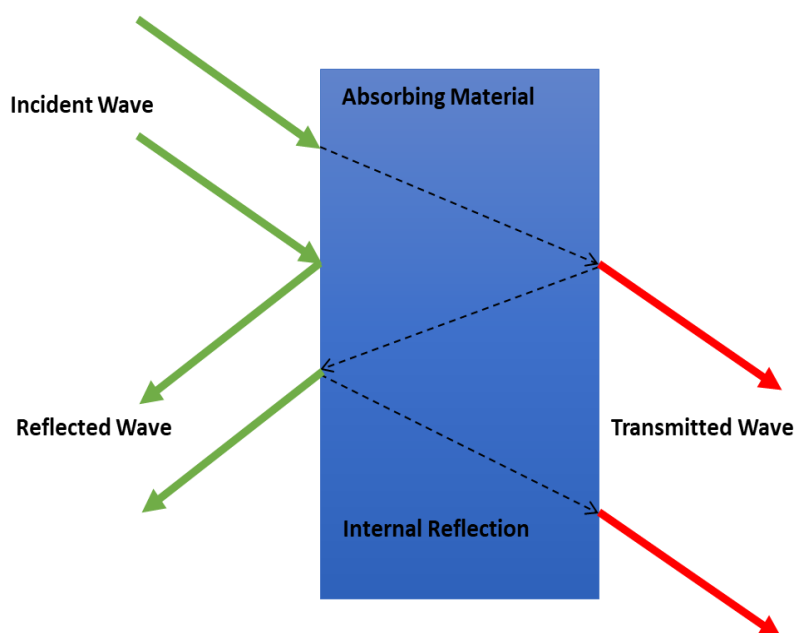


Figure 4: Wave propagation through absorbing material

For microwave absorption measurements, the layer's reflectivity is determined by its thickness and geometry. The incident wave is partially reflected from the

interface between the free space and material. The remaining gets penetrates into the material. The multiple reflections lead to the absorption of the most part of the incident wave, and some get transmitted through the material if there is no metal sheet. To increase absorption capacity, a metal surface is placed near the substrate; the metal sheet will reflect the penetrating wave back into the substrate. As a result, transmitting waves are negligible in microwave absorption with a metal source, so the reflection loss is calculated as the difference between the initial incident wave and the final reflected wave [25]. Reflection loss is the parameter used to determine the microwave absorption efficiency in the composite material by using the complex permittivity values. For an ideal EM wave absorption material, they must meet two requirements: (1) impedance matching between free space and the material surface to prevent wave reflection, which necessitates complex permittivity near complex permeability; and (2) materials should absorb incident waves as possible within absorbers, which necessitates materials with high magnetic or dielectric loss [5]. Perfect matching can be obtained by satisfying the Equation (1).

$$\frac{\mu_1}{\varepsilon_1} = \frac{\mu_0}{\varepsilon_0} \quad (1)$$

Where,  $\mu_0 = 4\pi * 10^{-7} H/m$  and permittivity  $\varepsilon_0 = 8.854 * 10^{12} f/m$  of the free space and  $\mu_1$  and  $\varepsilon_1$  are the permeability and permittivity of the absorbing material, respectively. In case of a perfect absorber the permeability and permittivity of the material equal to one that means the ratio is equal to 1. It is difficult to maintain this formula at microwave frequencies because the real component of relative permittivity remains nearly unchanged with microwave frequency variation [26]. There are two important parameters that will play an important role in the microwave absorption efficiency; these are the relative complex permittivity ( $\varepsilon_r$ ) and relative

complex permeability ( $\mu_r$ ). Relative complex permittivity can be described as the interaction of the material with the electric field applied, and it is expressed as  $\epsilon_r = \epsilon' - j\epsilon''$ , in which  $\epsilon'$  is the real part of the relative complex permittivity and  $\epsilon''$  the imaginary part of the permittivity. Similarly, relative complex permeability is the interaction of a material with the magnetic field applied and is expressed as  $\mu_r = \mu' - j\mu''$  where  $\mu', \mu''$  are the real and imaginary parts of the permeability, respectively. Equation (2) shows the relation between relative permittivity and permeability with the impedance of the absorbing material.

$$Z = \sqrt{\frac{\mu_r}{\epsilon_r}} \quad (2)$$

The real part of Permittivity  $\epsilon'$  and permeability  $\mu'$  denote the material's ability to store electric and magnetic fields, respectively. Similarly, the imaginary part of permittivity and permeability describes the dissipation of the energy or the loss ability of the electric and magnetic fields. The parameter loss tangent of dielectric  $\delta_e$  and magnetic  $\delta_m$  represents the ratio of the amount of energy dissipated to the amount of energy stored as in Equations (3) and (4).

$$\delta_e = \frac{\epsilon''}{\epsilon'} \quad (3)$$

$$\delta_m = \frac{\mu''}{\mu'} \quad (4)$$

$$\epsilon_r = \epsilon' - j \frac{\sigma}{\epsilon_0 \omega} \quad , \epsilon'' = \frac{\sigma}{\epsilon_0 \omega} \quad (5)$$

Another parameter is the material's conductivity as expressed in Equation (5) in terms of permittivity, and it's the capability of the material to conduct electric current. The nano-composite thickness plays an important role in the design of absorbing material with matched impedance. Increasing the thickness of nano-

composites transfers the reflection loss peaks to the low-frequency region, and also, the variation in the thickness can be used to tune the absorption frequency range. According to the theory of the transmission line, the reflection loss of electromagnetic radiation RL(dB) by a normal incident wave at the surface of single-layer material backed by a perfect conductor can be described as Equation (6) [19].

$$RL(dB) = 20 \text{ Log} \left| \frac{(Z_{in} - Z_0)}{(Z_{in} + Z_0)} \right| \quad (6)$$

$$Z_{in} = Z_0 \sqrt{\frac{\mu_r}{\epsilon_r}} \tanh \left[ j \frac{2\pi f t}{c} \right] \sqrt{\mu_r \epsilon_r} \quad (7)$$

Where  $Z_0$  the characteristic impedance of the free space is, approximately equal to 377 Ohms,  $Z_{in}$  is the input impedance of the metal-backed composite material and is obtained by Equation (7) and depends on the composite electric and magnetic properties.  $f$  is the EM wave frequency,  $t$  is the thickness of the absorber, and  $c$  is the velocity of light in free space.

Dielectric Salisbury screen idea is used for studying the microwave properties of the double-layered absorber. Figure 5 shows the basic configuration of the Salisbury absorbing screen illuminated by a normal incident by a plane wave.

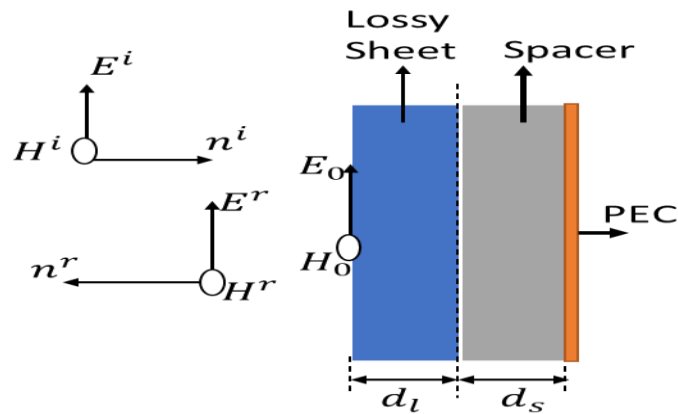


Figure 5: Dielectric salisbury screen

PEC (Perfect Electric conductor) is the first layer on the right side made of a thick metal slab and acts as a reflecting surface. PEC reflects all the energy associated with the incident wave. The spacer, which is usually made of a lossless dielectric material, is the second layer, and having a lower value of relative complex permittivity, the thickness of the lossless sheet is denoted by  $d_s$ . The third layer is the lossy sheet having a higher value of complex permittivity and it absorbs all the energy associated with the incident wave, the thickness of the layer is denoted by  $d_l$ . The lossy layer is characterized by the effective complex permittivity and the imaginary part of the permittivity represents the lossy term. Its absolute value relates to electrical conductivity. While the spacer is characterized by the real part of the effective complex permittivity [27].

The ratio between the amplitudes of the reflected and incident electric fields,  $E^r$  and  $E^i$ , is defined as the reflection coefficient  $R$  of the dielectric Salisbury screen is depicted in Figure 5.

$$R = \frac{E^r}{E^i} \quad (8)$$

The most general absorber configuration that can be envisaged consists of multiple planar layers of different homogeneous materials, and it can be modeled by a series of transmission line segments connected in cascade. Figure 6 shows the transmission line model of the dielectric Salisbury screen. Each segment has impedance and propagation constant and the segment length is given by the layer thickness ( $d_l, d_s$ ).



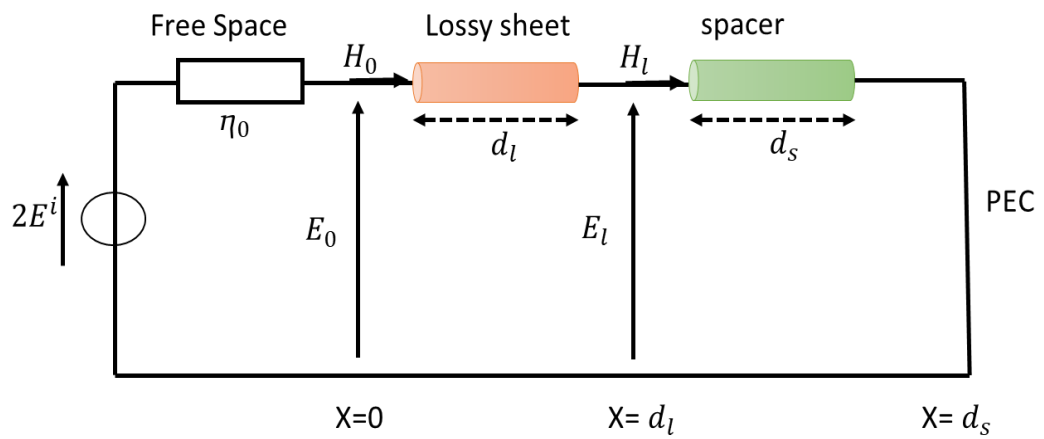


Figure 6: Dielectric salisbury screen transmission line model

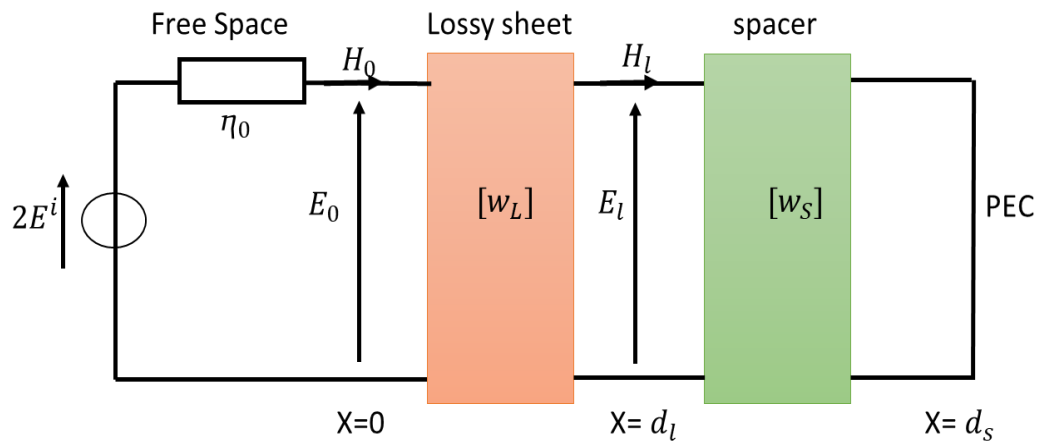


Figure 7: Transmission matrix representation

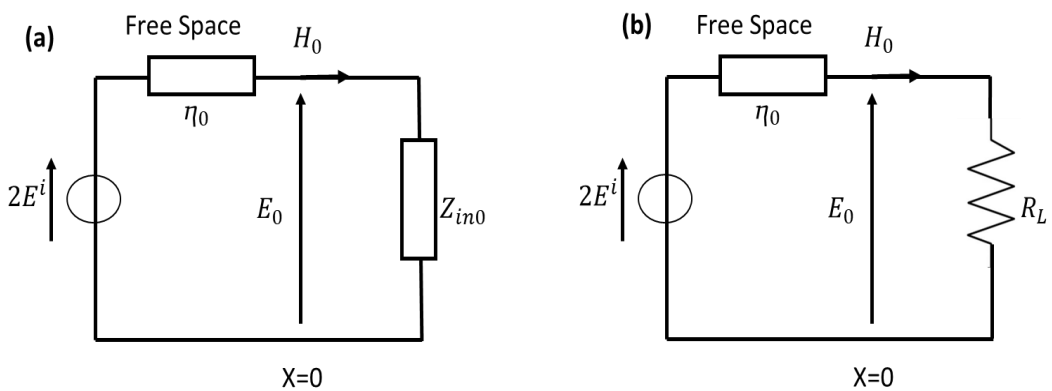


Figure 8: Equivalent circuit

Figure 7 shows the characterized salisbury screen by input to output transmission matrixes of lossy layer [ $w_L$ ] and spacer layer [ $w_S$ ]. The coefficients are given by [28]

$$w_{L11} = w_{L22} = \cosh(j\omega d_l c_0^{-1} \sqrt{\epsilon_l}) \quad (9)$$

$$w_{L12} = -\eta_0 \sinh(j\omega d_l c_0^{-1} \sqrt{\epsilon_l}) / \sqrt{\epsilon_l} \quad (10)$$

$$w_{L21} = -\epsilon_l \sinh(j\omega d_l c_0^{-1} \sqrt{\epsilon_l}) / \sqrt{\eta_0} \quad (11)$$

Here  $\omega = 2\pi f$ ,  $c_0 = 3 \cdot 10^8$  is the speed of light,  $\epsilon_l$  is the relative effective complex permittivity of the lossy sheet.  $\eta_0 = 377 \text{ Ohm}$  is the free space impedance.  $d_l$ , thickness of lossy layer. Similarly, derive the coefficients of transmission matrix [ $w_S$ ] as,

$$w_{S11} = \phi_{S22} = \cosh(j\omega d_s c_0^{-1} \sqrt{\epsilon_s}) \quad (12)$$

$$w_{S12} = -\eta_0 \sinh(j\omega d_s c_0^{-1} \sqrt{\epsilon_s}) / \sqrt{\epsilon_s} \quad (13)$$

$$w_{S21} = -\epsilon_s \sinh(j\omega d_s c_0^{-1} \sqrt{\epsilon_s}) / \sqrt{\eta_0} \quad (14)$$

$\epsilon_s$  is the relative effective complex permittivity of spacer and  $d_s$ , thickness of spacer.

Then the reflected electric field  $E^r$  is obtained by,

$$E^r = E_0 - E^i \quad (15)$$

Where  $E_0$  is the total transmitted field, by considering the Figure 8(a)  $E_0$  can be calculated as,

$$E_0 = \frac{2E^i Z_{in0}}{Z_{in0} + \eta_0} \quad (16)$$

$Z_{in0}$  is the input impedance of the system given by,

$$Z_{in0} = \frac{w_{L11} w_{S12} + w_{L12} w_{S11}}{w_{L21} w_{S12} + w_{L11} w_{S11}} \quad (17)$$

So, the reflection coefficient can be calculated as

$$R = \frac{|Z_{in0} - \eta_0|}{|Z_{in0} + \eta_0|} \quad (18)$$

By the theory of Salisbury screen, the lossy sheet is electrically thin and purely resistive, results in  $w_{L11} \approx 1, w_{L21} \approx \sigma_l d_l$ ,  $\sigma_L$  conductivity of the lossy layer. This implies

$$Z_{in0} = R_L \quad (19)$$

By combining (17) and (19), the minimum frequency at  $f_r$  is obtained, where  $R=0$  from Figure 8(b).  $R_L = (\sigma_l d_l)^{-1}$  is the sheet resistance of the lossy layer. Then  $d_l$

$$\sigma_l d_l = \frac{1}{\eta_0} \quad (20)$$

$$d_l = \frac{1}{\eta_0 \sigma_l} \quad (21)$$

For the two-layer absorber study the lossy layer thickness is found by Equation (21) and spacer thickness is varied to get the minimum reflection loss at the desired frequency.

## 2.1 Multiple Reflection Method

The multiple reflection method concept is to represent the wave reflected or transmitted from a complete layer as a sum of waves multiply reflected from individual layer interfaces. The method is well-known for a single layer sandwiched between two semi-infinite media. Figure 9 illustrates the multiple reflections in a single layer where, mediums with real dielectric permittivity  $\epsilon_0$  and real dielectric permittivity  $\epsilon_f$  on either side of the material with permittivity  $\epsilon_1$ .

A superposition of waves may be used to describe the wave reflected from a stack of layers: a) the wave reflecting from the interface  $\epsilon_0/\epsilon_1$ ; b) the wave transmitting

through the interface  $\epsilon_0/\epsilon_1$ , then passing through the layer, reflecting from the interface  $\epsilon_0=\epsilon_f$  passing through the layer once more and leaving the layer through the interface  $\epsilon_0=\epsilon_1$  and continuing this procedure, Thus the total reflection  $R_1$  can be obtained by summing up all the reflections.

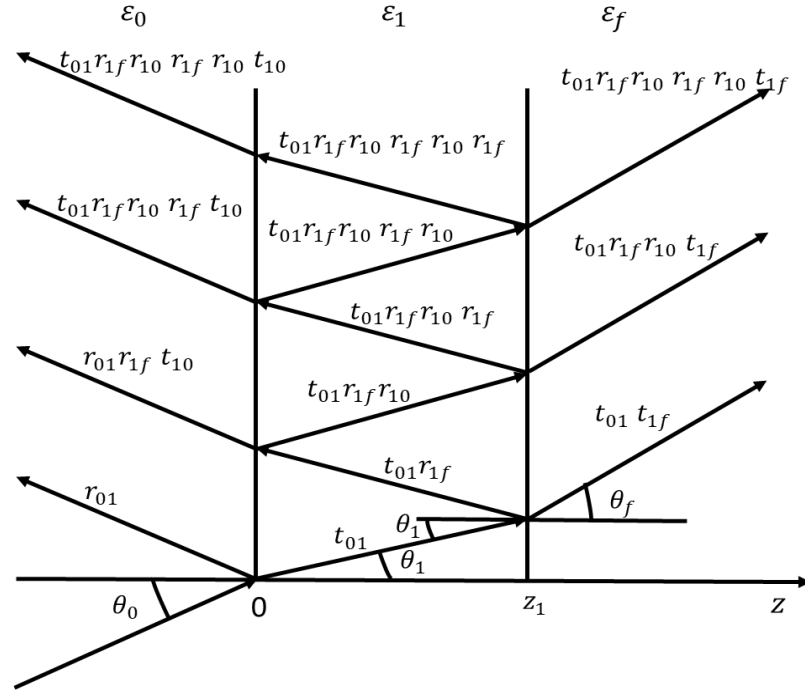


Figure 9: Multiple reflection in one layer

$$\begin{aligned}
 R_1 = & r_{01} + t_{01} \exp(ik_{1z}d_1) r_{1f} \exp(ik_{1z}d_1) t_{10} \\
 & + t_{01} \exp(ik_{1z}d_1) r_{1f} \exp(ik_{1z}d_1) r_{10} \exp(ik_{1z}d_1) r_{1f} \exp(ik_{1z}d_1) t_{10} \\
 & + \dots \quad (22)
 \end{aligned}$$

$k_{1z}$  is the wave vector of the incident wave in the medium  $\epsilon_1$  along the z-axis can be obtained by Equation (23)

$$k_{1z} = \pm \frac{\omega}{c} \sqrt{[(\epsilon'_1 + i\epsilon''_1) - \epsilon_0 \sin^2 \theta_0]} \quad (23)$$

$r_{01}$  is the wave reflected from the interface  $\varepsilon_0/\varepsilon_1$ ,  $t_{01}$  the wave penetrates through the interface  $\varepsilon_0/\varepsilon_1$ ,  $d_1$  is the thickness of the layer. Equation (22) continuous as an infinite geometric series, thus sum up to get a simplified equation as

$$R_1 = r_{01} + \frac{t_{01}t_{10}r_{1f} \exp(2ik_{1z}d_1)}{1 + r_{01}r_{1f} \exp(2ik_{1z}d_1)} = \frac{r_{01} + r_{1f} \exp(2ik_{1z}d_1)}{1 + r_{01}r_{1f} \exp(2ik_{1z}d_1)} \quad (24)[29]$$

For a two-layer material, the multiple reflection calculation is so tedious due to the complications in the internal reflection summation, as shown in Figure 10. Therefore, adopted the recursive calculation of the reflection coefficient, here finding the reflection coefficients for each interface by adding the internal reflections from the next interface, for example  $R_1$  is the total reflection coefficient from the interface  $\varepsilon_0/\varepsilon_1$  between the first layer and all other  $n - 1$  layers as done above obtain as.

$$R_n = r_{01} + \frac{t_{01}t_{10}r_1 \exp(2ik_{1z}d_1)}{1 + r_{01}r_1 \exp(2ik_{1z}d_1)} \quad (25)$$

Similarly, the wave reflected from the interface  $\varepsilon_0/\varepsilon_1$  is the sum of the waves reflected from the  $\varepsilon_2/\varepsilon_3$

$$r_1 = r_{12} + \frac{t_{12}t_{21}r_2 \exp(2ik_{2z}d_2)}{1 + r_{12}r_2 \exp(2ik_{2z}d_2)} \quad (26)$$

Thus, by generalizing this method, helps to find the total reflection coefficient for any arbitrary number of layers. For an  $\varepsilon_j/\varepsilon_{j+1}$  interface,

$$r_j = r_{j,j+1} + \frac{t_{j,j+1}t_{j+1,j}r_{j+1} \exp(2ik_{j+1,z}d_{j+1})}{1 + r_{j,j+1}r_{j+1} \exp(2ik_{j+1,z}d_{j+1})} \quad (27)$$

By using this equation, recursively can obtain the reflection coefficient for any number of layers. It's very useful for transverse electric and magnetic waves. This method is used in our study for the calculation of the reflection coefficient for double layer.

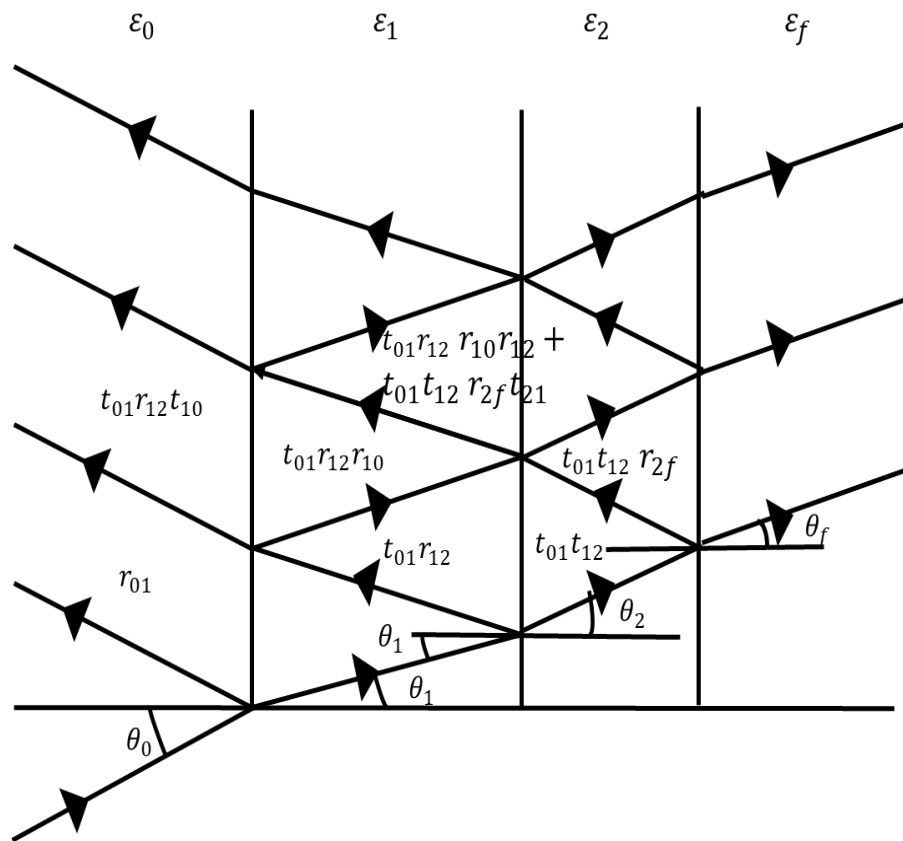


Figure 10: Multiple reflection in two layers

### Chapter 3: Materials and Morphological Study

This chapter discusses the samples used for this study; totally 14 cylindrical samples are used, which includes PU 0 Wt.%, 1 Wt.%, 5 Wt.%, 8 Wt.% and 10 Wt.% CNT with PU samples and 5 Wt.% (weight percentage) CNT functionalized with 5%, 10%, and 20% of Cobalt oxide (Co oxide), Iron oxide (Fe oxide) and Cobalt oxide (CoFe oxide) samples.

The Samples used in the study are purchased e from Nanocyl Company in Belgium. MWCNT used in the composite material has an inner diameter between 5-12 nm, and outer diameter varies from 30-50 nm. Figure 11 shows the SEM (scanning electron microscopy) image of the CNT in the composite.

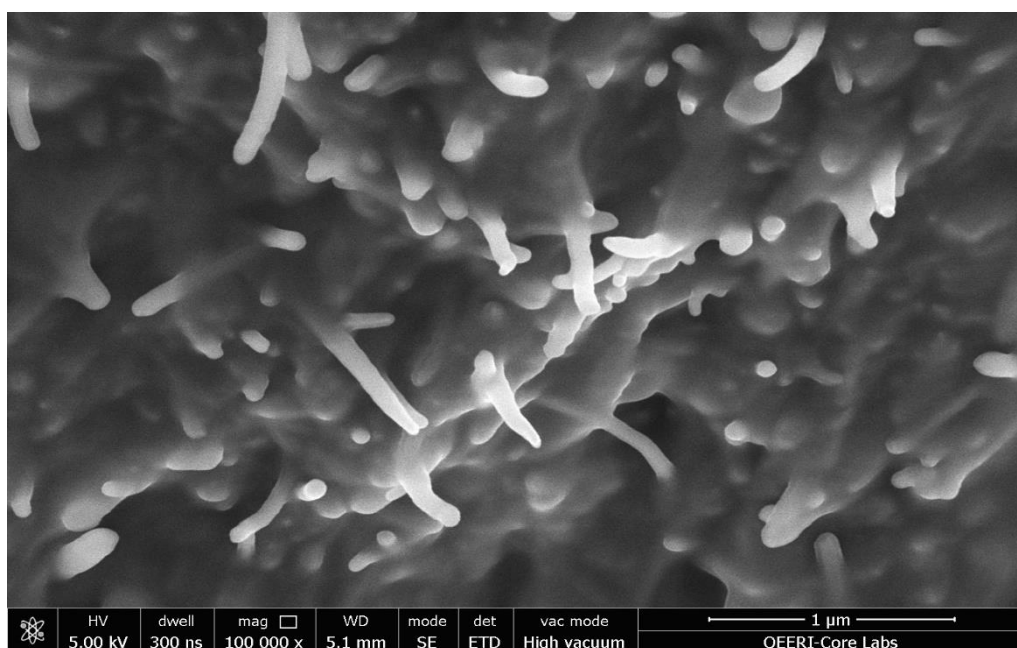


Figure 11: SEM image of CNT

The PU-CNT samples were made using various carbon nanotube weight percent (1%, -10 Wt.% CNT) are shown in Figure 12.

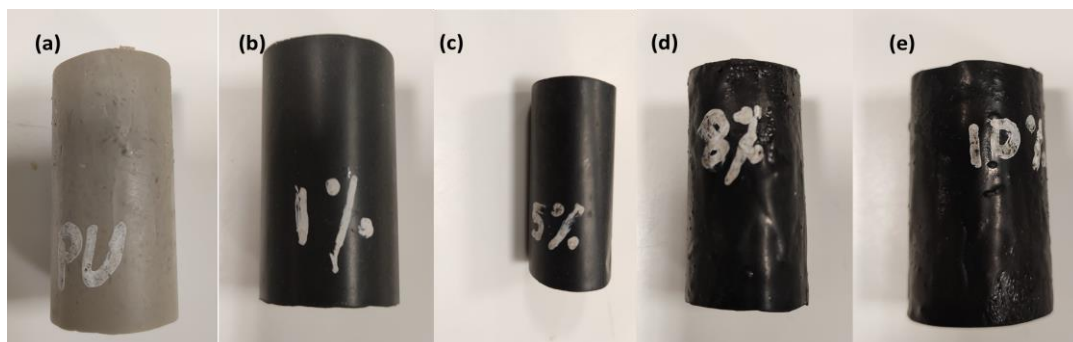


Figure 12: Samples with PU and different Wt.% of CNT (a) PU alone (b) PU + 1% CNT (c) PU + 5% CNT (d) PU + 8% CNT

The morphology of the nanoparticle is studied through the Scanning Electron Microscope (SEM), Transmission electron microscopy (TEM), and elemental mapping of the nanoparticles. Figure 13 depicts SEM image of PU impregnated with surface decorated MWCNTs. The image demonstrates a uniform distribution of the MWCNTs in the PU matrix.

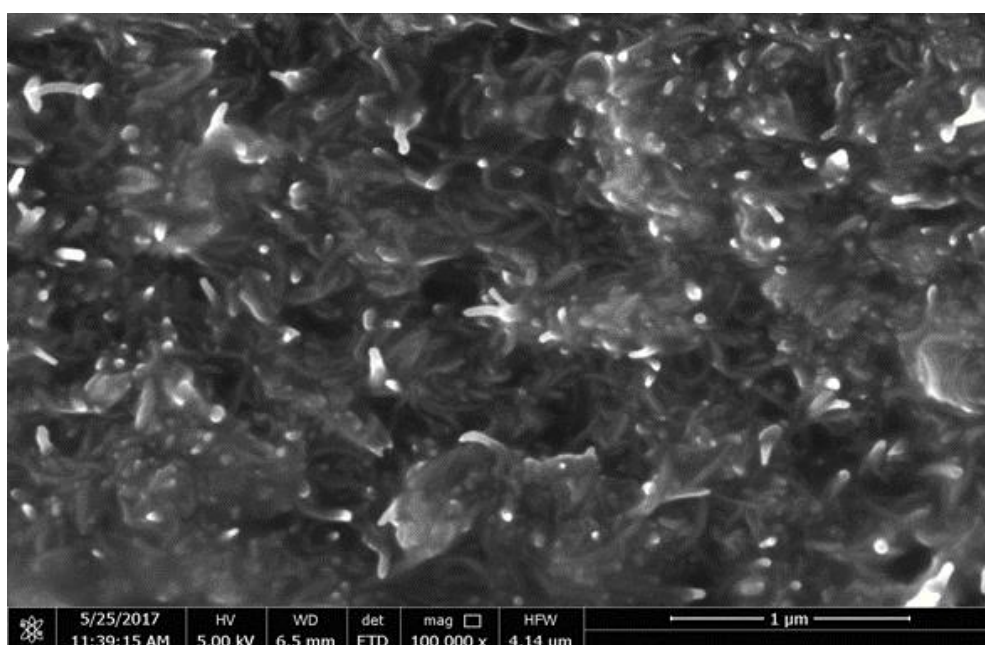


Figure 13: SEM of MWCNT in PU matrix



### 3.1 Functionalized CNT

Magnetic nanoparticles are added within or outside the CNT during functionalization. This procedure is normally carried out with a small number of nanoparticles. This condition is imposed so that there is no considerable magnetic loss in the composite. For functionalization of CNT, the magnetic nanoparticles are adsorbed into the external surface than the insertion to the CNT. Functional group insertion to the CNT has a better dielectric property, but this process is difficult and expensive, so the functionalization is carried out on the external surface. Figure 14(a), (b), and (c) shows the SEM image of cobalt iron oxide nanoparticles with a different magnification of 1000X, 50KX, and 600KX respectively. Table 3 describes the elements that present in the sample at the selected areas as shown in Figure 14(d) with their weight percent; samples contain C, O, Co, with the impurities like Cl, P, and Ni. Figure 15 depicts the TEM image of the cobalt iron oxide nanoparticles with CNT; the morphology of the cobalt nanoparticles depicts a rod shape with a size of about 5 nm in length and 2 nm in diameter. The iron nanoparticles decorating the MWCNTs have spherical morphology with average diameter of 5 nm. The elemental mapping of the individual particles of C, Co, Fe, and O are shown in Figure 16. TEM, SEM, and elemental mapping confirm the formation of crystalline cobalt iron oxide nanoparticles.

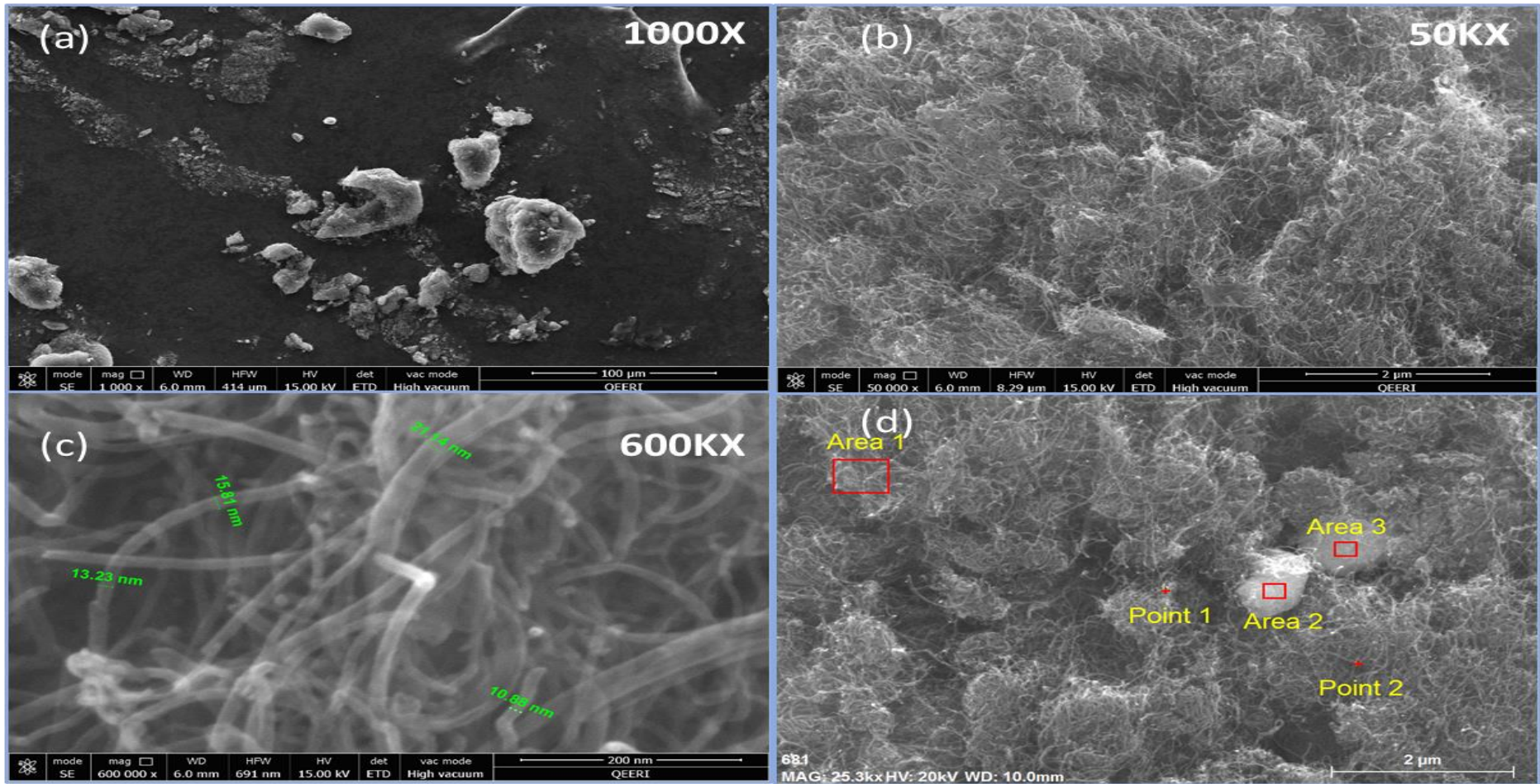


Figure 14: SEM images of CNT with cobalt-iron oxide nanoparticles with different magnifications (a) 1000X (b) 50 KX (c) 600 KX (d) Areas selected in the sample

Table 3: Elements present in the sample at different areas

|                | <b>Area 1</b> | <b>Area 2</b> | <b>Area 3</b> | <b>Point 1</b> | <b>Point 2</b> |
|----------------|---------------|---------------|---------------|----------------|----------------|
| <b>Element</b> | <b>Wt.%</b>   | <b>Wt.%</b>   | <b>Wt.%</b>   | <b>Wt.%</b>    | <b>Wt.%</b>    |
| <b>C</b>       | 92.40         | 92.75         | 78.29         | 92.27          | 92.60          |
| <b>O</b>       | 6.37          | 6.78          | 17.02         | 7.20           | 6.90           |
| <b>F</b>       | 0.06          | 0.00          | 0.00          | 0.04           | 0.02           |
| <b>Mg</b>      | 0.05          | 0.04          | 0.07          | 0.04           | 0.04           |
| <b>Al</b>      | 0.08          | 0.06          | 0.12          | 0.07           | 0.07           |
| <b>Si</b>      | 0.04          | 0.03          | 0.04          | 0.03           | 0.02           |
| <b>S</b>       | 0.01          | 0.01          | 0.00          | 0.02           | 0.02           |
| <b>Cl</b>      | 0.07          | 0.05          | 0.08          | 0.07           | 0.06           |
| <b>Ca</b>      | 0.00          | 0.01          | 0.05          | 0.01           | 0.00           |
| <b>Mn</b>      | 0.07          | 0.01          | 0.019         | 0.01           | 0.06           |
| <b>Fe</b>      | 0.50          | 0.08          | 2.71          | 0.10           | 0.08           |
| <b>Co</b>      | 0.34          | 0.16          | 1.43          | 0.15           | 0.13           |

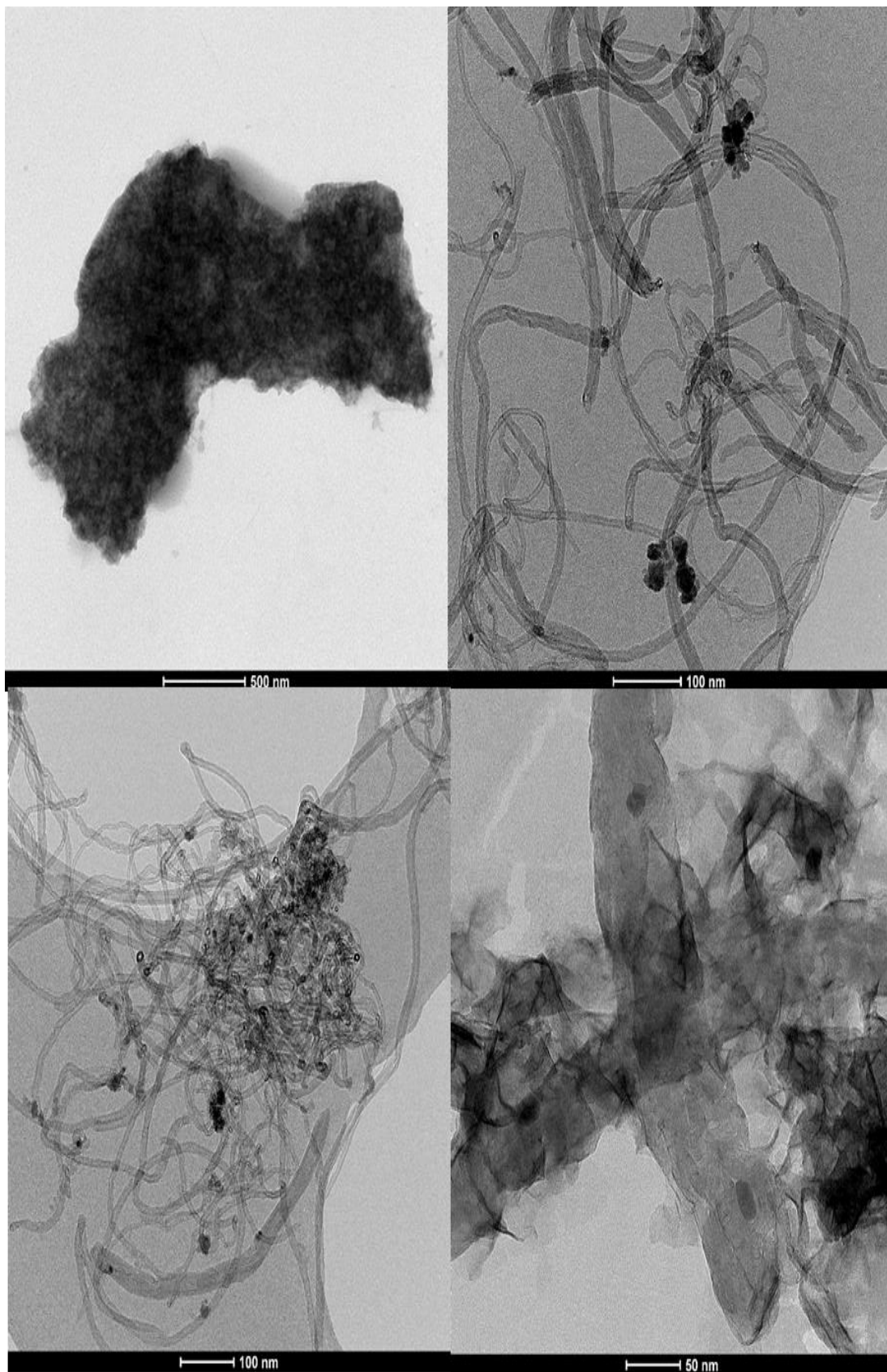


Figure 15: TEM images of CNT with cobalt-iron oxide nanoparticles

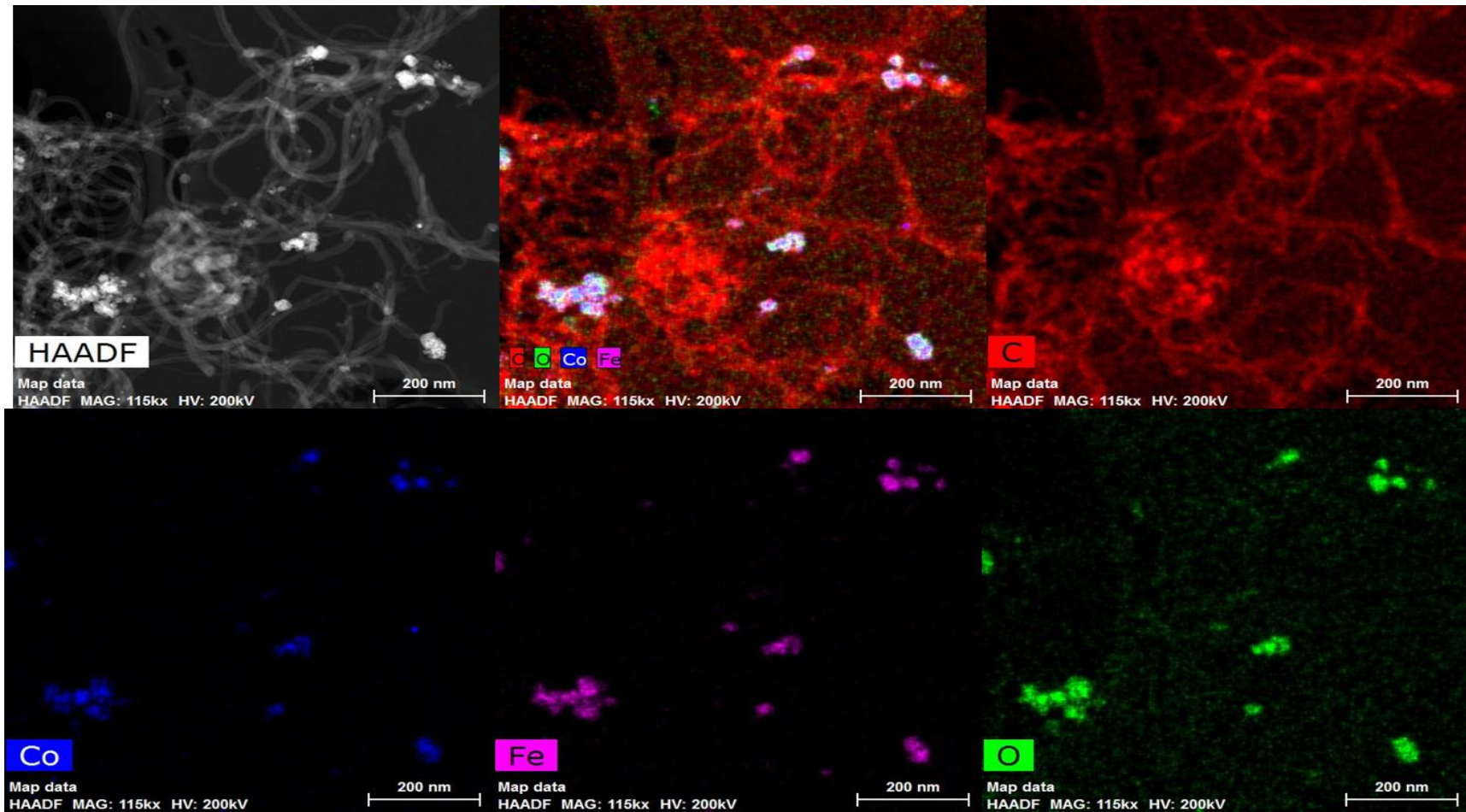


Figure 16: Elemental mapping of cobalt-iron oxide nanoparticle

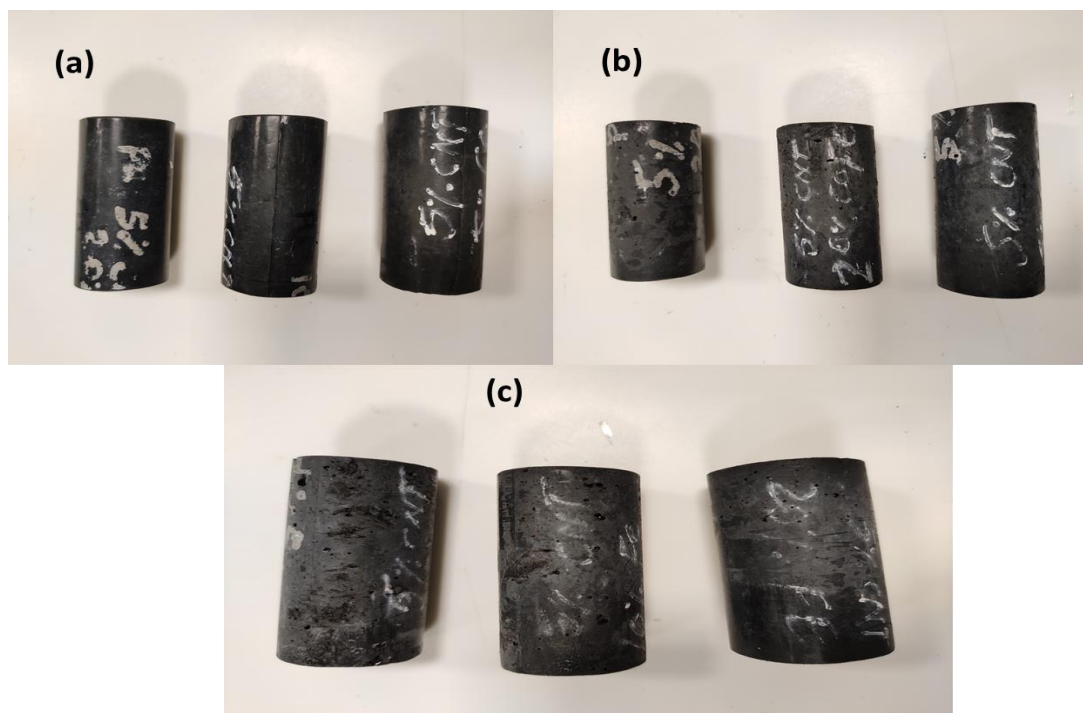


Figure 17: Functionalized CNT samples (a) PU + 5% CNT + xCo (b) PU + 5% CNT + xCoFe (c) PU + 5% CNT + xFe

The samples have a height of 4 inches and a diameter of 1 inch, as shown in Figure 17. The dielectric measurement was conducted at the two ends of the sample. Nonetheless, each sample was cut in half, and the measurements were done on 4 sides. The dielectric value measure was consistent at all 4 sides, this proves the homogeneity of the sample.

## Chapter 4: Measurement Techniques

The ability to measure an absorber's absorbing properties over the frequency band of interest is important. Different test methods are used to predict the absorption properties such as the wave-guide method [30], Free space method [31], and coaxial line method [32, 33]. An absorber's reflection coefficient is determined by the permittivity and permeability of its constituent materials. Measurement technique should have the ability to measure these parameters design efficient absorbers [34]. This work used the open-ended coaxial probe technique, the method has the benefit, not to rigidly fix the sample geometry to match the geometry of the sampling apparatus, the calibration process is simple and also the method can cover a wide range of frequency.

The open-ended coaxial probe is a section of the transmission line that has been cut off. By immersing the probe in a liquid or touching it to the flat face of solid material, the material is measured. As the fields at the probe end come into contact with the material, they "fringe" into the sample and changes the field. This method assumes sample the sample is a non-magnetic, isotropic, and homogeneous and has a flat surface for a solid sample. Because this technique assumes that interactions of the electromagnetic field with the non-contacting boundaries of the sample are not detectable by the probe, the sample must be dense enough and much larger than the diameter of the aperture of the open-ended coaxial line [35]. The system setup comprises a Vector Network Analyzer (VNA) (10 MHz to 70 GHz), DAK (Dielectric Assessment Kit) probe frequency range 200 MHz-50 GHz, ethernet cable, and computer. The connections are shown in the schematic diagram Figure 18 and the measurement setup arrangement used in our lab is shown in Figure 19.

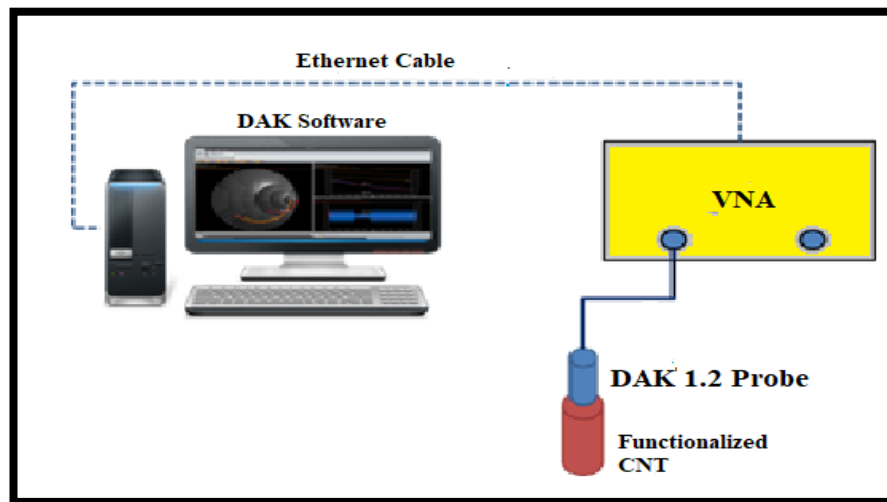


Figure 18: Schematic diagram of the measurement setup

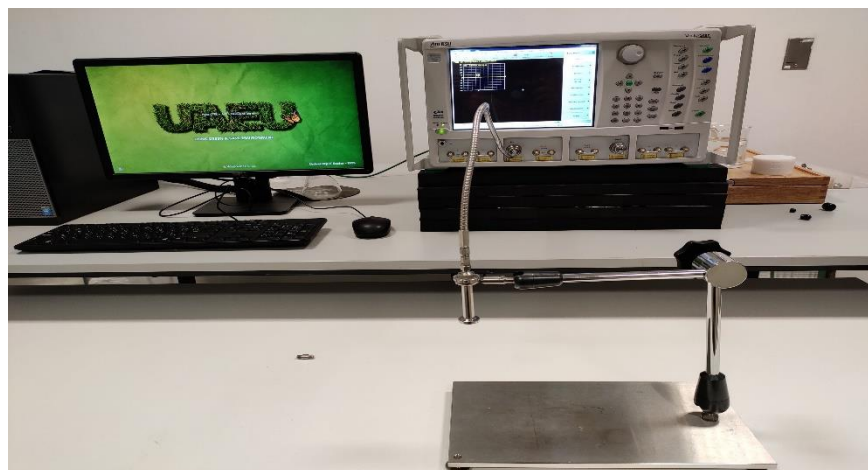


Figure 19: Measurement setup used in our lab

#### 4.1 Vector Network Analyzer and Scattering Parameters

A tuned receiver is the vector network analyzer. The microwave signal is transformed into the Intermediate frequency pass band. It's needed a reference to compare this signal to in order to determine its phase. When a signal's phase is 90 degrees, it differs from the reference signal by 90 degrees. There are two type of network analyzers are Scalar Network Analyzers (SNA) and vector Network Analyzers (VNA). Microwave signals are measured using SNAs, which transform



them to a DC voltage using a diode detector. This DC voltage is proportional to the incoming signal's magnitude. The detection method, on the other hand, ignores any details about the microwave signal's phase. While in VNA is needed access to both the magnitude and phase of a microwave signal [36]. This study used an Anritsu Vector Network Analyzer (VNA) of Vector Star MS4640B Series, it can measure broad range frequency from 70 KHz to 75 GHz as shown in Figure 20(b).

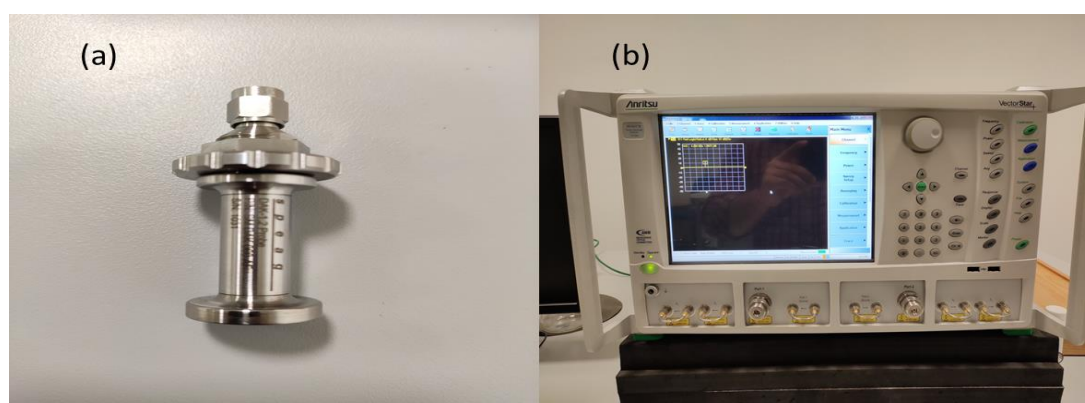


Figure 20: Instruments used (a) Speag DAK 1.2 probe (b) Anristu MS4647B VNA, 10 MHz to 70 GHz

The second characteristic of the VNA are it can measure the forward and reverse transmission. These can be called scattering parameters or ‘S’ parameters. Waves, rather than voltages or currents, are a simple way to define a network. This makes it easier to define reference planes. The definition in terms of incoming and outgoing waves has been added for practical purposes [37]. ‘S’ parameters describe the response of an N-port network to a signal. There are four ‘S’ parameters for a two-port network:  $S_{11}$ ,  $S_{12}$ ,  $S_{21}$ , and  $S_{22}$ , where the first subscript denotes the input port and the second subscript indicates the output port. The input reflection coefficient is  $S_{11}$ , the reverse transmission from port 2 to port 1 is  $S_{21}$ , the forward transmission from port 1 to port 2 is  $S_{12}$ , and the output reflection coefficient is  $S_{22}$ . The scattering matrix

is a mathematical term that fully explains how an electromagnetic wave propagates across a multi-port network. Figure 21 depicts the simple two-port network diagram.

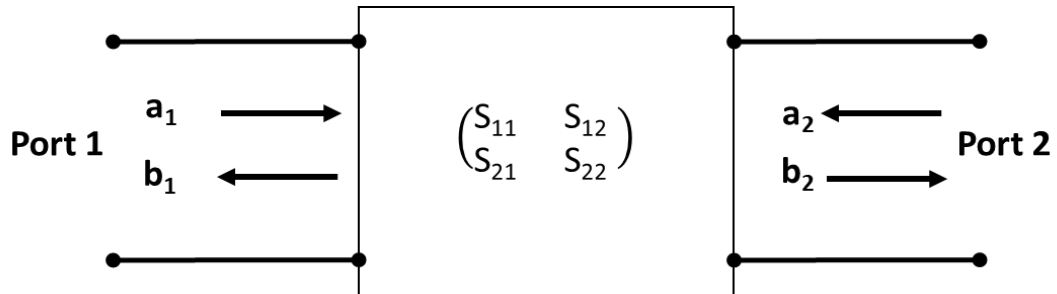


Figure 21: Schematic of a two-port network

From the Figure 21 the input to the port 1 are  $a_1$  and output is  $b_1$ , for port two  $a_2$  and  $b_2$  are the input and output respectively. Form a relation  $a$ ,  $b$  and 'S' in to matrix form as,

$$[b] = [s] * [a] \quad (28)$$

$$\begin{bmatrix} b_1 \\ b_2 \end{bmatrix} = \begin{bmatrix} S_{11} & S_{12} \\ S_{21} & S_{22} \end{bmatrix} * \begin{bmatrix} a_1 \\ a_2 \end{bmatrix} \quad (29)$$

Expressing the 's' parameters in a ratio form of  $a$  and  $b$  as,

$$S_{11} = \frac{b_1}{a_1}$$

$$S_{12} = \frac{b_1}{a_2}$$

$$S_{21} = \frac{b_2}{a_1}$$

$$S_{22} = \frac{b_2}{a_2}$$

Some of the properties of the  $n$ -port network are

- When  $S_{ij} = S_{ji}$  for all  $i$  and  $j$ ,  $n$ -port is reciprocal, the majority of passive components (resistors, capacitors, transformers, etc.) are reciprocal.

- If a two-port is reciprocal ( $S_{21} = S_{12}$ ) and the input and output reflection coefficients are equal ( $S_{22} = S_{11}$ ), it is said to be symmetric.
- If the S matrix is unitary then the N-port is passive and lossless.[37].

The permittivity and permeability of the material under test can be measured once the S-parameters of the coaxial sample holder with the samples have been determined. Using the S-parameters possible to measure the reflection coefficient (R), transmission coefficient (T) and absorption coefficient (A) [38]

$$T = |S_{12}|^2 = |S_{21}|^2 \quad (30)$$

$$R = |S_{11}|^2 = |S_{22}|^2 \quad (31)$$

$$A = I - R - T. \quad (32)$$

The probe DAK 1.2 as shown in Figure 20(a) developed by SPEAG.com is used to measure the frequency-dependent dielectric constant and it can be used for a wide frequency range from 5 – 50 GHz. Ethernet cable is connected between the VNA and the computer. The DAK software installed on the computer will extract the complex permittivity, permeability, tangent loss, and conductivity parameters from the ‘S’ parameter measurements by the VNA. This data can be used for the reflection loss calculations. The probe should be placed at an appropriate height, and the sample being examined is brought directly into contact with the probe. Ultimate care is taken to probe and coaxial cable movement once it is set, as dielectric measurements are very sensitive to the reflected signal.

## 4.2 Calibration

Calibration is a method of calculating systematic errors from measurements taken against established reference standards. The DAK has to be optimized for precise measurements; the calibration will normalize the magnitude and phase changes of the

probe and coaxial cable. There are two calibration methods available for the DAK system, Open, Short, and load (OSL) calibration and two loads (O-L<sub>1</sub>-L<sub>2</sub>) calibration.

Open calibration is carried out by exposing the probe to the open air, for short calibration a copper strip is connected to the probe using a connecting block. Then the load calibration is usually done by the deionized water, its dielectric properties are known. This work used a two-load calibration procedure for the calibration. In the two-load method, instead of short calibration another load of known dielectric properties is used, here the ethanol and teflon materials are used as the first and second load, respectively. The set-up for the calibration is shown in Figure 22.

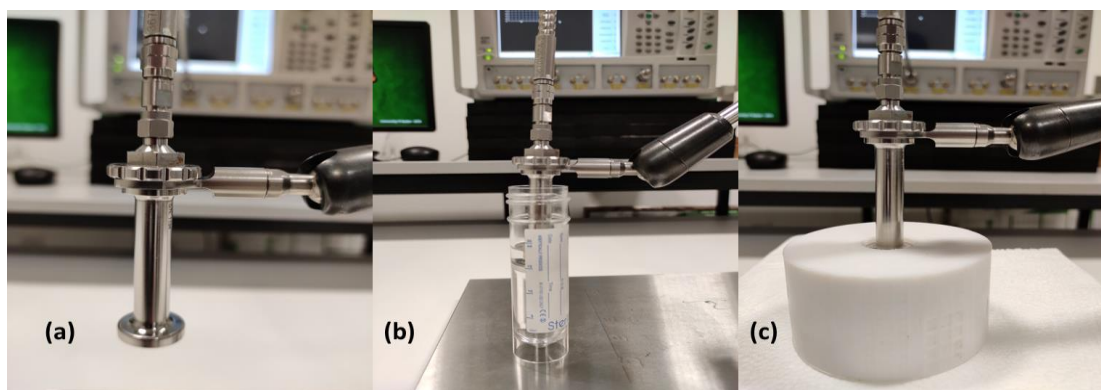


Figure 22: Calibration setup (a) Open (b) Ethanol as load 1 (c) Teflon as load 2

Figure 22(a) shows the open calibration where expose the probe in to the open space and check the smith chart on the DAK software follows the exact curve in the smith chart; then the open calibration is done. Figure 22(b) is the load 1 calibration using ethanol and the load 2 calibration using the solid teflon material (Figure 22c) and these materials parametric values are available on the DAK library. Once these calibrations are finished, again measures the material to check whether the material follows the same permittivity values available on the DAK material library. To study

the effectiveness of OSL and two loads calibration to measure the solid samples, analysis made based on the permittivity values obtained from the materials in the low and high frequency. For the measurement of materials DAK system provides two probes (1) Probe 3.5 can measure the frequency range from (200 MHz- 20 GHz) and (2) Probe 1.2 (5-50 GHz). Thus, frequency from (5-20 GHz) is a common range for both the probes, Hence, compared the solid (Teflon) measurement using two calibration methods and finalized that the two-load calibration with ethanol and teflon loads are the best option to measure the material in the (5-50 GHz) frequency range.

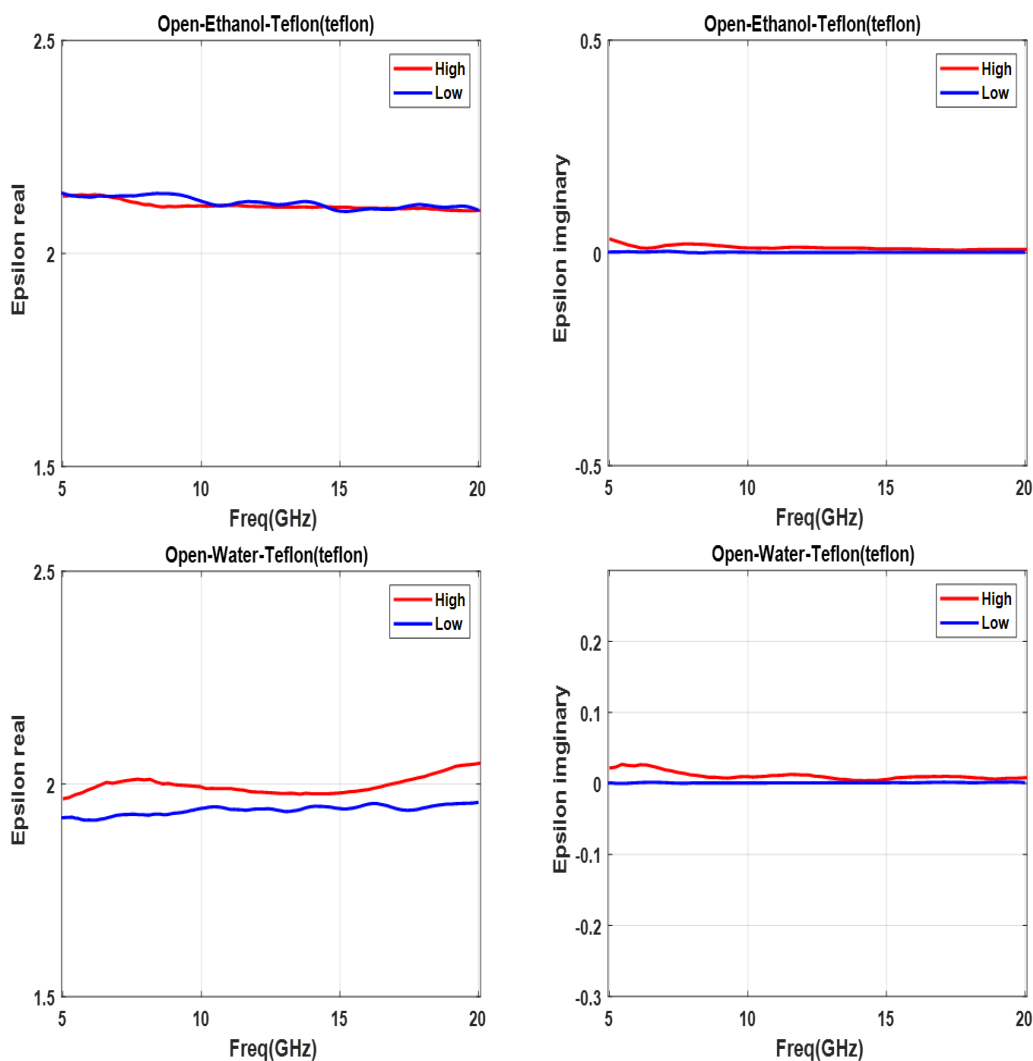


Figure 23: Measurement of teflon using O- $L_1$ - $L_2$  calibration with different loads

Figure 23 depicts the permittivity measurement of teflon in the high and low frequencies. The red color line denotes the high frequency using probe 1.2 and blue denotes the low-frequency measurement using 3.5 probe. Here used ethanol-teflon and water -teflon as the two loads for the two-load calibration and the measured sample is teflon (solid). So, by the evaluation understands that in the common frequency (5-20 GHz) ethanol- teflon load combination has the best similarities than another load combination.

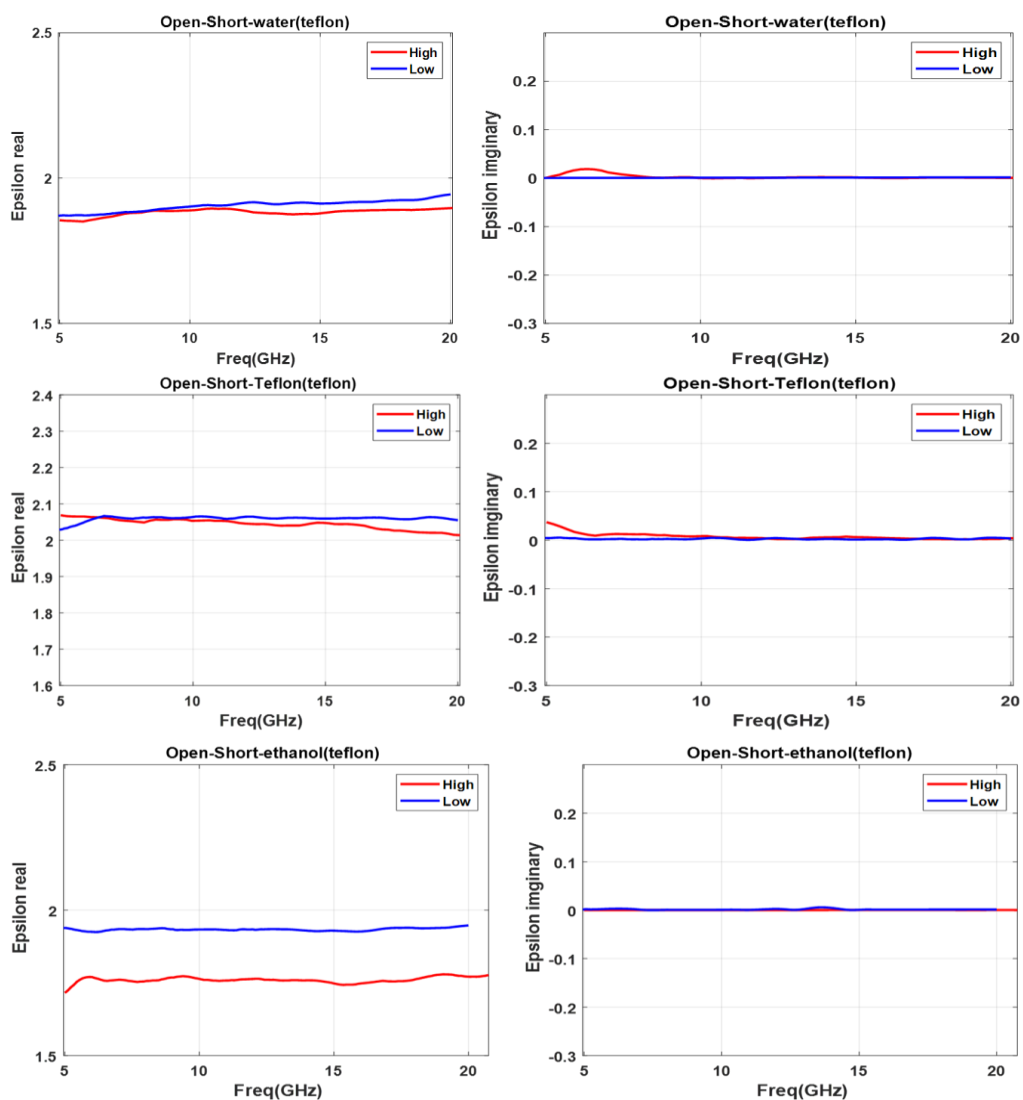


Figure 24: Measurement of teflon using OSL calibration with different loads

Similarly, the OSL calibration method measured the same material teflon using ethanol, water, and teflon as load references, as shown in Figure 24. But the results show that the real permittivity value is same as that of the two-load calibration. Also, for the short calibration is critical to get the exact central position of the smith chart in the high frequencies, thus from these results, consider the two-load calibration with ethanol-teflon is fine for the solid sample measurement. After the calibration, measurements can be completed. In each measurement of the sample, it's good to clean the probe with ethanol, and the measured data can be stored in-to the buffers available in the DAK software, and it can be exported into the disk. Using these obtained measurements, analyze the material's characteristics.

## Chapter 5: Measurements and Characterization of Samples

In this study, 3 sets of samples are measured in each set has three samples of functionalization at different concentration levels, along with PU and PU with 5% CNT composites. Functionalized samples consist of 5 weight percentage (wt. %) of CNT and 5%, 10%, and 20% concentration of functionalizing metal nanoparticles (Co, Fe, and CoFe), Thus set 1 consists of PU + 5% CNT with 5% Co, PU + 5% CNT with 10% Co and PU + 5% CNT with 20% Co, second sets of PU + 5% CNT with 5% CoFe, PU + 5% CNT with 10% CoFe and PU + 5% CNT with 20% CoFe, finally, the third sets consist of PU + 5% CNT with 5% Fe, PU + 5% CNT with 10% Fe and PU + 5% CNT with 20% Fe.

### 5.1 Permittivity Measurements

For an efficient absorber light-weight is an important criterion, especially for the stealth technology; thus, the selection of CNT concentration is critical to maintaining the sample weight. Figure 25 depicts the real and imaginary parts of the permittivity and tangent loss for the 0 Wt. %, 5 Wt. %, 8 Wt. %, and 10 Wt. % of CNT in the PU matrix. As the concentration of CNT increases the real and imaginary of permittivity value are increasing, a high value of 6.5 is obtained for the 10 Wt. % CNT but moving towards the high frequency, the real part of the permittivity is almost constant and imaginary part of permittivity are reducing to lower values, even near to zero for the imaginary values, while in the real part is almost constant in high frequencies. Considering the weight and the permittivity value 5 Wt. % selected for the functionalization of CNT to obtain an efficient absorber.



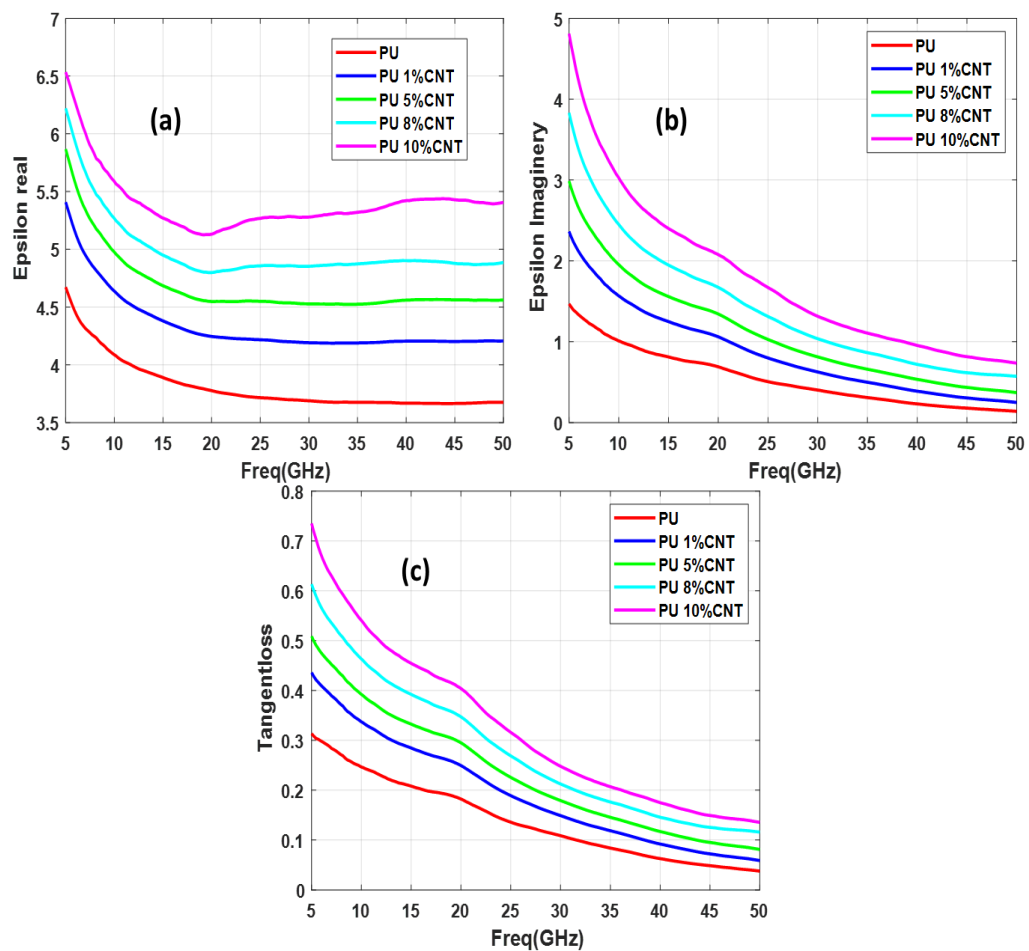


Figure 25: PU with different concentration of CNT a) Epsilon real (b) Epsilon imaginary (c) Tangent loss for 5-50 GHz frequency

Figures 26-28 depicts the effect of functionalization on the permittivity of the PU 5% CNT composite. The curves have a wavy shape or non-monotonous behavior, with several minima's and maxima's. SWCNT/cross-linked polyurethane composites have already shown this trend, the real part of the dielectric constant increases as the concentration of the functionalizing element (Co, CoFe, and Fe) increases [18]. When these three functionalized samples are compared, it can be shown that CoFe and Fe functionalized composite have the identical curve pattern for the real sections of the permittivity. The real portion of permittivity has a high value in the lower frequencies, then falls and starts to increase again at 32 GHz. Similarly, the imaginary part of

permittivity has a large value in the lower frequencies, while permittivity lowers near zero in the higher frequencies, which describes energy absorbed inside the absorber. The contributions of various types of polarizations such as inter-facial, atomic, orientation, and electronic polarizations play a major role in a material's complex permittivity properties. Percolation effect, CNT fiber aspect ratio, nanoparticle size, and other elemental characteristics all have a significant impact on the complex permittivity properties.

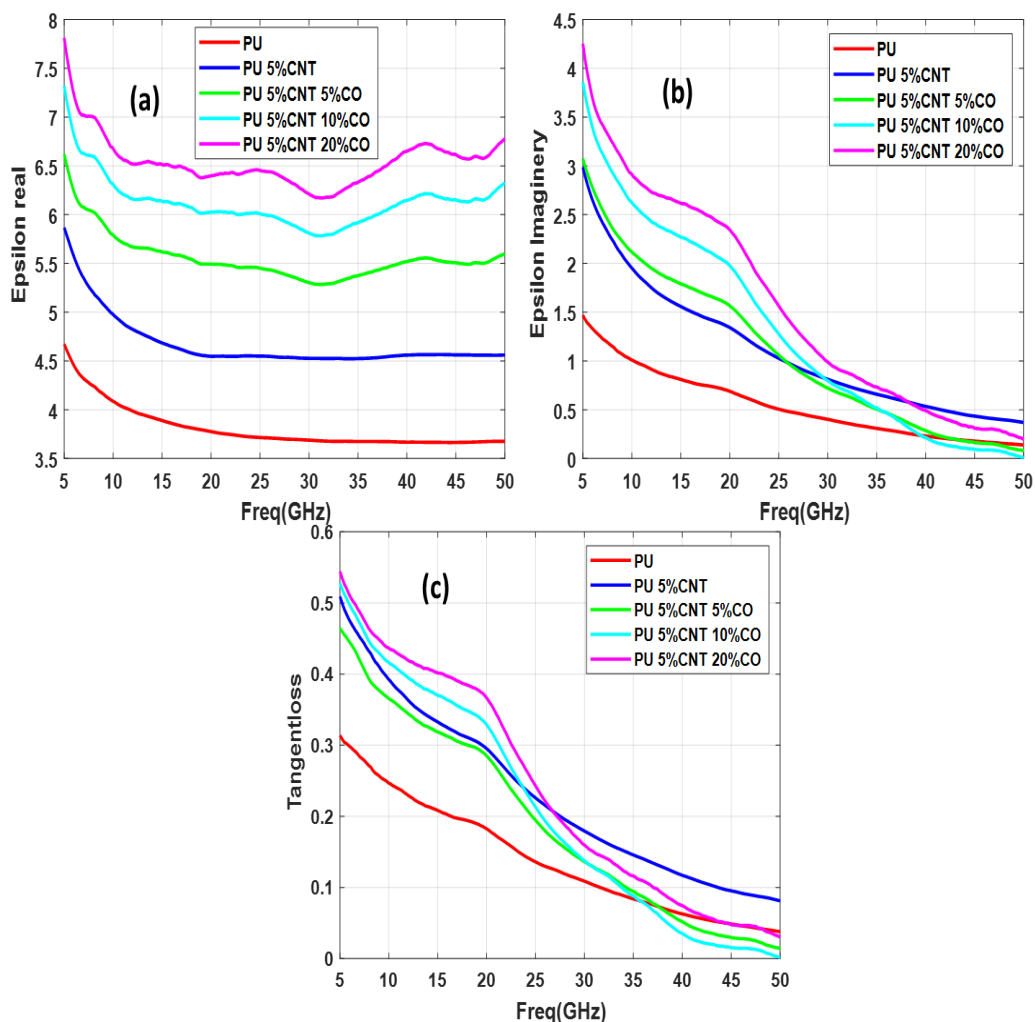


Figure 26: Functionalized with different concentration of Co a) Epsilon real (b) Epsilon imaginary (c) Tangent loss for 5-50 GHz frequency

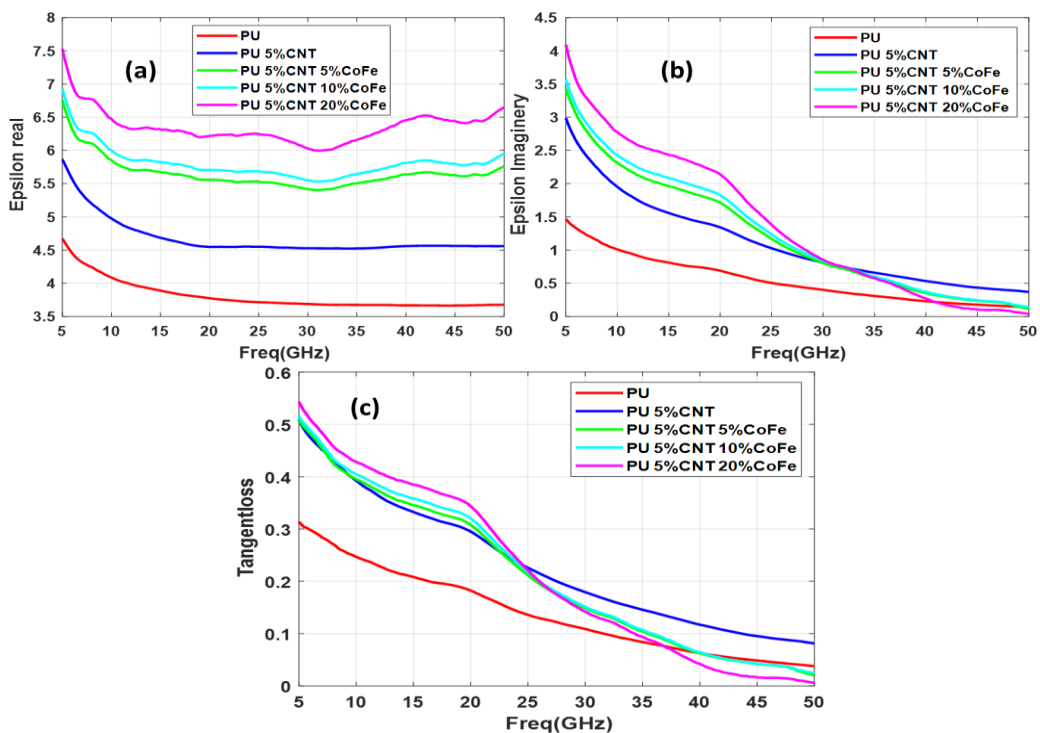


Figure 27: Functionalized with different concentration of CoFe a) Epsilon real (b) Epsilon imaginary (c) Tangent loss for 5-50 GHz frequency

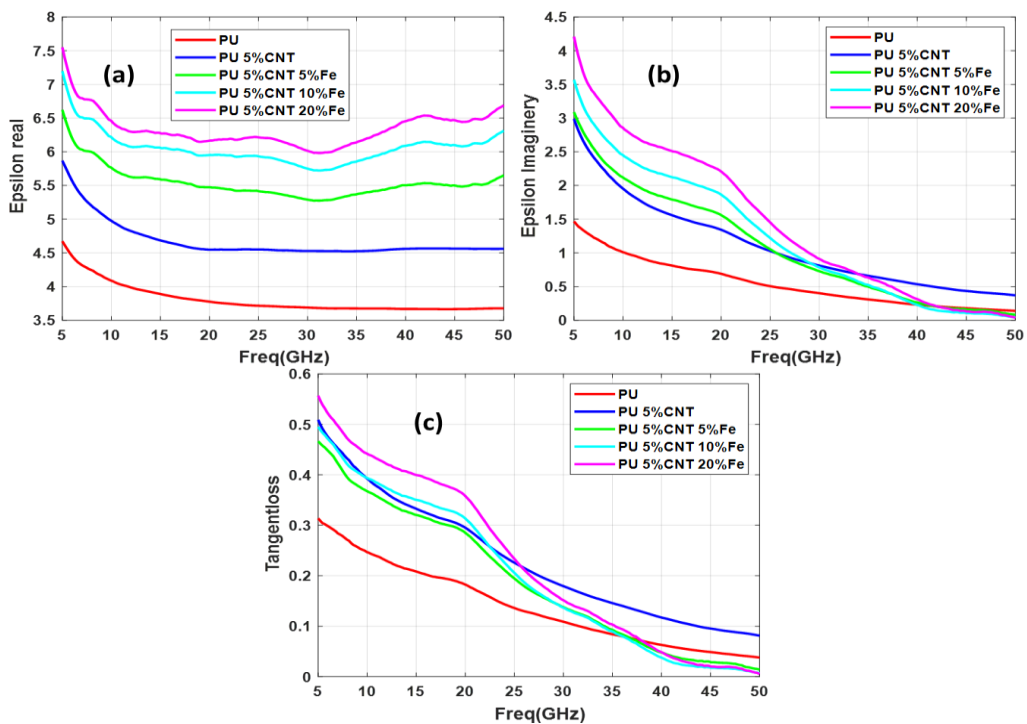


Figure 28: Functionalized with different concentration of Fe (a) Epsilon real (b) Epsilon imaginary (c) Tangent loss for 5-50 GHz frequency

## 5.2 Attenuation Calculation

A suitable matching EM impedance situation can reduce the incident microwave's reflectance to almost zero. The attenuation factor  $e^{-\alpha d}$ , governs the attenuation of electromagnetic energy inside the sample by lowering the wave amplitude in relation to the traveling distance  $d$ . The attenuation constant ( $\alpha$ ) is also influenced by the material's electric and magnetic properties and defined by

$$\alpha = \omega \left\{ \frac{\mu\epsilon}{2} \left[ 1 + \left( \frac{\sigma}{\omega\epsilon} \right)^2 \right]^{1/2} - 1 \right\}^{1/2} \quad (33)$$

Figure 29 shows the attenuation factor for PU, PU 5% CNT, PU + 5 % CNT+ (5%, 10%, and 20%) CoFe samples against varying thickness at center frequencies of C band (6 GHz), X band (10 GHz), Ku band (15.5 GHz), and K band (22.5 GHz). As the concentration of functionalizing element is increased the curve moves towards the lower thickness and the wave amplitude decreases to a factor of  $e^{-1}$  (about 37% of the original values) indicates by the dotted lines. The sample PU takes much thickness to attenuate the wave, as the concentration of functionalizing element increased, decreasing attenuation distance. The same trend is followed for the samples with Co and Fe functionalizing elements as added in the Appendix 2. Impending the metal oxide particles improved the absorption efficiency with reduced thickness, this will benefit for the aeronautical application.

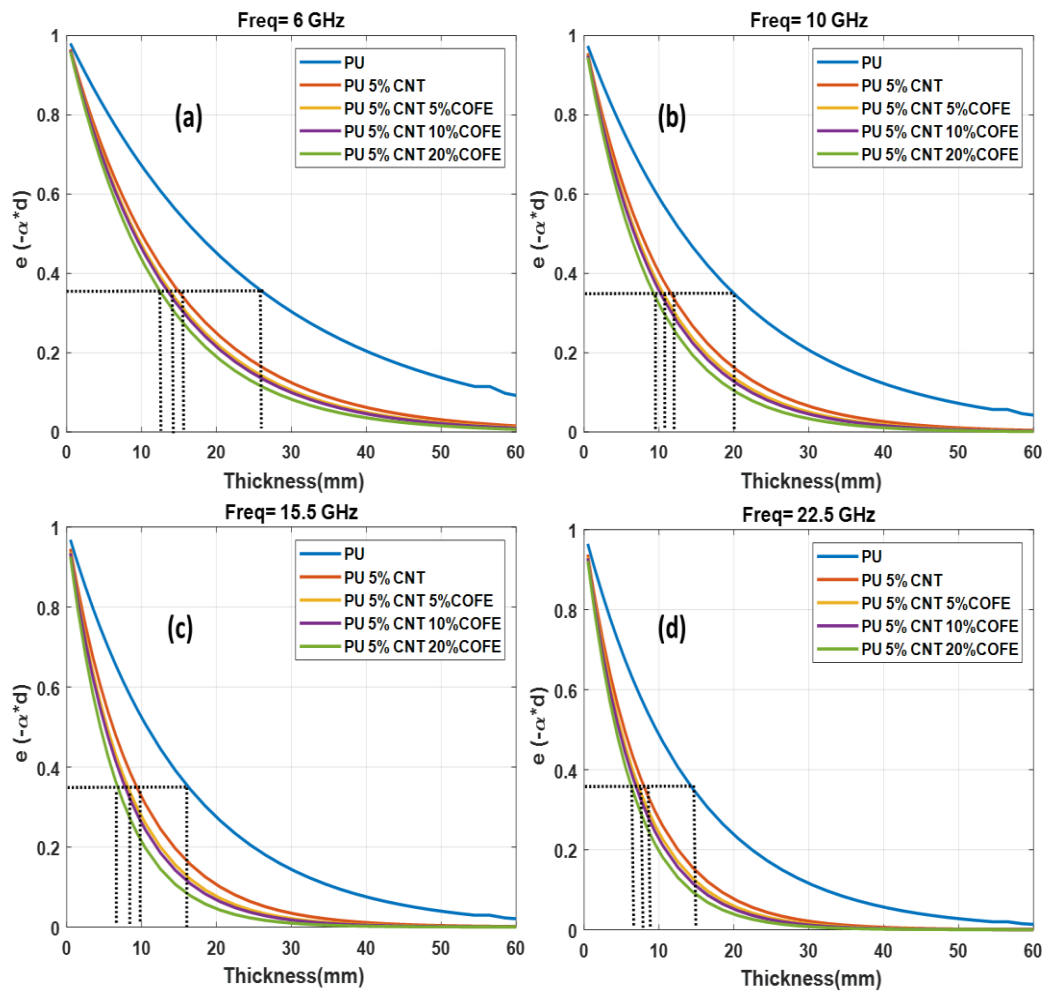


Figure 29: Attenuation factor for PU, PU 5% CNT, PU + 5% CNT + (5%, 10%, 20%) CoFe at different center frequencies (a) 6 GHz (b) 10 GHz (c) 15.5 GHz (d) 22.5 GHz

### 5.3 Impedance Calculation

The impedance matching between free space and the material-air interface  $Z_{in} = Z_0$  should be achieved for an ideal microwave absorbing material, as stated in chapter 2.  $Z_{in}$  can be computed using Equation 7. Figure 30 shows impedance patterns of the functionalized samples with pure PU and PU with 5% CNT. For all the samples follow almost the same pattern as the frequency increases, the impedance increases and follows a constant line. Also, the impedance decreased by reducing the Wt. % of the functionalizing element. Here the pure PU has the highest impedance value near

200 Ohm. To attain the impedance matching, the thickness is varied to match the free space impedance of 377 Ohm to the material's impedance.

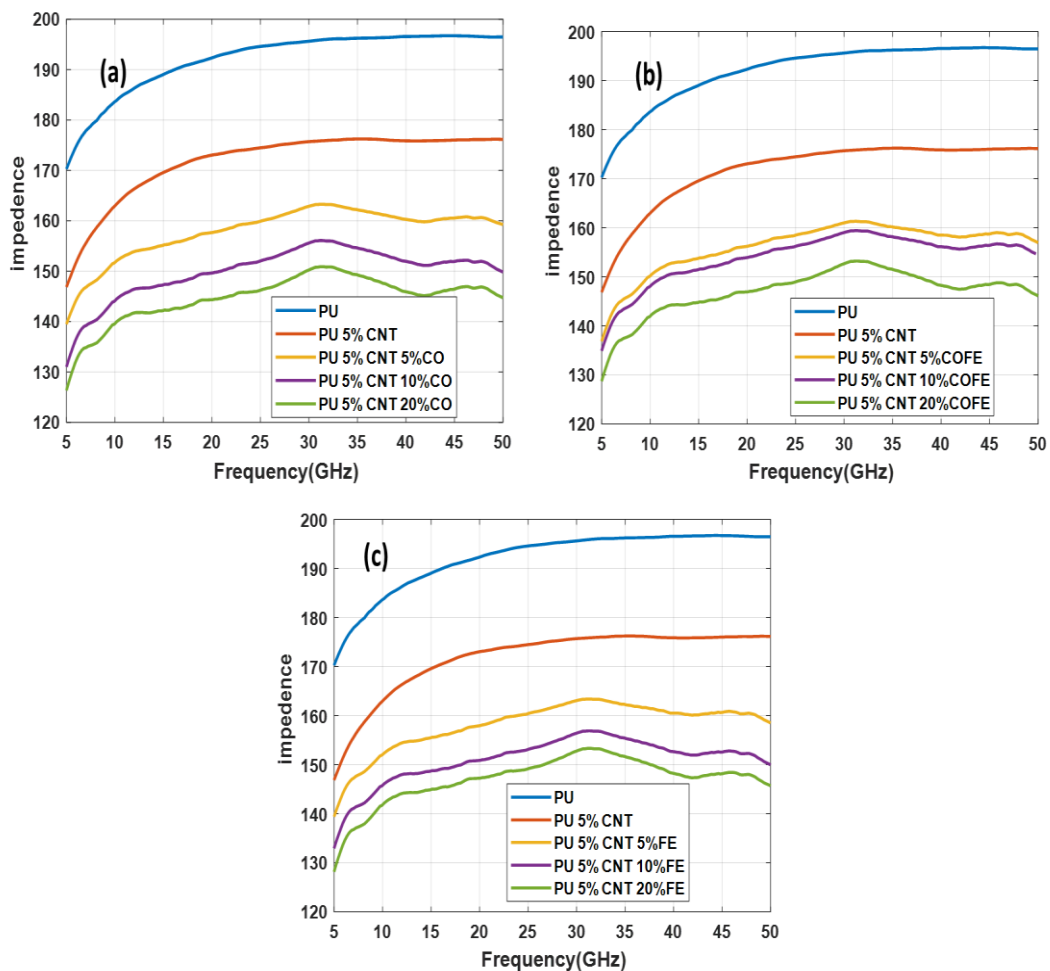


Figure 30: Comparison of impedance measurements for functionalized samples with PU and PU + 5% CNT

## Chapter 6: Reflection Loss Study of the Samples

This section discusses the reflection loss of the nine samples developed with the different concentrations (5%, 10%, and 20%) of the CNT composites with metal oxide (Co, CoFe, and Fe) functionalization. The reflection loss is calculated in the spectral range from 5-50 GHz, and in all the samples there are several minima of reflection are observed in the selected frequency range.

### 6.1 Reflection Loss for One-layer composite

The code in Appendix 1 is used to determine reflection loss for each sample using MATLAB. The single-layer composite using a metal sheet was calculated here. As a result, the wave is fully reflected back to the sample. The reflection loss for pure PU and PU mixed with 5% CNT at various thicknesses is shown in Figure 31(a and b). When using pure PU, the majority of the waves are reflected from the sample; however, when using PU with 5% CNT, the reflection is effectively reduced. With a small thickness of 4.5 mm, it shows multiple resonant at 7.5 GHz, 24 GHz, and 39.5 GHz. At 24 GHz frequency has a minima of -31 dB.

Functionalization of CNT with 5%, 10%, and 20% of Co nanomaterial are shown in Figure 32(a)-(c) with varying thickness of samples ranging from (0.5 mm-4.5 mm), the composite shows superior reflection values with small thickness in 5% as the concentration increases. With 1.5 mm thickness, Co composite has no effect on the reflection value, but when concentration is increased to 20%, the reflection value drops to -17 dB. The composite with a 20% Co content and a thickness of 3.5 mm achieves a minimum reflection of -43 dB. More performances of the samples are explained in the Table 4.

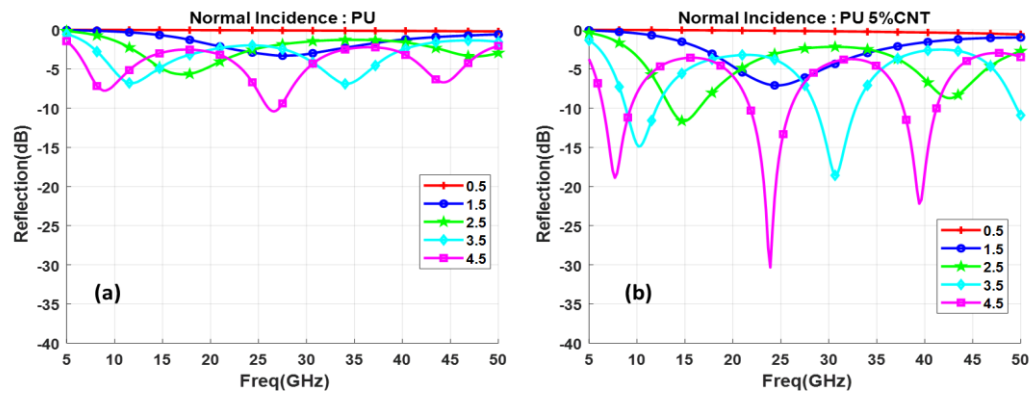


Figure 31: Reflection loss without functionalization (a) PU (b) PU 5% CNT at different thickness

Sample's permittivity increases as the concentration of functional elements increases; the minima relocate to a lower frequency zone. Two strong reflection loss minima below -30 dB can be seen in a 10% Co composite with thicknesses of 3.5 mm and 4.5 mm. This means that the vast majority of magnetic waves are absorbed by the system. Figure 33 shows that at 3.5 mm thickness, the reflection loss is -43 dB at 8 GHz frequency, with an absorption bandwidth of 3.5 GHz. In the high-frequency range, the reflection loss is -37.5 dB at 25.5 GHz.

Table 4: Performance of composite with Co functionalization

| CNT composite layer   | Spectral Bandwidth @ -10 dB (GHz) |                      | Minimum Reflection (dB) |                      | Thickness (mm) |
|-----------------------|-----------------------------------|----------------------|-------------------------|----------------------|----------------|
|                       | Low Frequency (<20)               | High Frequency (>20) | Low Frequency (<20)     | High Frequency (>20) |                |
| PU alone              | No                                | 1                    | -7.5                    | -10.5                | 4.5            |
| PU+5% CNT             | 3                                 | 3.5                  | -18.5                   | -31                  | 4.5            |
| PU+5% CNT with 5% Co  | 3.5                               | 4                    | -17                     | -20.5                | 3.5            |
| PU+5% CNT with 10% Co | 3.5                               | 4.5                  | -25.5                   | -37.5                | 3.5            |
| PU+5% CNT with 20% Co | 3                                 | 4                    | -43                     | 18                   | 3.5            |



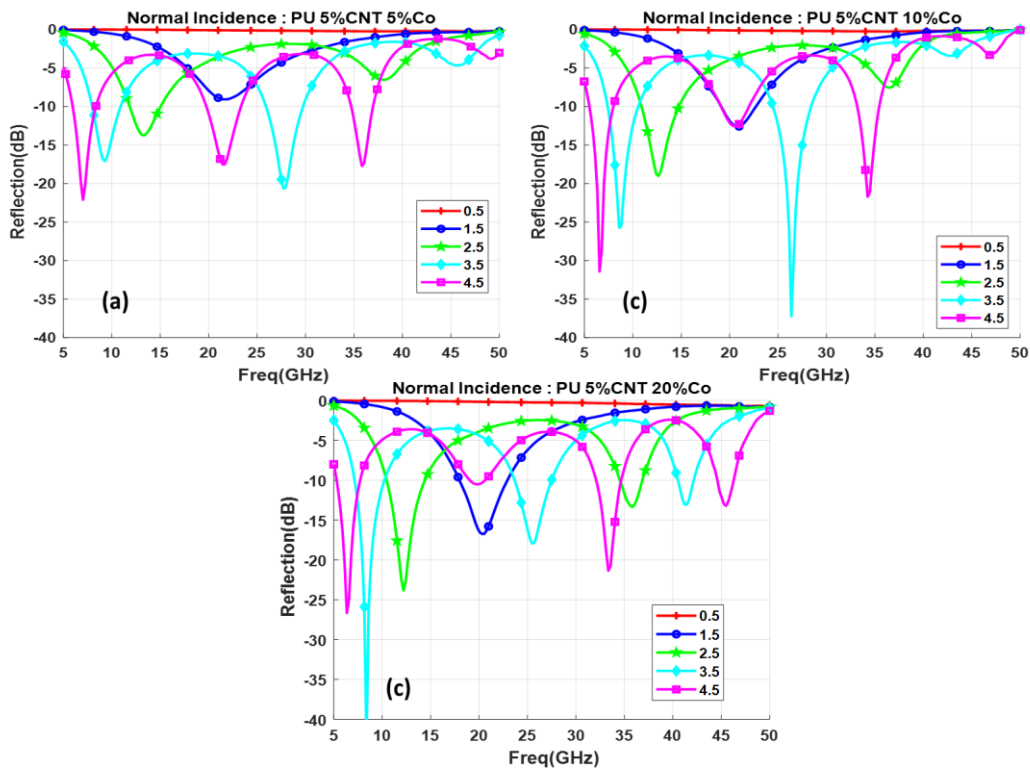


Figure 32: Reflection loss of Co functionalized composite (a) 5% Co (b) 10% Co (c) 20% Co with different thickness (mm)

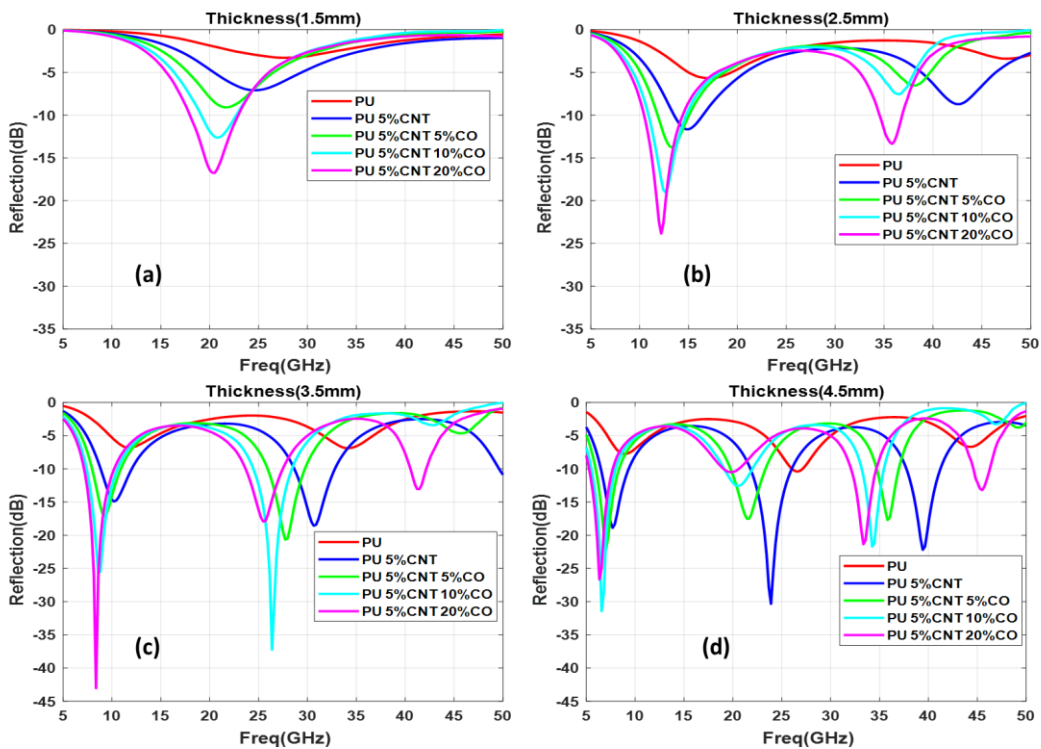


Figure 33: Comparison of reflection losses for different wt.% of Co element at different thickness (a) 1.5 mm (b) 2.5 mm (c) 3.5 mm (d) 4.5 mm

The reflection loss of a functionalized CNT composite with varying concentrations of CoFe oxide nanoparticles is shown in Figure 34. At the frequency 34 GHz with a narrow bandwidth, 10% of CoFe concentration has a minimum value of -36 dB reflection loss. At frequencies between 5 and 10 GHz, composite thicknesses ranging from 2.5 to 4.5 mm show minimal reflection.. The reflection loss of a functionalized CNT composite with varying concentrations of CoFe oxide nanoparticles is shown in Figure 34. When compared to Co functionalized, 5 % CoFe has better reflection minimas with -28 dB and is produced at 3.5 mm and 4.5 mm thickness. The CoFe values of 10% and 20% are nearly identical to the Co concentrations. Figure 35 depicts the reflection loss for various CoFe concentrations and thicknesses and Table 5 gives the total performance of the sample with CoFe functionalization. For 5% and 10% CoFe in the frequency range of 25-30 GHz, 3.5 mm thickness yields a 4.5 GHz bandwidth.

Table 5: Performance of composite with CoFe Oxide functionalization

| CNT composite layer    | Spectral Bandwidth @ -10 dB (GHz) |                       | Minimum Reflection (dB) |                       | Thick ness (mm) |
|------------------------|-----------------------------------|-----------------------|-------------------------|-----------------------|-----------------|
|                        | Low Frequency (<20)               | High Frequenc y (>20) | Low Frequenc y (<20)    | High Frequenc y (<20) |                 |
| PU + 5% CNT + 5% CoFe  | 3.5                               | 4.5                   | -20                     | -28                   | 3.5             |
| PU + 5% CNT + 10% CoFe | 3.5                               | 4.5                   | -22                     | -36                   | 3.5             |
| PU + 5% CNT + 20% CoFe | 3                                 | 3.5                   | -32                     | -24.5                 | 3.5             |

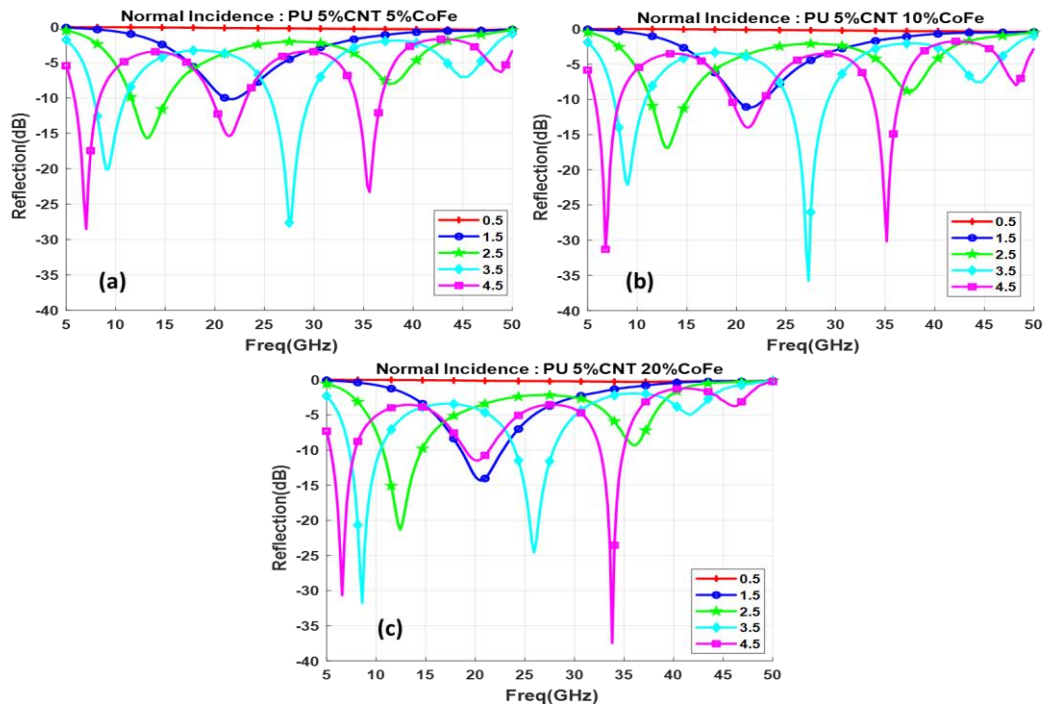


Figure 34: Reflection loss for CoFe functionalized composite (a) 5% CoFe (b) 10% CoFe (c) 20% CoFe with different thickness (mm)

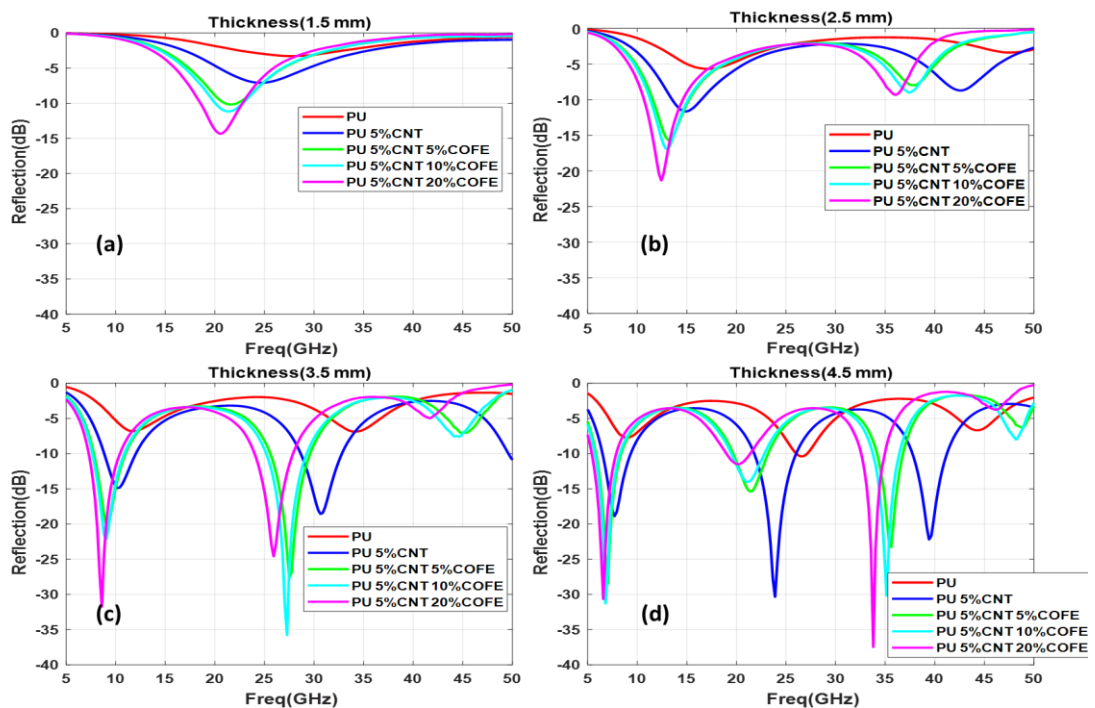


Figure 35: Comparison of reflection losses for different wt.% CoFe element at different thickness (a) 1.5 mm (b) 2.5 mm (c) 3.5 mm (d) 4.5 mm

For 10% and 20% Fe nanoparticle concentrations, resulted in a minimum reflection loss of -38 dB. However, the values are defined in two separate frequency bands. As illustrated in Figure 36(b), 10% Fe has this value in the higher frequency range, whereas 20% Fe has this value in the lower frequency range. However, as the bandwidth narrows, CoFe and Fe nanoparticle formed composites have almost identical curve behavior.

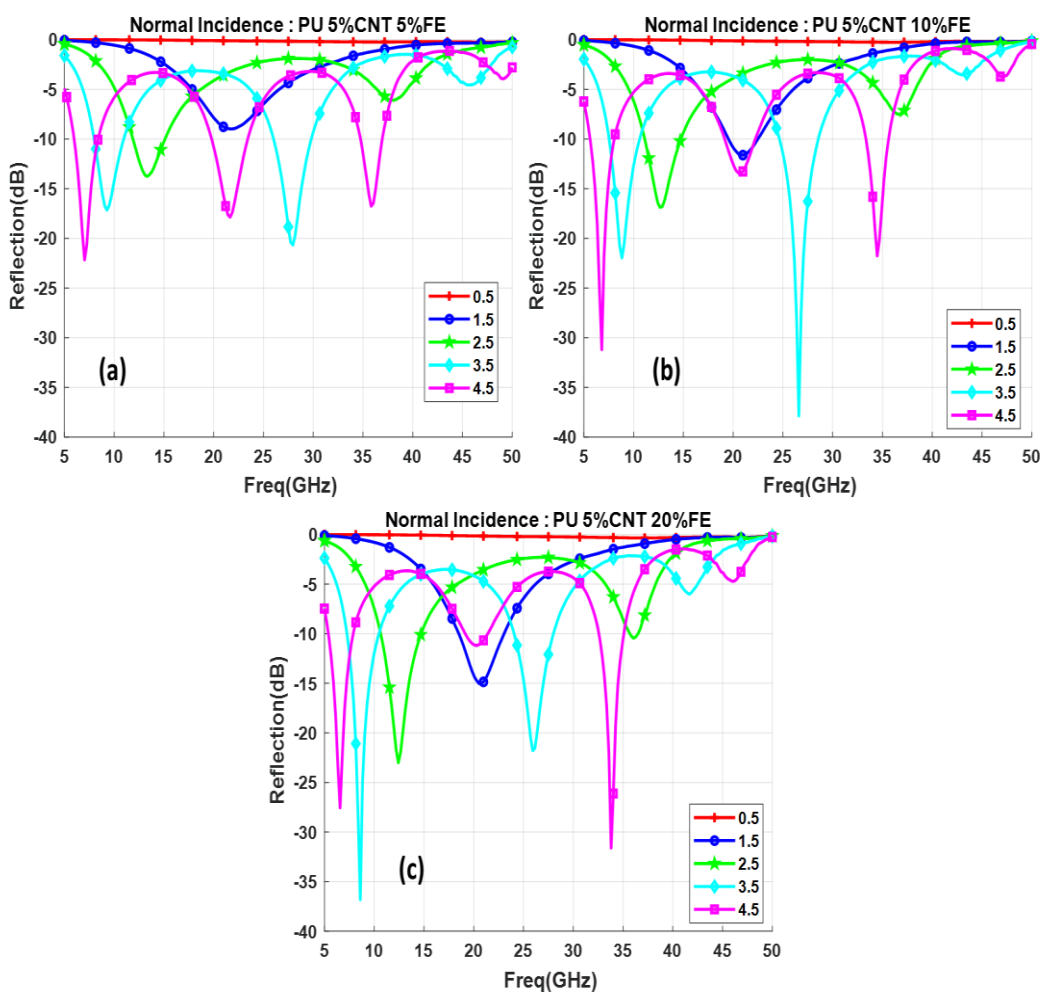


Figure 36: Reflection loss of Fe functionalized composite (a) 5% Fe (b) 10% Fe (c) 20% Fe with different thickness (mm)

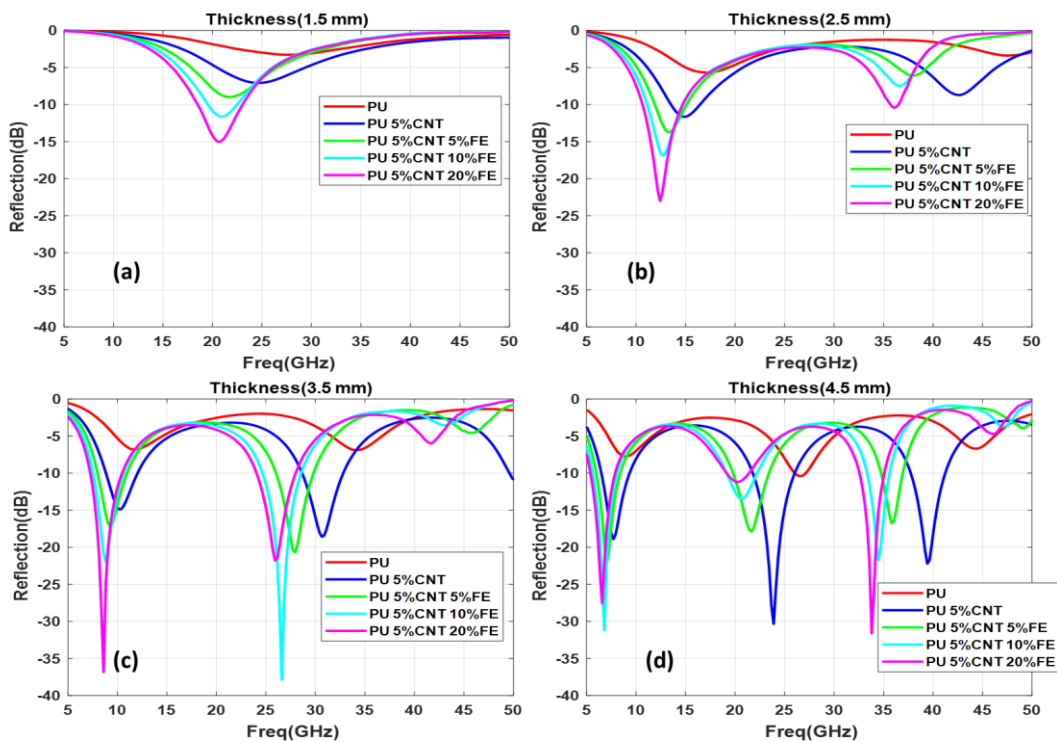


Figure 37: Comparison of reflection losses for different wt.% of Fe element at different thickness (a) 1.5 mm (b) 2.5 mm (c) 3.5 mm (d) 4.5 mm

Table 6: Performance of composite with Fe Oxide functionalization

| CNT composite layer  | Spectral Bandwidth @ -10 dB (GHz) |                      | Minimum Reflection (dB) |                      | Thickness (mm) |
|----------------------|-----------------------------------|----------------------|-------------------------|----------------------|----------------|
|                      | Low Frequency (<20)               | High Frequency (>20) | Low Frequency (<20)     | High Frequency (<20) |                |
| PU + 5% CNT + 5% Fe  | 3                                 | 3.5                  | -16.5                   | -20.5                | 3.5            |
| PU + 5% CNT + 10% Fe | 3                                 | 3.5                  | -22                     | -38                  | 3.5            |
| PU + 5% CNT + 20% Fe | 3                                 | 3.5                  | -37                     | -21.5                | 3.5            |

## 6.2 Reflection Loss for Two-layer composite

The reflection loss of single layer composites was discussed in the previous section; here, the reflection loss study was extended to double layer composites. In Chapter 2, the stack design is explained. The first layer is a lossy sheet with a high permittivity value and a predetermined thickness determined by Equation 21. The second layer is a lossless sheet with a low permittivity value and varying thickness. The PU sample is used in all calculations in the second layer, while the first layer is varied with different functionalized samples. MATLAB analysis was used to investigate the effect of reflection for the double layered composite with and without metal sheet.

As illustrated in Figures 38, 40, 41 and 42, double layer reflection loss is estimated for two frequencies of 10 GHz and 25 GHz backed by a metal layer. Figure 38 shows that the PU 5% CNT 10% Co and PU composite layer has a resonance at 10 GHz with a reflection loss of -18 dB; similarly, the composite layer has a resonance at 25 GHz with a reflection loss of -32 dB; and a minima appears in the lower frequency with 2 GHz bandwidth but a thickness of 4.4 mm. The composite covers the frequency band of 4 GHz at 10 GHz.

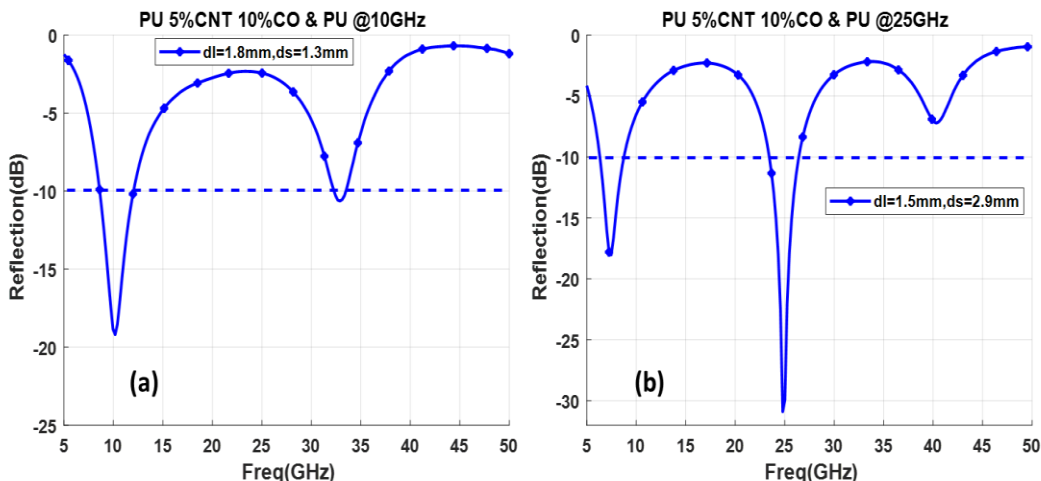


Figure 38: Reflection loss for PU 5% CNT 10% Co & PU composite backed with metal at (a) 10 GHz (b) 25 GHz

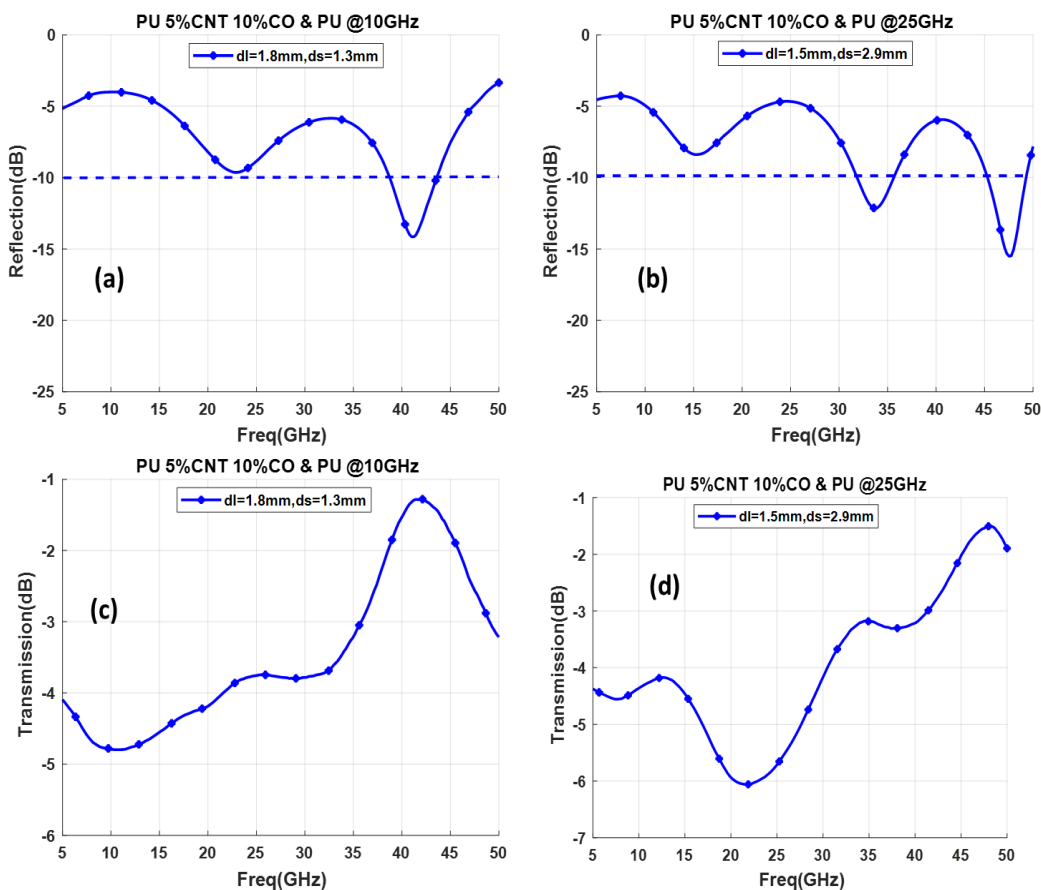


Figure 39: Reflection loss for PU 5% CNT 10% Co & PU with no metal backed at (a) 10 GHz (c) 25 GHz, (b) & (d) Transmission in PU 5% CNT 10% Co & PU composite at 10 GHz & 25 GHz

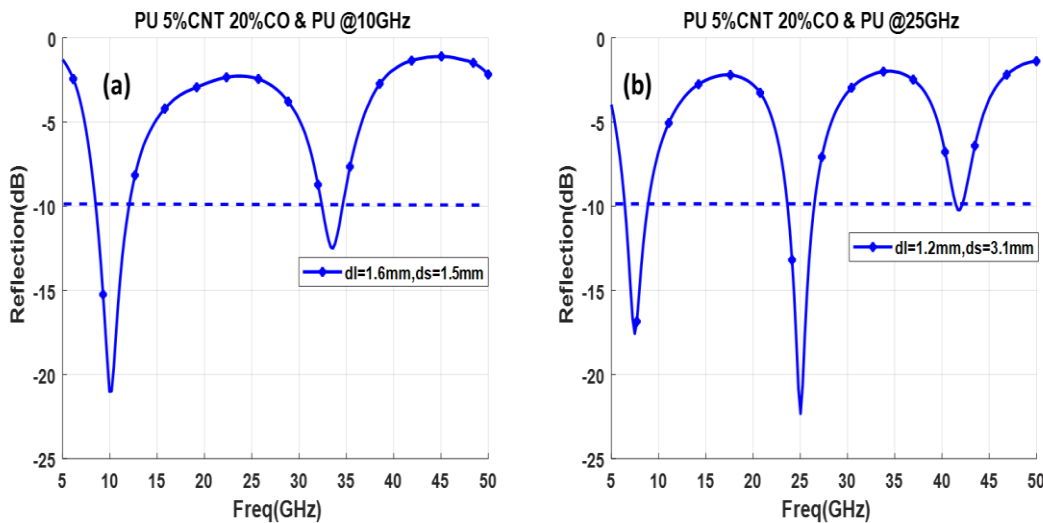


Figure 40: Reflection loss for PU 5% CNT 20% Co & PU composite backed with metal at (a) 10 GHz (b) 25 GHz

Furthermore, Figure 39 reveals a wide band in the higher frequency range for PU 5% CNT 10% Co and PU composite layer without a metal layer, but when plotting the transmission curve, it shows the bandwidth is due to the transmission via this sample. As a result, the absorption effect on the composite layer without the metal layer is minimal.

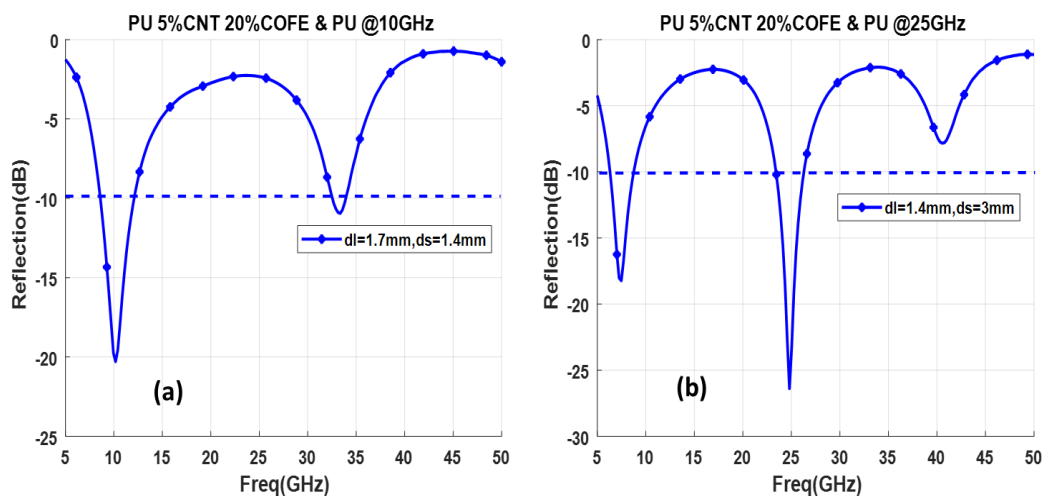


Figure 41: Reflection loss for PU 5% CNT 20% CoFe & PU composite backed with metal at (a) 10 GHz (b) 25 GHz



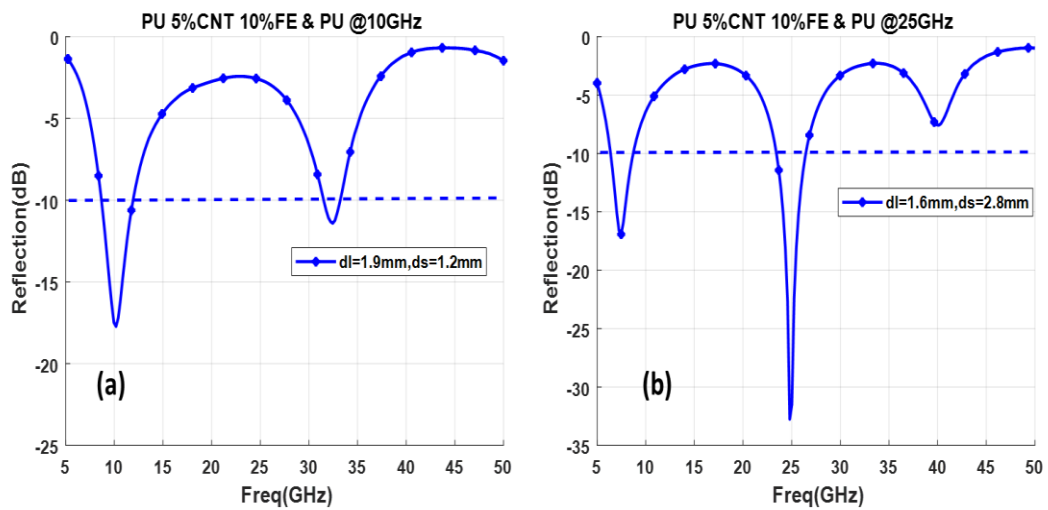


Figure 42: Reflection loss for PU 5% CNT 10% Fe & PU composite backed with metal at (a) 10 GHz (b) 25 GHz

The Co wt. % concentration is increased from 5 to 20%. Figure 40 shows a reduction in reflection from -18 to -21.5 dB at 10 GHz, as well as a modest resonance at higher frequencies around 33 GHz and no change in thickness of 3.1 mm.

Table 7: Performance of double layered composite

| CNT composite layer                     | Spectral Bandwidth<br>-10 dB (GHz) |                      | Minimum Reflection (dB) |                      | Thickness (mm) |
|---|------------------------------------|----------------------|-------------------------|----------------------|----------------|
|   | Low Frequency (<20)                | High Frequency (>20) | Low Frequency (<20)     | High Frequency (>20) |                |
| PU + 5% CNT with 10% Co & PU @ 10 GHz   | 4                                  | 1                    | -18                     | -10.5                | 3.1            |
| PU + 5% CNT with 10% Co & PU @ 25 GHz   | 1.5                                | 2.5                  | -18                     | -32                  | 4.4            |
| PU + 5% CNT with 20% Co & PU @ 10 GHz   | 4                                  | 2.5                  | -21.5                   | -12.5                | 3.1            |
| PU + 5% CNT with 20% Co & PU @ 25 GHz   | 2.5                                | 2.5                  | -17.5                   | -22.5                | 4.3            |
| PU + 5% CNT with 20% CoFe & PU @ 10 GHz | 4.5                                | 1.5                  | -20.5                   | -11                  | 3.1            |
| PU + 5% CNT with 20% CoFe & PU @ 25 GHz | 2.5                                | 2.5                  | -18                     | -27                  | 4.4            |
| PU + 5% CNT with 10% Fe & PU @ 10 GHz   | 4.2                                | 1.5                  | -17.5                   | -12                  | 3.1            |
| PU + 5% CNT with 10% Fe & PU @ 25 GHz   | 2                                  | 3                    | -17.5                   | -33                  | 4.4            |

When two-layer composite layer reflection was examined. The composite displays resonance at the target frequencies of 10 GHz and 25 GHz, and while the reflection loss values vary slightly, the thickness remains constant at 3.1 mm for all samples at 10 GHz. When comparing the loss of reflection with and without metal,

composite has higher transmission than wave absorption. Considering reflection at 25 GHz, the composite has a thickness of 4.4 mm. At 10 GHz, the composite of PU 5% CNT 10% Fe and PU has a better reflection loss of -17.5 dB, while at 25 GHz, the PU 5% CNT 10% Fe & PU has a reflection loss of -33 dB and also has a minima at 7 GHz with -17.5 dB. Detailed performance of the double layer composite is given in Table 7.

## Chapter 7: Conclusion

To demonstrate the effect of functionalization on the electromagnetic properties and absorption efficiency of CNT composites, several concentrations of nanoparticles are used to make functionalized CNT composites, and their dielectric properties are measured and compared to those of basic CNT composites. The open-ended coaxial probes method was used to measure electrical properties. The reflection loss properties of a metal-backed single layer slab were investigated, and a minimum reflection loss of -43 dB at 8 GHz with a thickness of 3.5 mm was obtained. In the frequency range of 25 to 35 GHz, 5% and 10% CoFe functionalized composite achieve a 4.5 GHz bandwidth. Thus, microwave absorption efficiency can be improved by using functionalized CNT composites with the appropriate thickness and concentration. As a result, this composite will be a viable choice for stealth applications that require a minimum weight and high absorption capability.

## References

- [1] A. Munir, "Microwave Radar Absorbing Properties of Multiwalled Carbon Nanotubes Polymer Composites: A Review," *Advances in Polymer Technology*, vol. 36, no. 3, pp. 362–370, Aug. 2017, doi: 10.1002/adv.21617.
- [2] X.-G. Sun *et al.*, "Microwave Absorption Characteristics of Carbon Nanotubes," *Carbon Nanotubes - Synthesis, Characterization, Applications*, Jul. 2011, doi: 10.5772/16514.
- [3] W. Emerson, "Electromagnetic wave absorbers and anechoic chambers through the years," *IEEE Transactions on Antennas and Propagation*, vol. 21, no. 4, pp. 484–490, Jul. 1973, doi: 10.1109/TAP.1973.1140517.
- [4] A. Delfini *et al.*, "Advanced Radar Absorbing Ceramic-Based Materials for Multifunctional Applications in Space Environment," *Materials (Basel)*, vol. 11, no. 9, p. 1730, Sep. 2018, doi: 10.3390/ma11091730.
- [5] J. Huo, L. Wang, and H. Yu, "Polymeric nanocomposites for electromagnetic wave absorption," *J Mater Sci*, vol. 44, no. 15, pp. 3917–3927, Aug. 2009, doi: 10.1007/s10853-009-3561-1.
- [6] Z. Wang *et al.*, "Magnetite Nanocrystals on Multiwalled Carbon Nanotubes as a Synergistic Microwave Absorber," *J. Phys. Chem. C*, vol. 117, no. 10, pp. 5446–5452, Mar. 2013, doi: 10.1021/jp4000544.
- [7] S. W. Phang, R. Daik, and M. H. Abdullah, "Poly(4,4'-diphenylene diphenylvinylene) as a non-magnetic microwave absorbing conjugated polymer," *Thin Solid Films*, vol. 477, no. 1, pp. 125–130, Apr. 2005, doi: 10.1016/j.tsf.2004.08.120.
- [8] X. Huang, P. Jiang, and T. Tanaka, "A review of dielectric polymer composites with high thermal conductivity," *IEEE Electrical Insulation Magazine*, vol. 27, no. 4, pp. 8–16, Jul. 2011, doi: 10.1109/MEI.2011.5954064.
- [9] K. S. Jayaraj, S. Walpalage, and S. M. Egodage, "Review on development of natural rubber/nanoclay nanocomposites," in *2015 Moratuwa Engineering Research Conference (MERCon)*, Apr. 2015, pp. 18–23. doi: 10.1109/MERCon.2015.7112313.
- [10] Nornikman H *et al.*, "Parametric Study of a Pyramidal Microwave Absorber Design," *IEICE Proceedings Series*, vol. 35, no. 1C02-1, Oct. 2008, DOI:10.34385/proc.35.1C02-1.
- [11] R. Kaur and G. D. Aul, "Review on Microwave Absorbing Material using Different Carbon Composites," *International Journal of Engineering Research & Technology*, vol. 3, no. 5, May 2014, <https://www.ijert.org/review-on-microwave-absorbing-material-using-different-carbon-composites>

- [12] M. I. Hussein *et al.*, “Microwave Absorbing properties of metal functionalized-CNT-polymer composite for stealth applications,” *Scientific Reports*, vol. 10, no. 1, Art. no. 1, Sep. 2020, doi: 10.1038/s41598-020-72928-1.
- [13] Y. Li *et al.*, “Multiband microwave absorption films based on defective multiwalled carbon nanotubes added carbonyl iron/acrylic resin,” *Physica B: Condensed Matter*, vol. 404, pp. 1343–1346, May 2009, doi: 10.1016/j.physb.2008.12.015.
- [14] T. Tanaka, G. C. Montanari, and R. Mulhaupt, “Polymer nanocomposites as dielectrics and electrical insulation-perspectives for processing technologies, material characterization and future applications,” *IEEE Transactions on Dielectrics and Electrical Insulation*, vol. 11, no. 5, pp. 763–784, Oct. 2004, doi: 10.1109/TDEI.2004.1349782.
- [15] A. Saib *et al.*, “Carbon nanotube composites for broadband microwave absorbing materials,” *IEEE Transactions on Microwave Theory and Techniques*, vol. 54, no. 6, pp. 2745–2754, Jun. 2006, doi: 10.1109/TMTT.2006.874889.
- [16] M. Ates, A. A. Eker, and B. Eker, “Carbon nanotube-based nanocomposites and their applications,” *Journal of Adhesion Science and Technology*, vol. 31, no. 18, pp. 1977–1997, Sep. 2017, doi: 10.1080/01694243.2017.1295625.
- [17] X. Shen *et al.*, “Preparation and electromagnetic performance of coating of multiwall carbon nanotubes with iron nanogranule,” *Journal of Magnetism and Magnetic Materials*, vol. 288, pp. 397–402, Mar. 2005, doi: 10.1016/j.jmmm.2004.08.035.
- [18] Z. Liu *et al.*, “Microwave Absorption of Single-Walled Carbon Nanotubes/Soluble Cross-Linked Polyurethane Composites,” *J. Phys. Chem. C*, vol. 111, no. 37, pp. 13696–13700, Sep. 2007, doi: 10.1021/jp0731396.
- [19] R. C. Che *et al.*, “Fabrication and microwave absorption of carbon nanotubes/CoFe<sub>2</sub>O<sub>4</sub> spinel nanocomposite,” *Appl. Phys. Lett.*, vol. 88, no. 3, p. 033105, Jan. 2006, doi: 10.1063/1.2165276.
- [20] D.-L. Zhao, X. Li, and Z.-M. Shen, “Preparation and electromagnetic and microwave absorbing properties of Fe-filled carbon nanotubes,” *Journal of Alloys and Compounds*, vol. 471, no. 1, pp. 457–460, Mar. 2009, doi: 10.1016/j.jallcom.2008.03.127.
- [21] F. Wen, F. Zhang, and Z. Liu, “Investigation on Microwave Absorption Properties for Multiwalled Carbon Nanotubes/Fe/Co/Ni Nanopowders as Lightweight Absorbers,” *J. Phys. Chem. C*, vol. 115, no. 29, pp. 14025–14030, Jul. 2011, doi: 10.1021/jp202078p.
- [22] M. S. Mustaffa *et al.*, “An investigation of microstructural, magnetic and microwave absorption properties of multi-walled carbon nanotubes/Ni<sub>0.5</sub>Zn<sub>0.5</sub>Fe<sub>2</sub>O<sub>4</sub>,” *Sci Rep*, vol. 9, no. 1, p. 15523, Oct. 2019, doi: 10.1038/s41598-019-52233-2.

- [23] H. Hekmatara, M. Seifi, and K. Forooraghi, "Microwave absorption property of aligned MWCNT/Fe<sub>3</sub>O<sub>4</sub>," *Journal of Magnetism and Magnetic Materials*, vol. 346, pp. 186–191, Nov. 2013, doi: 10.1016/j.jmmm.2013.06.032.
- [24] L. Huang *et al.*, "Challenges and future perspectives on microwave absorption based on two-dimensional materials and structures," *Nanotechnology*, vol. 31, no. 16, p. 162001, Apr. 2020, doi: 10.1088/1361-6528/ab50af.
- [25] Y. Wang, Y. Du, P. Xu, R. Qiang, and X. Han, "Recent Advances in Conjugated Polymer-Based Microwave Absorbing Materials," *Polymers*, vol. 9, no. 1, Art. no. 1, Jan. 2017, doi: 10.3390/polym9010029.
- [26] W. J. Wang, C. G. Zang, and Q. J. Jiao, "Ni-Coated Carbon Nanotubes/Mn-Zn Ferrite Composite as Viable Microwave Absorbing Materials," *Advanced Materials Research*, 2012. vol. 399–401, Nov. 2011, pp. 310–314. doi: 10.4028/www.scientific.net/amr.399-401.310.
- [27] A. G. D'Aloia *et al.*, "Electromagnetic absorbing properties of graphene–polymer composite shields," *Carbon*, vol. 73, pp. 175–184, Jul. 2014, doi: 10.1016/j.carbon.2014.02.053.
- [28] D. A. Lampasi *et al.*, "Effect of Grain Size and Distribution on the Shielding Effectiveness of Transparent Conducting Thin Films," *IEEE Transactions on Electromagnetic Compatibility*, vol. 56, no. 2, pp. 352–359, Apr. 2014, doi: 10.1109/TEMC.2013.2282085.
- [29] G. V. Morozov, R. G. Maev, and G. W. F. Drake, "Multiple reflection method for electromagnetic waves in layered dielectric structures," *Quantum Electron.*, vol. 31, no. 9, p. 767, Sep. 2001, doi: 10.1070/QE2001v031n09ABEH002042.
- [30] V. H. Nguyen *et al.*, "Measurement of complex permittivity by rectangular waveguide method with simple specimen preparation," in *2014 International Conference on Advanced Technologies for Communications (ATC 2014)*, Oct. 2014, pp. 397–400. doi: 10.1109/ATC.2014.7043419.
- [31] F. J. F. Gonçalves *et al.*, "Free-Space Materials Characterization by Reflection and Transmission Measurements using Frequency-by-Frequency and Multi-Frequency Algorithms," *Electronics*, vol. 7, no. 10, Art. no. 10, Oct. 2018, doi: 10.3390/electronics7100260.
- [32] R. Zajíček, J. Vrba, and K. Novotný, "Evaluation of a Reflection Method on an Open-Ended Coaxial Line and its Use in Dielectric Measurements," *Acta Polytechnica*, vol. 46, no. 5, p. 5, May 2006 doi: <https://doi.org/10.14311/882>
- [33] J. Wang *et al.*, "Open-Ended Coaxial Cable Selection for Measurement of Liquid Dielectric Properties via the Reflection Method," *Mathematical Problems in Engineering*, vol. 2020, Article ID 8942096, 8 pages, Oct 2020. <https://doi.org/10.1155/2020/8942096>.
- [34] P. G. Lederer, "An Introduction to Radar Absorbent Materials (RAM)," ROYAL SIGNALS AND RADAR ESTABLISHMENT MALVERN (ENGLAND), Feb. 1986. Available: <https://apps.dtic.mil/sti/citations/ADA169895>.

- [35] C. Tsipogiannis, "Microwave materials characterization using waveguides and coaxial probe," *undefined*, 2012. Available: /paper/Microwave-materials-characterization-using-and-Tsipogiannis/cfbc5ae2d8f5dec1ef666e5cae60feb9e70b2d33.
- [36] "VectorStar Family of RF,  $\mu$ W, mmW VNAs MS4640B Series | Anritsu America." <https://www.anritsu.com/en-us/test-measurement/products/ms4640b-series> (accessed Mar. 25, 2021). Available: <https://www.anritsu.com/en-US/test-measurement/products/ms4640b-series>.
- [37] F. Caspers, "RF engineering basic concepts: S-parameters," *arXiv:1201.2346 [physics]*, Jan. 2012. Available: <http://arxiv.org/abs/1201.2346>.
- [38] S. Kumar, Arti, P. Kumar, N. Singh, and V. Verma, "Steady microwave absorption behavior of two-dimensional metal carbide MXene and Polyaniline composite in X-band," *Journal of Magnetism and Magnetic Materials*, vol. 488, p. 165364, Oct. 2019, doi: 10.1016/j.jmmm.2019.165364.



### List of Publications

1. M. Kallumottakkal, M. I. Hussein, and M. Z. Iqbal, "Recent Progress of 2D Nanomaterials for Application on Microwave Absorption: A Comprehensive Study," *Frontiers in Materials*, vol. 8, p. 34, 2021, doi: 10.3389/fmats.2021.633079.
2. M. Kallumottakkal *et al.*, "Functionalized-CNT Polymer Composite for Microwave and Electromagnetic Shielding," *Polymers*, vol. 13, no. 22, Art. no. 22, Jan. 2021, doi: 10.3390/polym13223907.

## Appendices

### Appendix 1

#### 1. Permittivity and tangent loss Plotting

```
clear all
close all
clc

%% Reading Multiple files

filename1='PU_0% CNT.xls';
Data1 = xlsread(filename1);
Freq=Data1(:,1).*10^6;
epsR=Data1(:,33);
epsI=Data1(:,34);
tangentloss1=Data1(:,36);

filename2='PU_5% CNT.xls';
Data2 = xlsread(filename2);
Freq1=Data2(:,1).*10^6;
epsR2=Data2(:,33);
epsI2=Data2(:,34);
tangentloss2=Data2(:,36);

filename3='PU_5% CNT_5% CO.xls';
Data3 = xlsread(filename3);
Freq2=Data3(:,1).*10^6;
epsR3=Data3(:,33);
epsI3=Data3(:,34);
tangentloss3=Data3(:,36);

filename4='PU_5% CNT_10% CO.xls';
Data4 = xlsread(filename4);
Freq3=Data4(:,1).*10^6;
epsR4=Data4(:,25);
epsI4=Data4(:,26);
tangentloss4=Data4(:,28);

filename5='PU_5% CNT_20% CO.xls';
Data5 = xlsread(filename5);
Freq4=Data5(:,1).*10^6;
epsR5=Data5(:,33);
epsI5=Data5(:,34);
tangentloss5=Data5(:,36);
```

```
%% Plotting real part of permittivity
```

```
figure;
Freq=Freq./10^9;
plot(Freq,epsR,'r',Freq,epsR2,'b',Freq,epsR3,'g',Freq,epsR4,'c',Freq,epsR5,'m','LineWidth',2);
set(gca,'FontSize',12)
set(gca,'fontweight','bold')
xlabel('\bf \fontsize{14}Freq(GHz)');
ylabel('\bf \fontsize{14}Epsilon real');
grid;
legend('PU','PU 5%CNT','PU 5%CNT 5%CO','PU 5%CNT 10%CO','PU 5%CNT 20%CO');
```

```
%% Plotting imaginary part of permittivity
```

```
figure;
plot(Freq,epsI,'r',Freq,epsI2,'b',Freq,epsI3,'g',Freq,epsI4,'c',Freq,epsI5,'m','LineWidth',2);
set(gca,'FontSize',12)
set(gca,'fontweight','bold')
xlabel('\bf \fontsize{14}Freq(GHz)');
ylabel('\bf \fontsize{14}Epsilon Imaginary');
grid;
legend('PU','PU 5%CNT','PU 5%CNT 5%CO','PU 5%CNT 10%CO','PU 5%CNT 20%CO');
```

```
%% Plotting tangent loss
```

```
figure;

plot(Freq,tangentloss1,'r',Freq,tangentloss2,'b',Freq,tangentloss3,'g',Freq,tangentloss4,'c',Freq,tangentloss5,'m','LineWidth',2);
set(gca,'FontSize',12)
set(gca,'fontweight','bold')
xlabel('\bf \fontsize{14}Freq(GHz)');
ylabel('\bf \fontsize{14}Tangent loss');
grid;
legend('PU','PU 5%CNT','PU 5%CNT 5%CO','PU 5%CNT 10%CO','PU 5%CNT 20%CO');
```

## 2. One-layer composite backed with metal

This code plots the reflection, transmission and insertion of a single layer dielectric slab backed with metal

```
clear all
```

```

close all
clc
d= [2 3 4 5]; %thickness in millimeters
leg= num2str(d.',2);
n=length(d);
theta=45;
eps1=1;
eps4=1;
d=d.*10^-3;

%% Reading Multiple files
[~,sheet_name]=xlsinfo('PU_AVG.xls');
for k=1:numel(sheet_name)
    data{k}=xlsread('PU_AVG.xls',sheet_name{k});
end;

    Freq = data{k}(:,1).*10^6;% Freq in GHZ;
    m = k; %% no of times measurements were
    done;

epsR=data{k}(:,2);
epsI=data{k}(:,3);
eps2=epsR-1i*epsI;
c=3e8;

% slab2

epsR1=1;
eps0=8.85e-12;
sigma=41e6;
epsI1 = sigma./(2*pi*Freq*eps0);
eps3=epsR1-1i*epsI1;

kz1=2*pi*(Freq/c).*sqrt(eps2);
kz2=2*pi*(Freq/c).*sqrt(eps3);

%%normal incidence%%

r1n=(sqrt(eps1)-sqrt(eps2))./(sqrt(eps1)+sqrt(eps2));
r2n=(sqrt(eps2)-sqrt(eps3))./(sqrt(eps2)+sqrt(eps3));
r3n=(sqrt(eps3)-sqrt(eps4))./(sqrt(eps3)+sqrt(eps4));

%% total reflection

for i=1:n

X2n=(r2n+r3n.*exp(-1i*2*kz2*d(i)))./(1+(r2n.*r3n).*exp(-1i*2*kz2*d(i)));
X1n=(r1n+X2n.*exp(-1i*2*kz1*d(i)))./(1+(r1n.*X2n).*exp(-1i*2*kz1*d(i)));

```

```

Rn(:,i)=(abs(X1n).^2);
end

%% plotting Normal Incidence

Freq=Freq./10^9;
col = {[1 0 0]; [0 0 1]; [0 1 0];[0 1 1];[1 0 1];[1 0.8 0.4];[1 0.5 0];[.6 .3 .5];[0 0
0];[0.3 0.5 1];[0.3 1 0.8];[1 0.2 0.5];[0.2 0.8 1];[0.1 0.5 0.7]};
m=['+', 'o', 'p', 'd', 's', '^', '<', '>', '*', 'v', 'h', 'x', '+', 'o'];

figure;

for i=1:4

line_fewer_markers(Freq,10*log10(abs(Rn(:,i))),15,'Color',col{i},'Marker',m(i),'Mar
kerSize',5,'LineWidth',2);
hold on;

end
hold off;

xlim([0 20]);
set(gca,'FontSize',12)
set(gca,'fontweight','bold')
xlabel('\bf \fontsize{14}Freq(GHz)');
ylabel('\bf \fontsize{14}Reflection(dB)');
grid;
legend(leg);
legend(leg,'Location','southwest');
title ('Normal Incidence : PU_AVG');

```

### Two-layer composite backed with metal

This code plots the reflection of a two-layer dielectric slab backed with metal

```

close all
clear all

% first layer

f=25.025*10^9;
c=3e8;
epsr1=6.00783;
lamdaL=(c)/(f*sqrt(epsr1));
sigma=1.77417;
d=(1/(120*pi*sigma)) % (dl-high epsilon lossy sheet) thickness of slab1 in meters
% second layer

```

```

epsrs=3.7152975;
lamdaS=(c)/(f*sqrt(epsrs));
d2=lamdaS/2.18% (lossless sheet PU (ds) thickness of slab2 in meters
theta=60; %polarization angle

%%% slab 1 file reading
filename1='PU_5% CNT_10% CO_AVG.xlsx';
eps1=1;
eps5=1;
Data1 = xlsread(filename1);
Freq=Data1(:,1).*10^6;
epsR=Data1(:,2);
epsI=(Data1(:,3));
eps2=epsR-1i*epsI;
c=3e8;

%%% slab2 file reading
filename2='PU_AVG.xlsx';
Data2 = xlsread(filename2);
epsR1=Data2(:,2);
epsI1=(Data2(:,3));
eps3=epsR1-1i*epsI1;

% slab3
epsR2=1;
eps0=10^-9/(36*pi);
sigma=41e6;
epsI2 = sigma./(2*pi*Freq*eps0);
eps4=epsR2-1i*epsI2;

kz1=2*pi*(Freq/c).*sqrt(eps2);
kz2=2*pi*(Freq/c).*sqrt(eps3);
kz3=2*pi*(Freq/c).*sqrt(eps4);

%%% normal incidence%%%
r1n=(sqrt(eps1)-sqrt(eps2))./(sqrt(eps1)+sqrt(eps2));
r2n=(sqrt(eps2)-sqrt(eps3))./(sqrt(eps2)+sqrt(eps3));
r3n=(sqrt(eps3)-sqrt(eps4))./(sqrt(eps3)+sqrt(eps4));
r4n=(sqrt(eps4)-sqrt(eps5))./(sqrt(eps4)+sqrt(eps5));

%%% total reflection

X3n=(r3n+r4n.*exp(-1i*2*kz3*d))./(1+(r3n.*r4n).*exp(-1i*2*kz3*d));
X2n=(r2n+X3n.*exp(-1i*2*kz2*d2))./(1+(r2n.*X3n).*exp(-1i*2*kz2*d2));
X1n=(r1n+X2n.*exp(-1i*2*kz1*d))./(1+(r1n.*X2n).*exp(-1i*2*kz1*d));

Rn=(abs(X1n).^2);

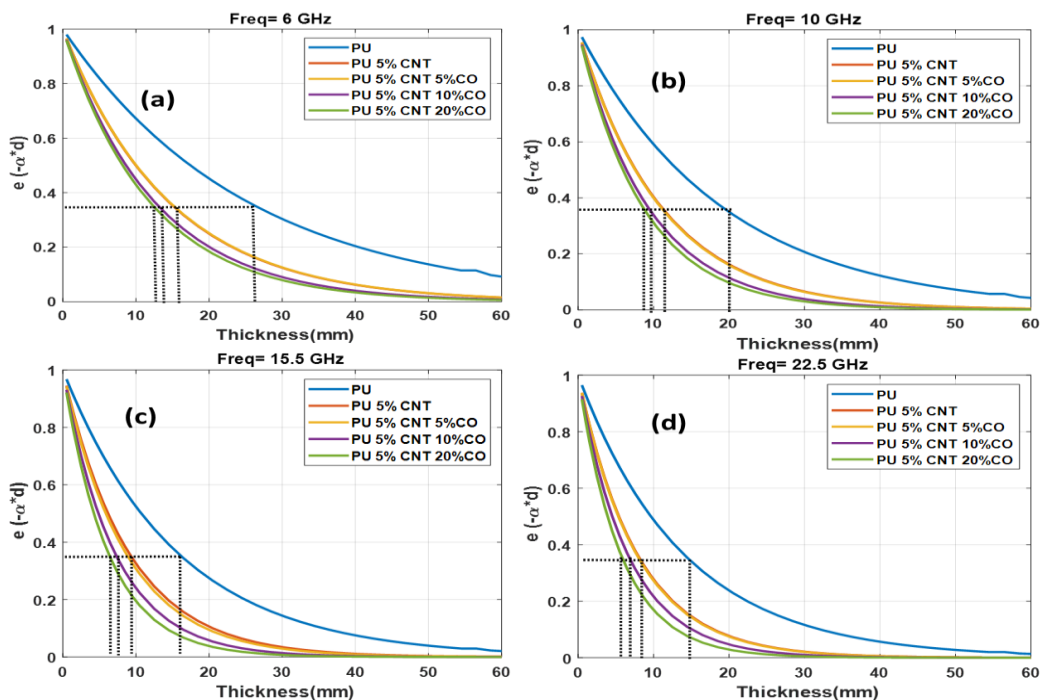
Freq=Freq./10^9;

```

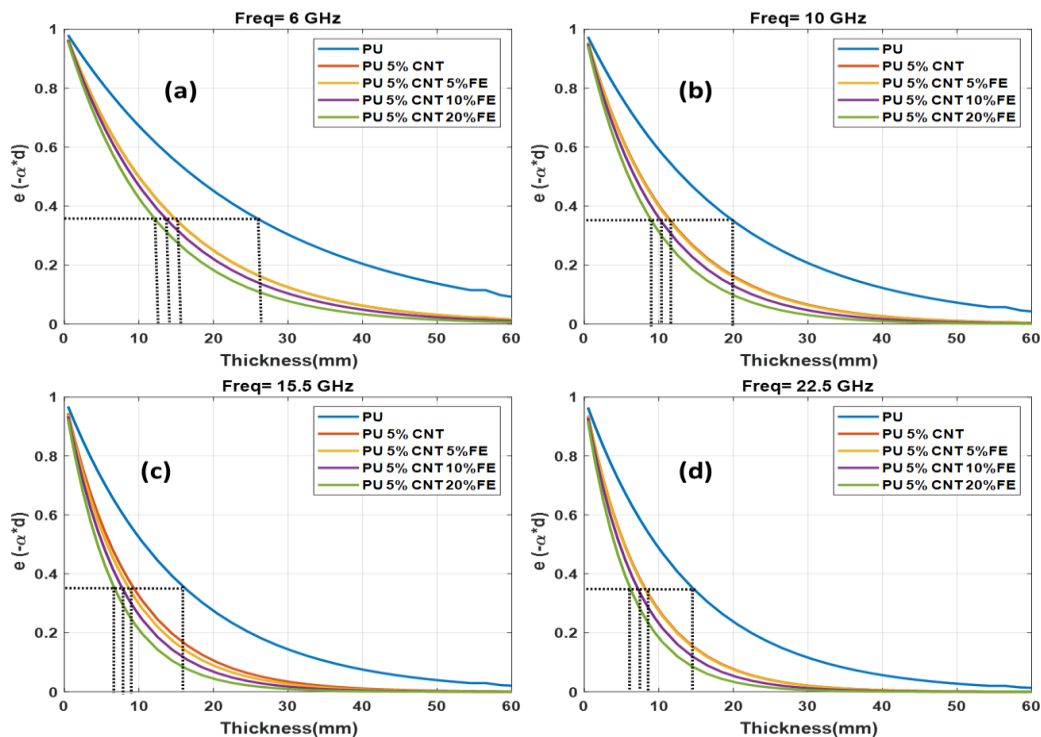
```
col = {[0 0 1]};
m=['*'];
figure;
for i=1:1
line_fewer_markers(Freq,10*log10(abs(Rn(:,i))),15,'Color',
col{i},'Marker',m(i),'MarkerSize',5,'LineWidth',2);
hold on;
end
hold off;

%%%plot%%
set(gca,'FontSize',12)
set(gca,'fontweight','bold')
xlabel('\bf \fontsize{ 14 }Freq(GHz)');
ylabel('\bf \fontsize{ 14 }Reflection(dB)');
grid;
xlim([5 50])
title('Normal Incidence');
legend('dl=1.2mm,ds=3.1mm');
```

## Appendix 2



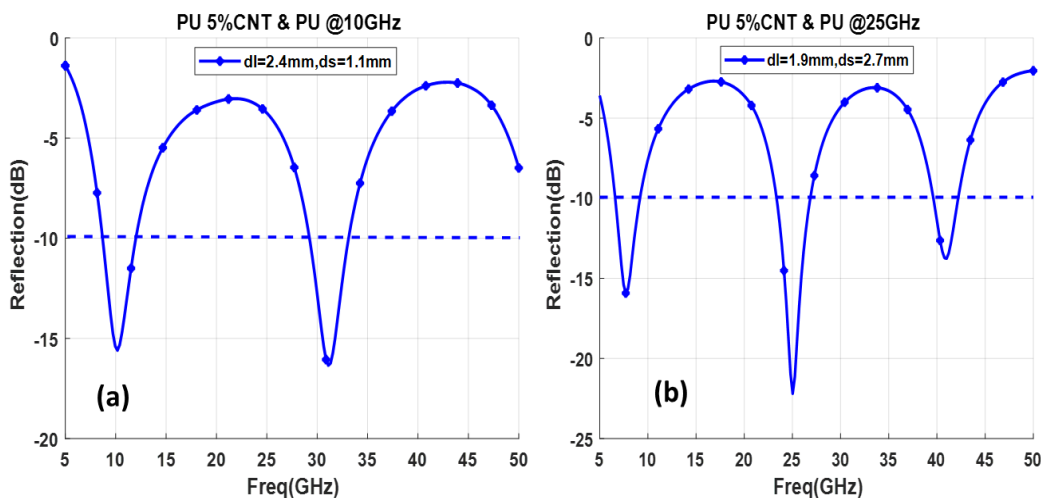
Attenuation factor for PU, PU 5% CNT, PU + 5% CNT+ (5%, 10%, 20%) Co at different center frequencies



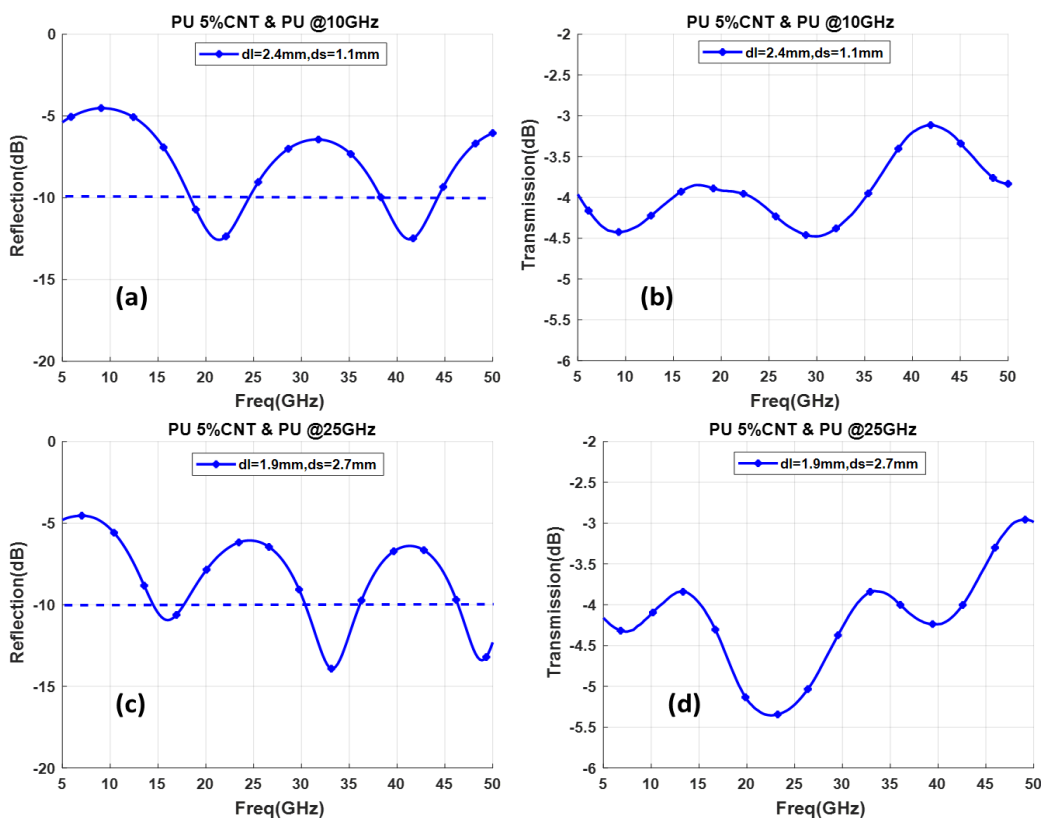
Attenuation factor for PU, PU 5% CNT, PU + 5% CNT + (5%, 10%, 20%) Fe at different center frequencies.



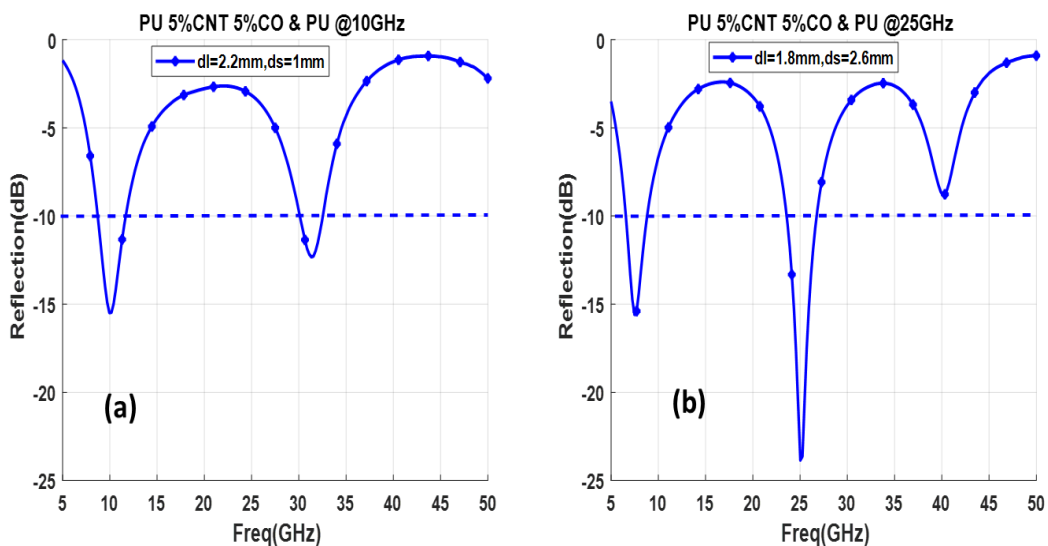
### Appendix 3



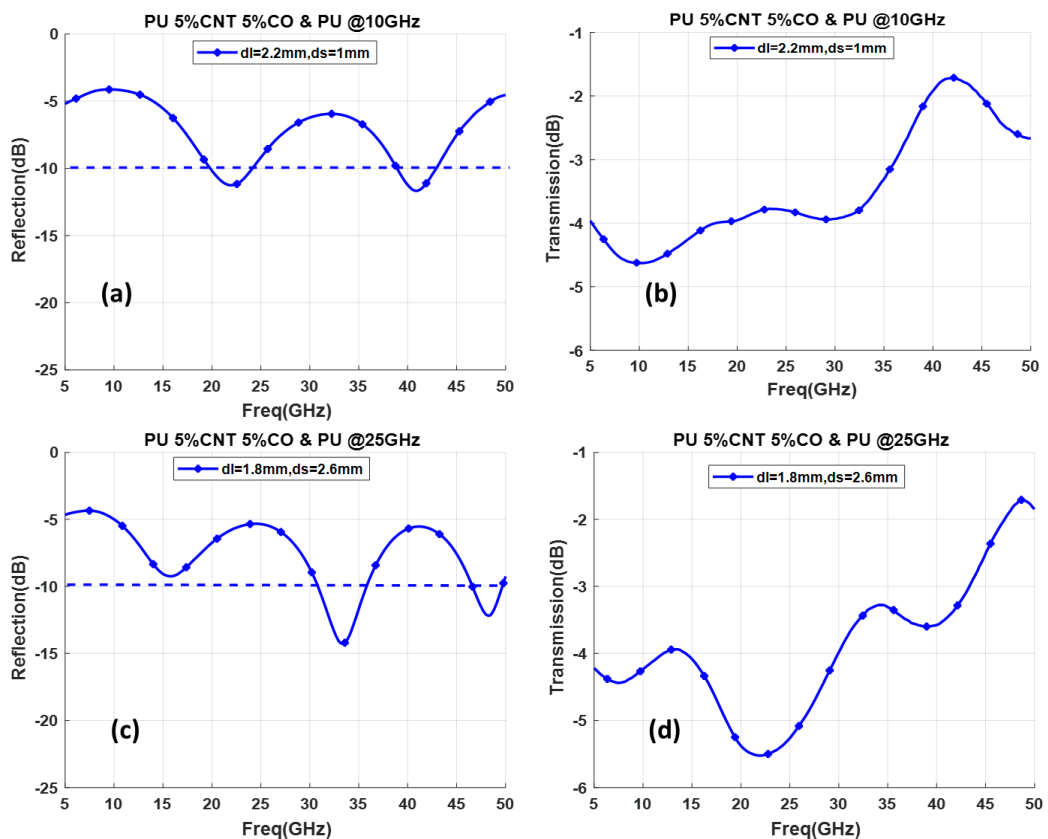
Reflection loss for PU 5% CNT & PU composite backed with metal at (a) 10 GHz (b) 25 GHz



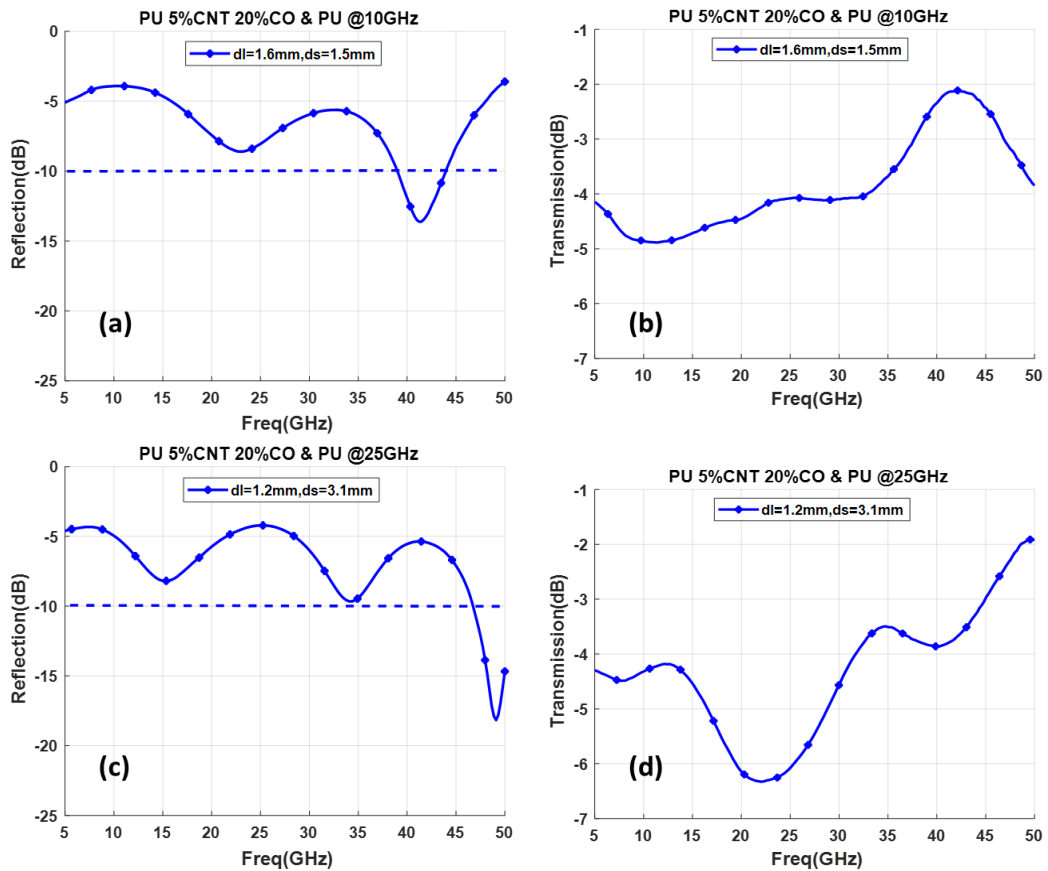
Reflection loss for PU 5% CNT & PU composite with no metal backed at (a) 10 GHz (c) 25 GHz. (b) & (d) Transmission in PU 5% CNT & PU composite at 10 GHz and 25 GHz



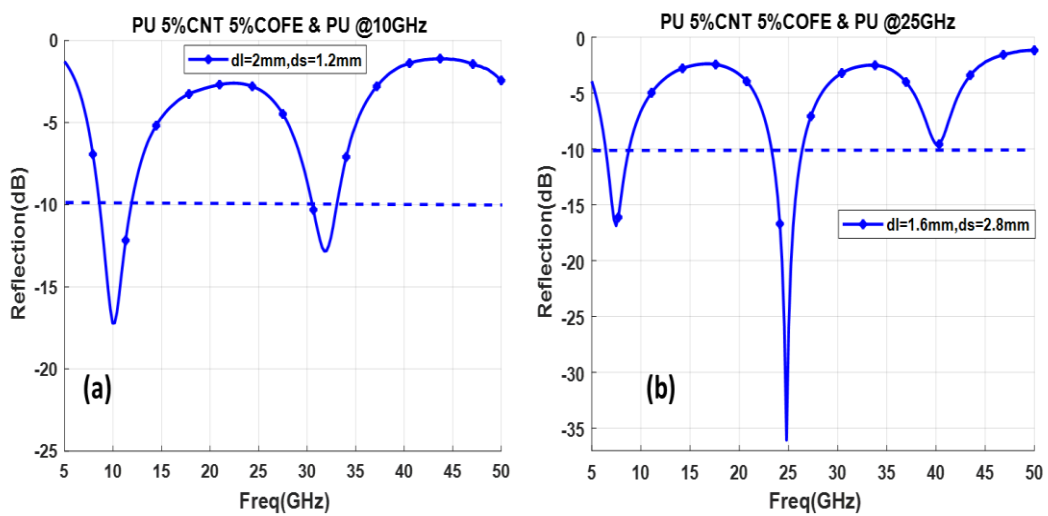
Reflection loss for PU 5% CNT 5% Co & PU composite backed with metal at (a) 10 GHz (b) 25 GHz



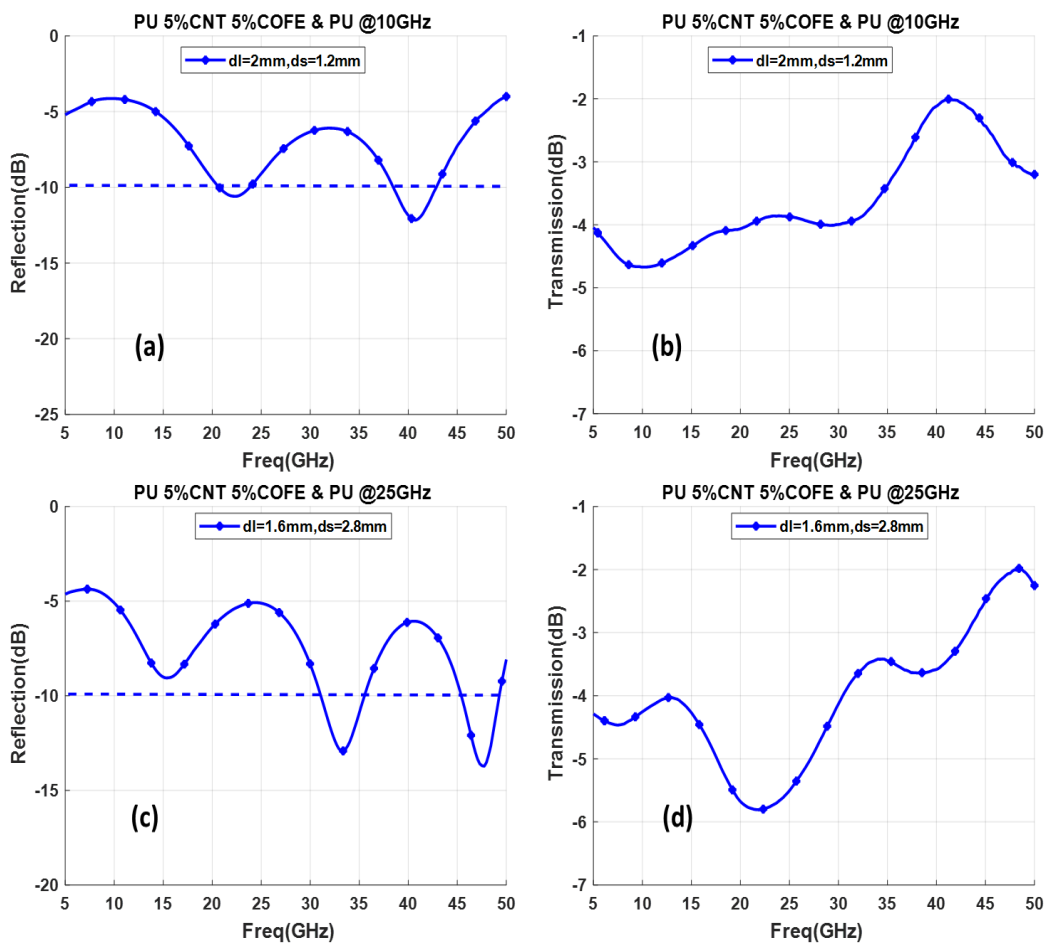
Reflection loss for PU 5% CNT 5% Co & PU composite with no metal backed at (a) 10 GHz (c) 25 GHz. (b) & (d) Transmission in PU 5% CNT 5% Co & PU composite at 10 GHz and 25 GHz



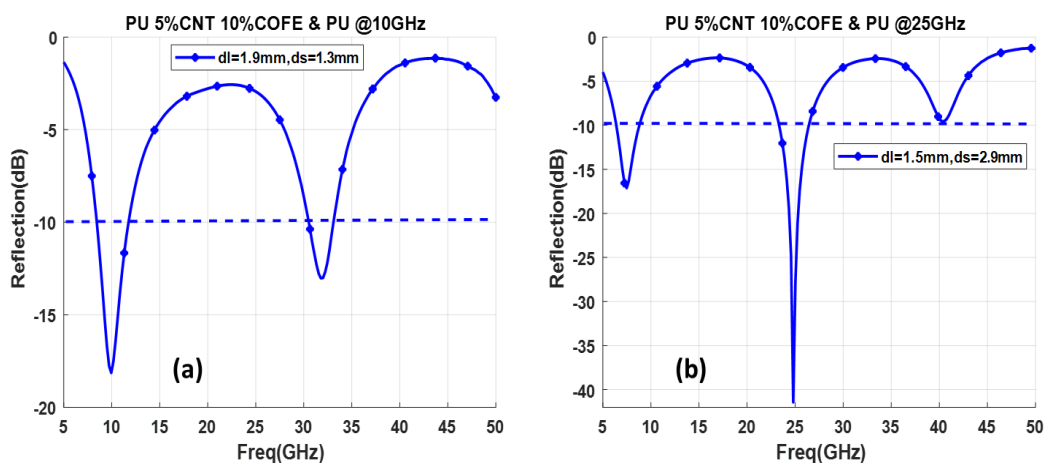
Reflection loss for PU 5% CNT 20% Co & PU composite with no metal backed at (a) 10 GHz (c) 25 GHz. (b) & (d) Transmission in PU 5% CNT 20% Co & PU composite at 10 GHz and 25 GHz



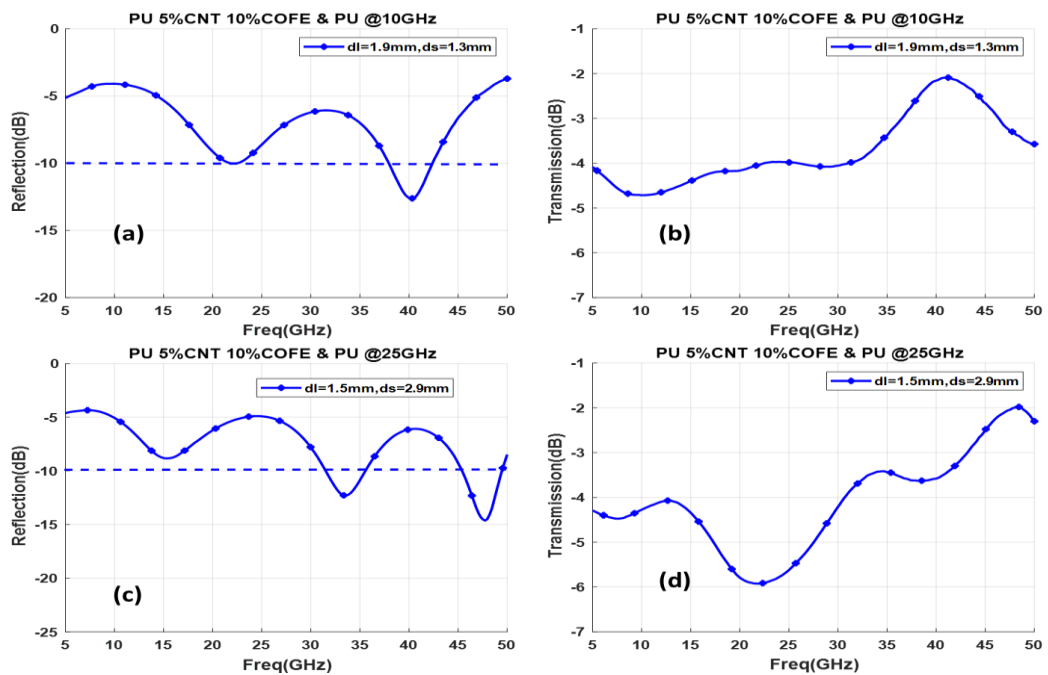
Reflection loss for PU 5% CNT 5% CoFe & PU composite backed with metal at (a) 10 GHz (b) 25 GHz



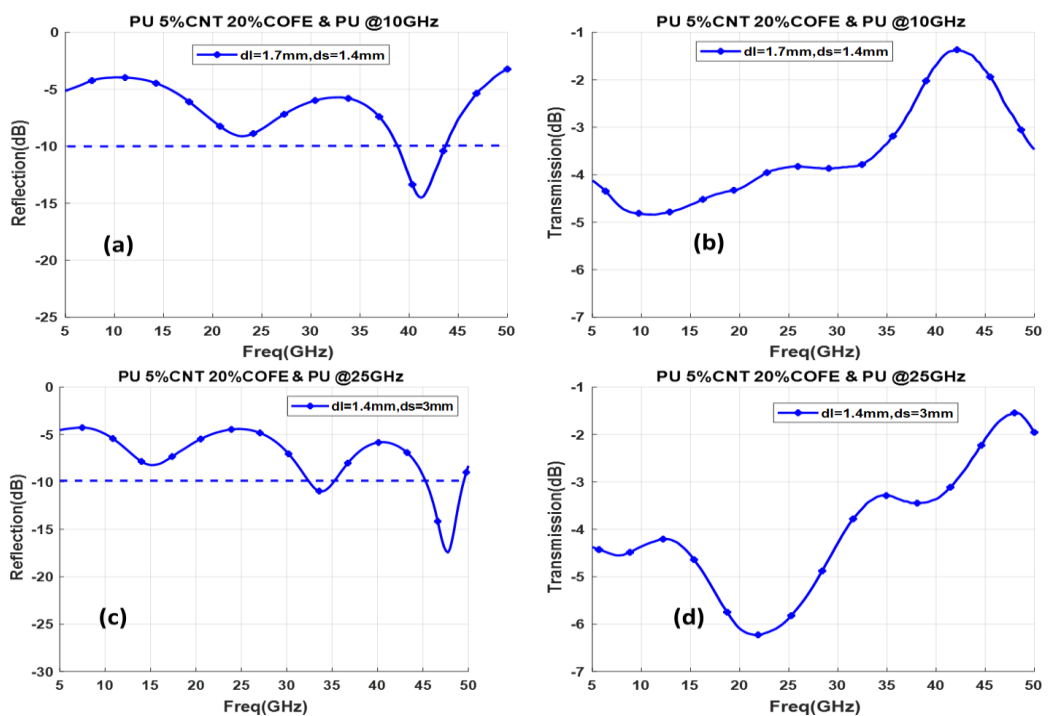
Reflection loss for PU 5% CNT 5% CoFe & PU composite with no metal backed at (a) 10 GHz (c) 25 GHz. (b) & (d) Transmission in PU 5% CNT 5% CoFe & PU composite at 10 GHz and 25 GHz



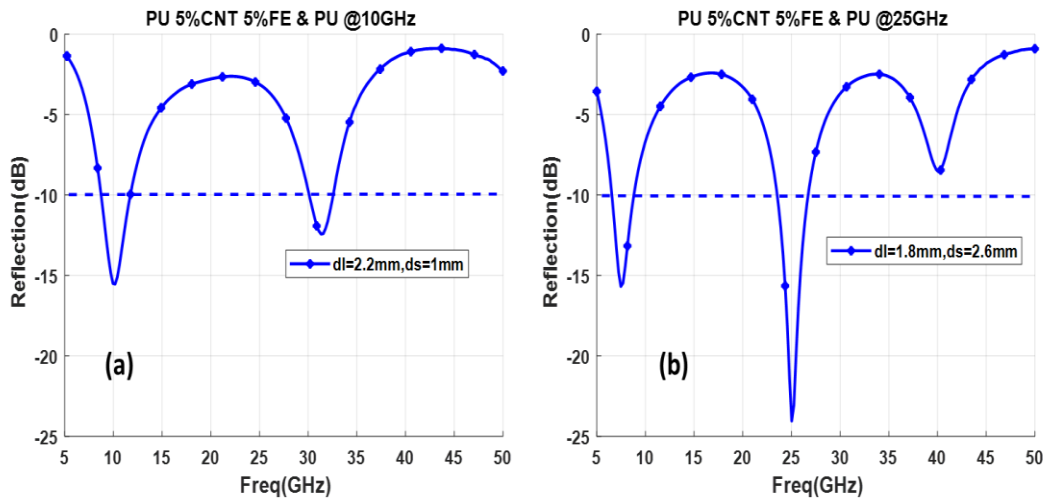
Reflection loss for PU 5% CNT 10% CoFe & PU composite backed with metal at (a) 10 GHz (b) 25 GHz



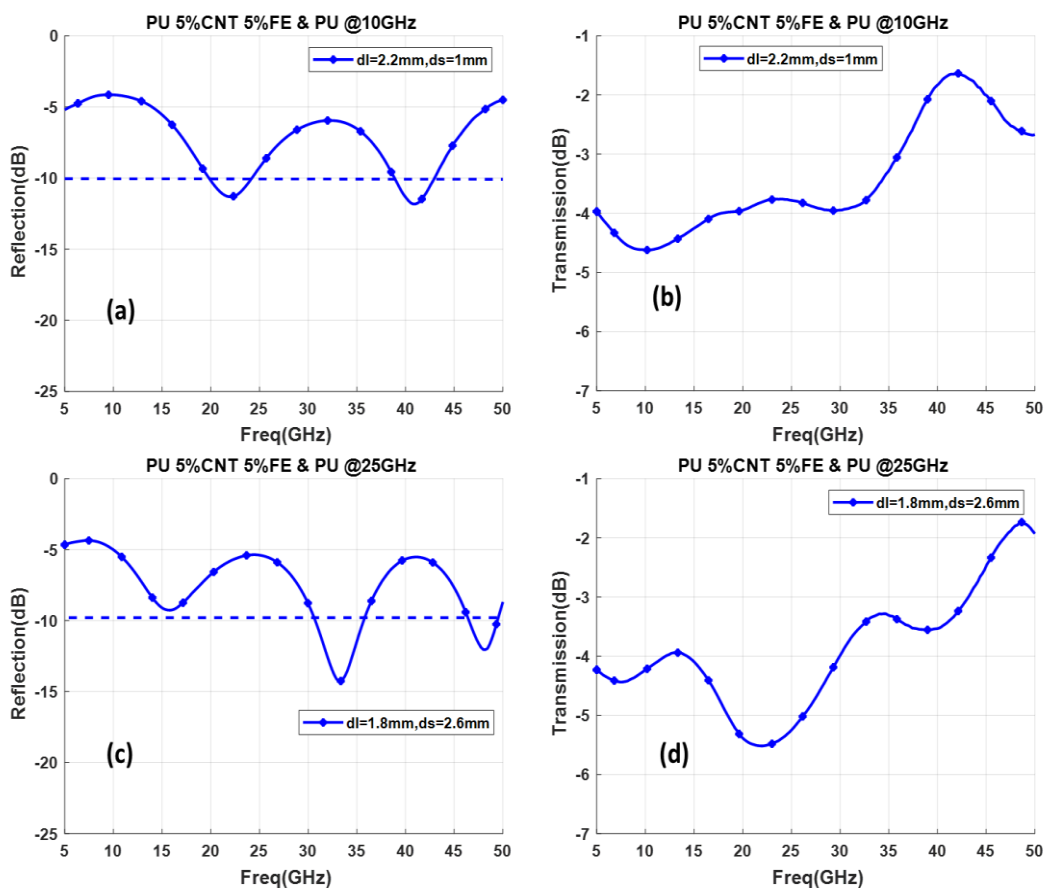
Reflection loss for PU 5% CNT 10% CoFe & PU composite with no metal backed at (a) 10 GHz (c) 25 GHz. (b) & (d) Transmission in PU 5% CNT 10% CoFe & PU composite at 10 GHz and 25 GHz



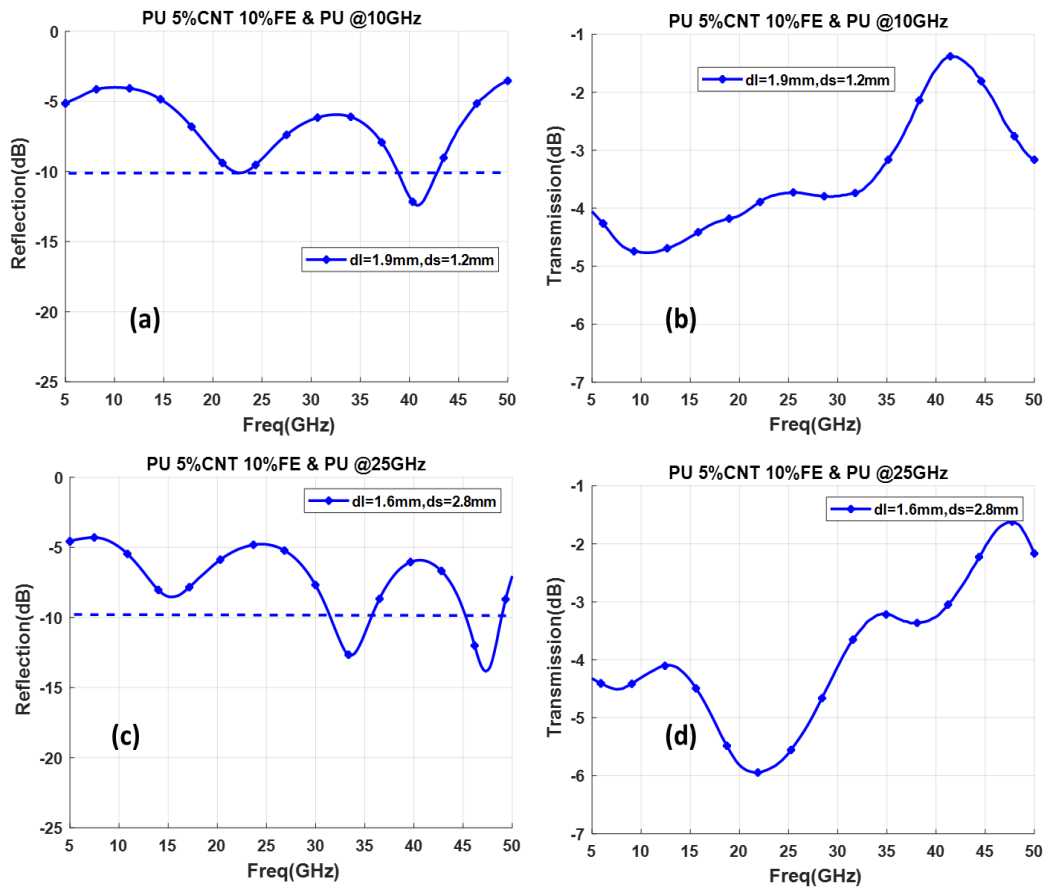
Reflection loss for PU 5% CNT 20% CoFe & PU composite with no metal backed at (a) 10 GHz (c) 25 GHz. (b) & (d) Transmission in PU 5% CNT 20% CoFe composite at 10 GHz and 25 GHz



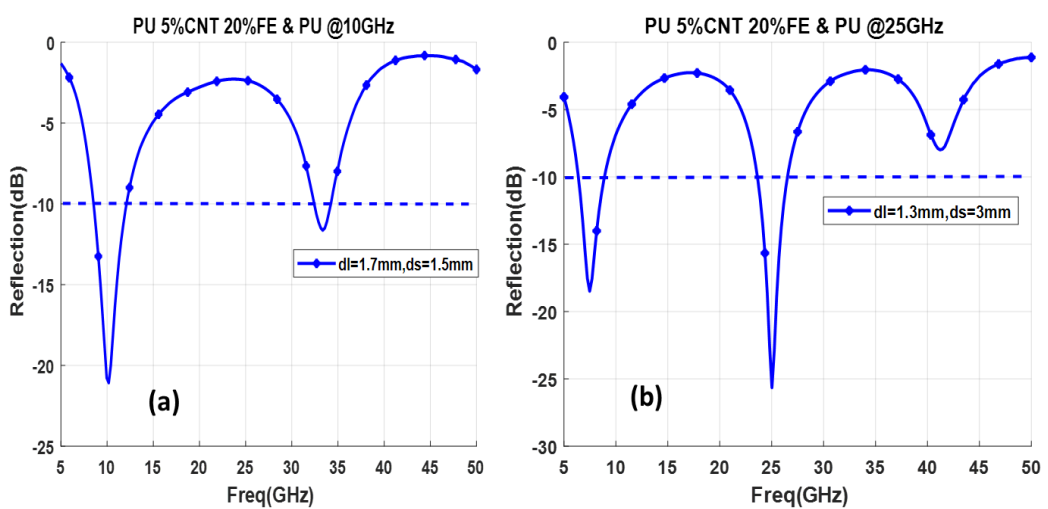
Reflection loss for PU 5% CNT 5% Fe & PU composite backed with metal at (a) 10 GHz (b) 25 GHz



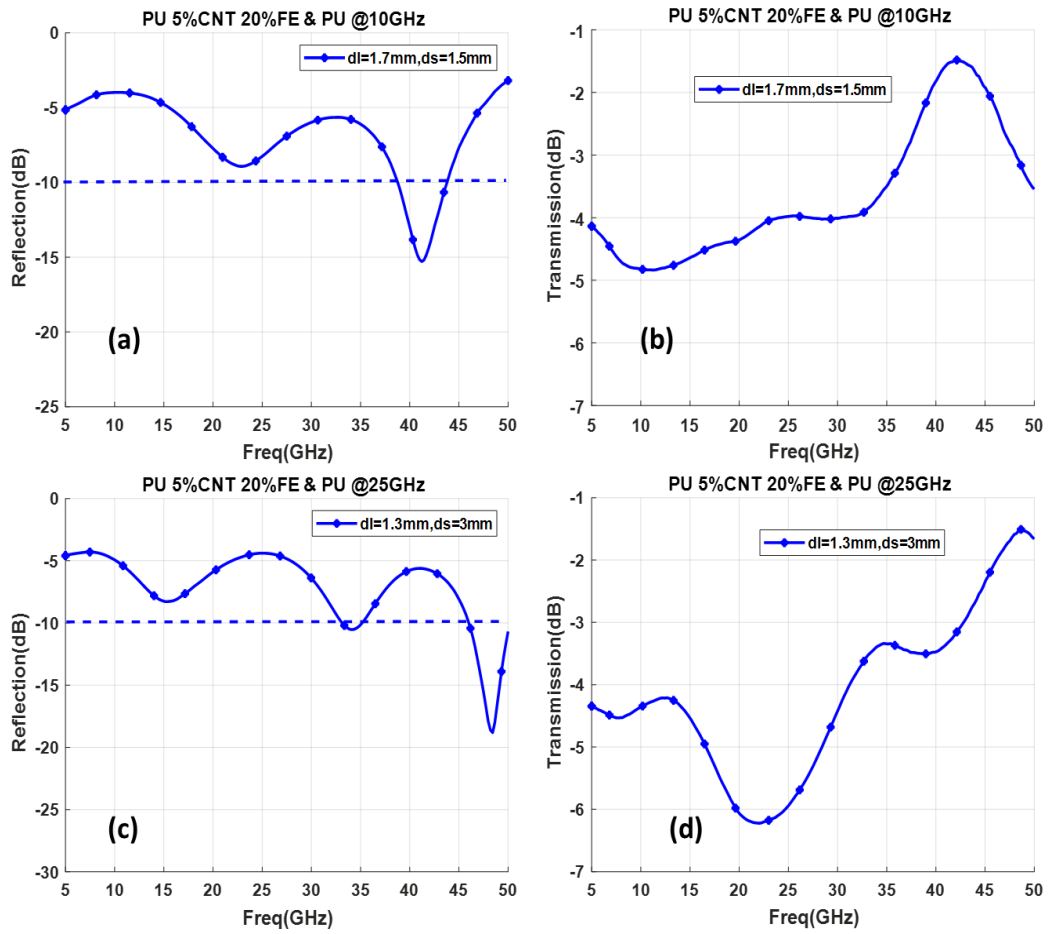
Reflection loss for PU 5% CNT 5% Fe & PU composite with no metal backed at (a) 10 GHz (c) 25 GHz. (b) & (d) Transmission in PU 5% CNT 5% Fe & PU composite at 10 GHz and 25 GHz



Reflection loss for PU 5% CNT 10% Fe & PU composite with no metal backed at (a) 10 GHz (c) 25 GHz. (b) & (d) Transmission in PU 5% CNT 10% Fe & PU composite at 10 GHz and 25 GHz



Reflection loss for PU 5% CNT 20% Fe & PU composite backed with metal at (a) 10 GHz (b) 25 GHz



Reflection loss for PU 5% CNT 20% Fe & PU composite with no metal backed at (a) 10 GHz (c) 25 GHz. (b) & (d) Transmission in PU 5% CNT 20% Fe & PU composite at 10 GHz and 25 GHz